

FATIGUE PRE-CRACKING LIFE ESTIMATION FOR FRACTURE  
TOUGHNESS TEST SPECIMENS

A THESIS SUBMITTED TO  
THE GRADUATE SCHOOL OF NATURAL AND APPLIED SCIENCES  
OF  
MIDDLE EAST TECHNICAL UNIVERSITY

BY

AMIR ALIPOUR GHASABI

IN PARTIAL FULFILLMENT OF THE REQUIREMENTS  
FOR  
THE DEGREE OF MASTER OF SCIENCE  
IN  
MECHANICAL ENGINEERING

JUNE 2018



Approval of the thesis:

**FATIGUE PRE-CRACKING LIFE ESTIMATION FOR FRACTURE  
TOUGHNESS TEST SPECIMENS**

submitted by **AMIR ALIPOUR GHASABI** in partial fulfillment of the requirements for the degree of **Master of Science in Mechanical Engineering Department, Middle East Technical University** by,

Prof. Dr. Halil Kalıpçılar  
Dean, Graduate School of **Natural and Applied Sciences**

\_\_\_\_\_

Prof. Dr. M. A. Sahir Arıkan  
Head of department, **Mechanical Engineering**

\_\_\_\_\_

Prof. Dr. F. Suat Kadiođlu  
Supervisor, **Mechanical engineering Department, METU**

\_\_\_\_\_

**Examining Committee Members:**

Prof. Dr. Metin Akkök  
Mechanical Engineering Department, METU

\_\_\_\_\_

Prof. Dr. F. Suat Kadiođlu  
Mechanical Engineering Department, METU

\_\_\_\_\_

Prof. Dr. Bülent Doyum  
Mechanical Engineering Department, METU

\_\_\_\_\_

Assoc. Prof. Dr. Demirkan ÇÖKER  
Aerospace Engineering Department, METU

\_\_\_\_\_

Prof. Dr. Bora Yıldırım  
Mechanical Engineering Department, Hacettepe University

\_\_\_\_\_

Date: \_\_\_\_\_

**I hereby declare that all information in this document has been obtained and presented in accordance with academic rules and ethical conduct. I also declare that, as required by these rules and conduct, I have fully cited and referenced all material and results that are not original to this work.**

Name, Last Name: AMIR ALIPOUR GHASABI

Signature :

## **ABSTRACT**

### **FATIGUE PRE-CRACKING LIFE ESTIMATION FOR FRACTURE TOUGHNESS TEST SPECIMENS**

ALIPOUR GHASABI, AMIR

M.S., Department of Mechanical Engineering

Supervisor : Prof. Dr. F. Suat Kadioğlu

June 2018, 102 pages

This study is done for predicting fatigue crack initiation life and propagation life of a crack initiated at a notch and grown to a desired length. Both numerical analysis and experimental study was done for single edge notch bend type specimen. Crack initiation life prediction was done using strain-life approach applying different available models. For this purpose 2-D and 3-D finite element model of the specimen was created in Abaqus. By simulating the 2-D and 3-D model under static loading, notch maximum stress was found to calculate the notch elastic stress concentration factor. Applying Neuber's rule local stresses and strains of notched part was calculated. These values were then compared to values found by elasto-plastic analysis done for 3-D model in Abaqus. Then, fatigue crack initiation life was predicted. For the propagation part, the required number of cycles to grow the initiated crack from 1 mm length to a desired length was calculated by using Walker and Paris equations. At the end the predicted lives were compared to experimental ones. It is found that reasonable agreement could be obtained, and the established procedure could be used in planning the preparation stages of cracked beam specimens.

Keywords: Fatigue Crack Initiation Life, Crack Propagation, FEA,

## ÖZ

### KIRIK ÖRGÜ TEST ÖRNEKLERİ İÇİN CATLAKTAN ONCE YORULMA CYCLE HESAPLAMASI

ALIPOUR GHASABI, AMIR

Yüksek Lisans, Makina Mühendisliđi Bölümü

Tez Yöneticisi : Prof. Dr. F. Suat Kadiođlu

HAZIRAN 2018, 102 pages

Bu alıřma, bir entikte bařlatılan ve istenilen uzunlukta büyütölmüş bir atlađın yorulma atlađı bařlama ömrünü ve yayılma ömrünü kestirmek için yapılmıřtır. Hem sayısal analiz hem de deneysel alıřma, tek kenarı entikli eđilme tipi deney numunesi için yapıldı. atlak bařlama inisasyon ömrü tahmini, mevcut farklı modelleri uygulayan gerinim-ömür yaklařımı kullanılarak yapıldı. Bu amaçla Abaqus'ta örnek iki ve üç boyutlu sonlu eleman modeli oluřturuldu. Statik yüklenme altında iki boyutlu modelin simüle edilmesiyle, entik elastik gerilme konsantrasyon faktörü için entik maksimum gerilme hesaplanmıřtır. Neuber'in kuralını uygulamak, yerel gerilmeler ve entikli kısım gerinimleri hesaplandı. Bu deđerler daha sonra Abaqus'ta 3-D modeli için yapılan elasto-plastik analizi ile bulunan deđerlerle karřılařtırıldı (sadece on evrim için). Daha sonra yorulma atlađı bařlama ömrü tahmin edildi. Yayılma kısmı için, bařlatılan atlađın 1 mm'den 6.4 mm'ye kadar uzatılması için gereken evrim sayısı, Walker denklemi kullanılarak hesaplanmıřtır. Sonunda tahmin edilen ömürler deneysel olanlarla karřılařtırıldı. Olduka uyumlu sonuçlar elde edildiđi ve uygulanan yöntemin atlak ieren kiriř numunelerinin hazırlık ařamalarının planlanmasında kullanılabileceđi bulunmuřtur.

Anahtar Kelimeler: Yorulma atlađı Bařlatma Ömrü, atlak yayılması, Sonlu Elemanlar Analizi

To My Beloved Mom and Dad

## **ACKNOWLEDGMENTS**

I would first like to express my sincere gratitude to my supervisor Prof. Dr. F. Suat Kadioglu for his great guidance, useful comments and criticisms throughout this study.

Beside my supervisor, I shall thank the members of my thesis examining committee for their insightful comments and valuable suggestions.

Finally, I would like to thank my family especially my parents Soraiya and Ahmad for their deep love, patience and support throughout my life.

This study has been partially funded by TUBITAK 1001 project, code 214M06Z “An experimental investigation on vibration of cracked beams”.

## TABLE OF CONTENTS

ABSTRACT .....	v
ÖZ.....	vi
ACKNOWLEDGMENTS.....	viii
TABLE OF CONTENTS .....	ix
LIST OF TABLES .....	xi
LIST OF FIGURES.....	xii
CHAPTERS	
1. INTRODUCTION.....	1
1.1 Introduction .....	1
1.2 Previous Investigations .....	2
1.3 Motivation and the Scope of the Thesis .....	4
1.3.1 Thesis Objectives .....	5
1.4 Thesis Structure.....	5
2. LITERATURE REVIEW AND BACKGROUND.....	7
2.1 Introduction and Historical Overview .....	7
2.2 Fatigue Design.....	8
2.3 Fatigue Loading.....	9
2.4 Steady State Cyclic Stress-Strain Relation.....	11
2.5 Fatigue Life .....	14
2.6 Strain-Life ( $\epsilon$ -N) Approach .....	15
2.7 Estimate of strain-Life fatigue Properties .....	19
2.8 Mean Stress Effects .....	20
2.8.1 Modified Morrow Approach .....	21
2.8.2 Manson-Halford Model.....	22
2.8.3 Smith, Watson, and Topper (SWT) Parameter .....	23
2.8.4 Walker Mean Stress Equation .....	23
2.9 Material Response at Notch Tip.....	24

2.9.1 Elastic Stress Concentration Factor .....	24
2.9.2 The Fatigue Notch Factor $K_f$ .....	25
2.9.3 Notch Sensitivity Factor $q$ and Empirical estimations for $K_f$ .....	26
2.9.4 Strain Life Approach in Notched Members.....	29
2.9.4.1 The Linear Rule .....	31
2.9.4.2 Neuber's Rule .....	32
2.9.4.3 Glinka's Rule .....	34
2.10 Review of Linear Elastic Fracture Mechanics (LEFM).....	36
2.10.1 Loading Modes .....	36
2.10.2 Stress Intensity Factor.....	37
2.10.3 Monotonic and Cyclic Plastic Zone.....	39
2.11 Fatigue Crack Growth (FCG) .....	40
2.11.1 Mean Stress Effects for FCG .....	43
2.11.1.1 The Walker Equation for FCG.....	43
2.12 Fracture Toughness Testing.....	44
2.12.1 Specimen Configurations.....	44
2.12.2 Fatigue Pre-cracking .....	46
2.12.3 Measurement Tools.....	47
2.12.4 $K_{Ic}$ Testing.....	48
2.12.4.1 ASTM E 399 .....	48
3. LIFE PREDICTIONS .....	51
3.1 Geometry, Loading and Boundary Conditions of Problem .....	51
3.2 Material of the Specimen .....	53
3.3 Stress Analysis of Specimen in Abaqus® .....	54
3.4 Calculation of Elastic and Fatigue Stress Concentration Factor, $K_t$ and $K_f$ ...	63
3.5 Cyclic Material Properties and Calculation of Cyclic Local Stresses and Strains .....	65
3.6 Fatigue Crack Initiation Life Prediction .....	72
3.7 Fatigue Crack Growth Life Prediction.....	76
3.8 Total Fatigue Life .....	81
4. EXPERIMENTAL ANALYSES .....	83
5. COMPARISONS, CONCLUSION AND FUTURE WORK.....	93
REFERENCES .....	99

## LIST OF TABLES

### TABLES

Table3.1: Chemical composition of al 6082 .....	53
Table3. 2: Physical and mechanical properties of al 6082 T651 .....	54
Table3. 3: Applied load and corresponding $\sigma_{max}$ , $\sigma_{nom}$ , and $K_t$ .....	63
Table3. 4: fatigue stress concentration factor.....	65
Table3. 5: Strain-life and cyclic properties of 6082 T6 aluminum alloy .....	65
Table3. 6: Cyclic local stresses and strains .....	69
Table3. 7: local stresses and strains at the end of ten cycles obtained from 2-D and 3-D analysis in Abaqus. (E) is total strain. (LE) is the logarithmic strain which is true strain.....	72
Table3. 8: Fatigue crack initiation life predictions .....	74
Table3. 9: FCG material data[10],[51],[52] .....	78
Table3. 10 Total fatigue life up to crack length of 16.4 mm.....	81
Table 5. 1 Fatigue crack initiation life (numerical & experimental).....	94

## LIST OF FIGURES

### FIGURES

Figure2. 1 Drawing of a fatigue failure in an axle, sketched by Joseph Glynn following The Versailles accident, 1842[18].....	7
Figure2. 2 Fatigue design flow chart originated by H. S. Reemsnyder from Bethlehem Steel Corp. and slightly modified by H. O. Fuchs. It was created for use by the Society of Automotive Engineers Fatigue Design and Evaluation (SAEFDE) Committee University of Iowa's annual short course on Fatigue Concepts in Design. ....	8
Figure2. 3 Schematic ground-air-ground flight spectrum.....	10
Figure2. 4 Schematic for constant amplitude cyclic loading.....	10
Figure2. 5 Bauschinger effect. <b>(a)</b> Tension loading. <b>(b)</b> Compression loading. <b>(c)</b> Tension loading followed by compression loading. ....	11
Figure2. 6 Stable cyclic stress-strain hysteresis loop[15].....	12
Figure2. 7 Construction of a cyclic stress-strain curve.[15].....	13
Figure2. 8 Concept of strain-life approach[23].....	15
Figure2. 9 Schematic of a total strain-life curve.[15].....	16
Figure2. 10 Mean stress relaxation under strain-controlled cycling with a mean strain.....	20
Figure2. 11 Mean stress effect on fatigue life of SAE 1045 hardened steel.....	21
Figure2. 12 A plate with a hole.....	25
Figure2. 13 Effect of a notch on the rotating bending $S-N$ behavior of an aluminum alloy, and comparisons with strength reductions using $K_t$ and $K_f$ [35].....	26
Figure2. 14 Notch sensitivity curves .....	27
Figure2. 15 Neuber constant curves for steel and T-series aluminum alloys .....	28
Figure2. 16 Local and nominal stresses and strains of a notched member[15] .....	29
Figure2. 17 Concentration factors variation with local (notch) stress .....	30
Figure2. 18 Determination of local stress and strain using Neuber's rule.....	32
Figure2. 19 Strain energy density method .....	35

Figure2. 20 Three modes of crack extension .....	37
Figure2. 21 SENB in bending .....	38
Figure2. 22 Fatigue crack length versus number of cycles to fracture .....	40
Figure2. 23 Fatigue crack growth rate, a schematic sigmoidal behavior.....	42
Figure2. 24 schematic mean stress effect on FCG .....	43
Figure2. 25 Standardized test specimens: (a) compact specimen, (b) disk-shaped compact specimen, (c) single-edge-notched bend SE(B) specimen, (d) middle tension (MT) specimen, and (e) arc-shaped specimen.[45] .....	45
Figure2. 26 Three-point bending apparatus for testing SE(B) specimens .....	46
Figure2. 27 Fatigue pre-cracking of a typical specimen, a fatigue crack is initiated at the notch tip through cyclic loading.....	46
Figure2. 28 Measurement of the crack-mouth-opening displacement with a clip gage. ....	47
Figure2. 29 Three types of load-displacement behavior in a $K_{Ic}$ test.....	49
Figure3. 1 Geometry and dimensions of SENB specimen drawn by SOLIDWORKS software. Dimensions are in [mm] .....	52
Figure3. 2 Schematic of specimen loading and boundary conditions.....	53
Figure3. 3 (a): 2-D half model created by Abaqus. (b): 3-D quarter model created by Abaqus.....	55
Figure3. 4 Loading and boundary conditions defined in Abaqus, (a): 2-D model, (b): 3-D model.....	55
Figure3. 5 Applied loading as a pressure load over a very small area. (a): 2-D model, (b): 3-D model.....	56
Figure3. 6 Support boundary condition. (a): 2-D model, (b): 3-D model.....	57
Figure3. 7 (a): x-symmetry boundary condition for 2-D model. (b) & (c): x-symmetry & z-symmetry BC for 3-D model .....	57
Figure3. 8 Meshing controls of specimen model in Abaqus. (a): 2-D model, (b): 3-D model.....	58
Figure3. 9 Meshing pattern of specimen model in Abaqus. (a): 2-D model, (b): 3-D model.....	59
Figure3. 10 Fine mesh around notch of specimen 2-D model in Abaqus.....	60
Figure3. 11 Fine mesh around notch tip of specimen 3-D model in Abaqus.....	60

Figure3. 12 Stress distribution around notch tip analyzed by Abaqus. (a): 2-D model, (b): 3-D model.....	61
Figure3. 13 Stress distribution extending from notch root to surface where the loading is applied. ....	61
Figure3. 14 (a) 3-D quarter model stress analysis with plane strain boundary condition. (b) stress distribution of notch tip through thickness of model .....	62
Figure3. 15 Determination of cyclic local stresses and strains and their ranges using Neuber's rule for material reference[47]. (a) & (b) using $K_t$ ; (c) & (d) using $K_{fneuber}$ ; (e) & (f) using $K_{fPeterson}$ . All by 2-D model result. And by 3-D model result: (g) & (h) using $K_{fneuber}$ ; (i) & (j) using $K_{fPeterson}$ .....	68
Figure3. 16 (a): Al 6082 T6 stress-strain plot[50] (b): Defined Amplitude in Abaqus for ten cycles.....	70
Figure3. 17 maximum and minimum local stresses after ten cycles. (a) and (b) for 2-D analysis and (c) and (d) for 3-D analysis .....	71
Figure3. 18 FCG life prediction using Walker equation for the initiated crack to grow from 1 [mm] length to 6.5 [mm] length. (a) Crack length versus Number of cycles; (b) $\Delta K$ versus Number of cycles; (c) $K_{max}$ versus Number of cycles .....	80
Figure 4. 1 (a): Gage resistance chart, (b): Specimen with bonded gages.....	83
Figure 4. 3 (a): DARTEC machine, (b): Fractured specimen.....	84
Figure 4. 5 Pilot test results as: (a) load-N, (b) displacement-N, (c) & (d) displacement-N & stiffness-N between 2000 cycles and 5500 cycles, and (e) crack propagation gage resistance-time. From (b), it can be seen that a small increase in displacement from 2000 cycles to 5500 cycles is due to crack growth. ....	85
Figure 4. 6 Photographs of specimen 1 with bonded gages.....	86
Figure 4. 7 Photographs of specimen 2 with bonded gages.....	86
Figure 4. 8 The testing setup with specimen.....	87
Figure 4. 9 After test photographs of specimen with residual stresses .....	88
Figure 4. 10 After test photographs of specimen without residual stresses.....	88
Figure 4. 11 Test one results. (a): maximum and minimum magnitudes of load versus N. (b): maximum and minimum values of displacement versus N. (c): crack length (acquired using krak gage) versus N. It should be noted that notch depth is included in crack length. ....	90
Figure 4. 12 Test two results. (a): maximum and minimum magnitudes of load versus N. (b): maximum and minimum values of displacement versus N. (c): crack length (acquired using krak gage) versus N. (d): crack length (acquired using crack propagation gage) versus N. ....	91

Figure 5. 1 Fatigue crack initiation and propagation life. (These are obtained by both numerical and experimental analyses for specimen without residual stresses.)  
(a): 0.1 mm assumed initiated crack length. (b): 1 mm assumed crack initiation length.....95

Figure 5. 2 Crack initiation and propagation life of specimens with and without residual stresses .....96

## LIST OF ABBRAVATIONS

HCF	high cycle fatigue
LCF	low cycle fatigue
FCG	fatigue crack growth
LEFM	linear elastic fracture mechanics
FEA	finite element analysis
ASTM	American Society for Testing Materials
CAD	computer aided design
SWT	Smith-Watson-Topper

## LIST OF SYMBOLS

$K_{max}$	maximum stress intensity
$K$	stress intensity factor
$K_a$	critical stress intensity for fast fracture at a given finite notch radius
$S$	nominal stress, Span length
$N$	number of cycles
$N_f$	number of cycles to failure
$a$	crack length
$R$	stress ratio
$e$	nominal strain
$\sigma$	local (notch) stress
$\varepsilon$	local (notch) strain
$P$	load
$\sigma_m$	mean stress
$\sigma_{max}$	maximum stress
$\sigma_{min}$	minimum stress
$\gamma$	Walker equation constant
$C$	Paris equation coefficient
$m$	Paris equation constant
$G$	energy release rate
$E$	modulus of elasticity
$\nu$	Poisson's ratio



# CHAPTER I

## INTRODUCTION

### 1.1 Introduction

To design a structure to prevent failure while subjected to static loading is straight forward, but in reality there are few components which are solely under static loading. So failure under cyclic loadings or in another words fatigue is a chief concern. Fatigue is a major mechanical failure phenomenon. Many books and papers point out that it causes 50 percent to 90 percent of all mechanical failures. Fatigue is mostly described in 3 stages: fatigue crack initiation, stable crack propagation and unstable crack propagation.[1][2][3]

There can be two points of view to look at this problem, one is to prevent a crack initiation in the component, the other is when crack is initiated, to detect it and prevent it from propagating unstably before catastrophic failure occurs. Many industries like ship, aircraft, nuclear and automotive industries major considerations is preventing components to initiate crack and this is usually achieved by over-conservative design.[1]

Generally there are geometrical discontinuities and notches in mechanical components and structures, for example in aircraft industries fuselages need holes for their assembly. When there are external forces, these discontinuities are places where stress concentration will be produced and changing the diameter of holes or discontinuities will change stress concentration value. These stresses are usually higher than the nominal stresses and could result in crack initiation if precautions like

machining of holes in high quality or induction of residual stresses are not taken into account in manufacturing these components. So it is very useful to study crack initiation in the vicinity of notches.[2]

While preventing crack initiation is one of the design concerns, knowledge of crack growth is also important. In real life many components contain cracks or very sharp crack-like notches. In these cases calculating the crack growth rate is useful to maintain operating stress limits and inspection intervals.[1]

## 1.2 Previous Investigations

Fatigue life prediction of structures with discontinuities has been extensively studied, Topper, Wetzel and Morrow used master plots of Neuber's rule vs life based on smooth specimen fatigue results to accurately predict fatigue of notched aluminum alloy plates subjected to completely reversed loading.[4]

Forman investigated crack initiation from flaws of changing radii (0.025 – 3.18 mm) in 7075-T6 aluminum. He used the ratio  $K_{max}/K_a$  to analyze the data where  $K_a$  depends on notch radius.[5]

In another research by Morrow, Lawrence and others, cyclic properties of material was defined at first. They used a finite element analysis to find the stresses at given notch configuration. Then by using a computer model and cycle by cycle damage summation they find the crack initiation life.[6]

Other researchers like Glinka used equivalent strain-energy density method in prediction of fatigue crack initiation.[7]

Buch, Vormwald and Seeger investigated the fatigue crack initiation time under the constant amplitude loading by the local stress-strain method and concluded that estimated accuracy mainly depended on the fatigue notch factor.[8]

Jiang applied a continuum mechanics approach for crack initiation and crack growth predictions, here a single fatigue damage criterion can model both stages. A rule is that any material point fails and form a fresh crack if the total accumulated fatigue damage reaches a limit.[9]

For the crack propagation phase, studies have been done as well. For example, Andraus and Baragatti studied the initiation and propagation of cracks in two different metal beams, one consist of 6082-T6 aluminum alloy and the other Fe430 steel. Their motivation for doing this, is to study the vibrations of cracked beams through the introduction of an actual fatigue crack instead of – as is usual – a narrow slot.[10]

Recently in the investigation of Ranganathan, he used short crack growth approach for consideration of crack initiation stage in estimation of total fatigue life.[11]

The research of Benachours, Hadjoui and Benguediab on fatigue crack initiation and propagation in 2024 T351 alloy plate specimen with double through cracks emanating from a hole show that crack initiation and propagation were dependent on specimen geometry and applied stresses, fatigue life is related to crack initiation and growth, crack initiation is related to applied mean stress, stress concentrations and material properties.[12]

Majid R. Ayatollahi et al. studied mixed mode fatigue crack initiation and growth in a CT specimen repaired by stop hole technique. They developed a numerical method which well predicts fatigue life extension of repaired specimens. In this study, the crack growth retardation and the location of fatigue crack initiation from stop-hole edge under different mode-mixities are examined. Different loading conditions were created by using a mixed-mode CT specimen made of Al\_6061-T651. The numerical results show that in the existence of stop holes the reduction in the stress concentration becomes larger for mode-II loading conditions.[13]

### 1.3 Motivation and the Scope of the Thesis

This thesis is motivated by the need for preparing several beam specimens containing sharp fatigue edge cracks, to be used in a (now concluded) TÜBİTAK project on vibrations of cracked beams [14]. Although such cracked beam specimens could be produced in an ad hoc manner through fatigue loading of beams with notches of arbitrary shape (such as a short saw cut or a saw cut terminating at a drilled hole) in three or four point bending configuration, initial trials show that such an effort is quite ineffective and a more methodical approach is required.

Such a systematic approach should lead to the determination of fatigue loading conditions and a suitable notch geometry, such that

- the specimen should not break due to unstable crack growth,
- the specimen should not undergo any appreciable (macroscopic) plastic deformation,
- A crack of desired depth could be grown in a reasonable time.

In order to measure fracture toughness of materials, fatigue pre-cracking is commonly employed. In other words fatigue cracks are produced ahead of sharp notches under controlled loading. Although the standards such as ASTM E399 and ASTM E1820 provide several recommendations to apply this procedure in a speedy and orderly fashion, a method to estimate the crack initiation life and the life for a certain amount of crack extension is not described.

Hence, in this thesis, both low cycle fatigue methods (strain life approach) and fracture mechanics methods (based on  $da/dN$  vs  $\Delta K$ ) are used to estimate the number of loading cycles required to have a crack of desired length ahead of a sharp notch. The recommendations (regarding notch geometry, loading configurations and load magnitudes) given in the above mentioned standards are not strictly followed but are taken as guidelines. Elastic and elasto-plastic finite element analyses were made using commercial finite element software ABAQUS® to obtain the required stress and strain concentration factors. A 1D stress analysis by using Neuber rule is

adopted in LCF calculations. The results are compared with actual experimental results, and the test and various analysis results are evaluated.

### **1.3.1 Thesis Objectives**

The main objectives of this thesis can be summarized as follows:

- To calculate the pre-cracking life of fracture toughness test specimen under constant amplitude loading
- To estimate the propagation life of an initiated crack to desired length
- And comparing the above results with experimental ones.

### **1.4 Thesis Structure**

The first chapter of thesis is an introduction to this whole study. The basic concepts of fatigue and life estimation theories are reviewed in chapter two. Next, modeling and life calculations of crack initiation and propagation phases are established in chapter three, then experimental procedure and results are presented in chapter four. Then the comparisons of numerical and experimental results are done in chapter five finishing with conclusion and future work.



## CHAPTER II

### LITERATURE REVIEW AND BACKGROUND

#### 2.1 Introduction and Historical Overview

There are many types of mechanical failures in engineering world, but the most common one is fatigue which is caused by repeated loading. Although the number of failures are very tiny compared to successes, the cost to lives and injuries and dollars are still high, so there is a need for proper fatigue design which includes modeling, analyses and testing. If fatigue designs, modelings and simulations can get close to reality then the confidence in engineering results will increase.[15]

Fatigue have been studied for nearly 160 years, the very first fatigue failure was detected in railways industry in 1840. It was reported that railroad axels failed regularly at shoulders.[16] The word fatigue was introduced in 1840s and 1850s to describe failure due to repeated stress. The first experiments was performed by August Wohler during 1850s and 1860s in Germany, the tests were concerned with railroad axel failures. He introduced the concept of S-N diagram and fatigue limit and figured out that for fatigue, the range of stress is more important than the maximum stress.[17]

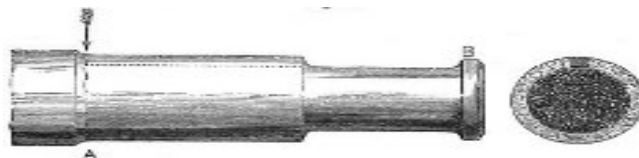


Figure2. 1 Drawing of a fatigue failure in an axle, sketched by Joseph Glynn following The Versailles accident, 1842[18]

## 2.2 Fatigue Design

There are similarities and differences in fatigue design methods, the differences have arisen from the facts that a component or structure may be

- safety important or safety unimportant
- expensive or inexpensive
- simple or complex
- produced for one end product or thousands or millions of products
- a modification or a new one

Adequate computer added engineering (CAE) and computer aided manufacturing (CAM) capabilities may or may not be available to the designers.

In all these above situations a common design flow chart can be produced as shown in figure 2.2.

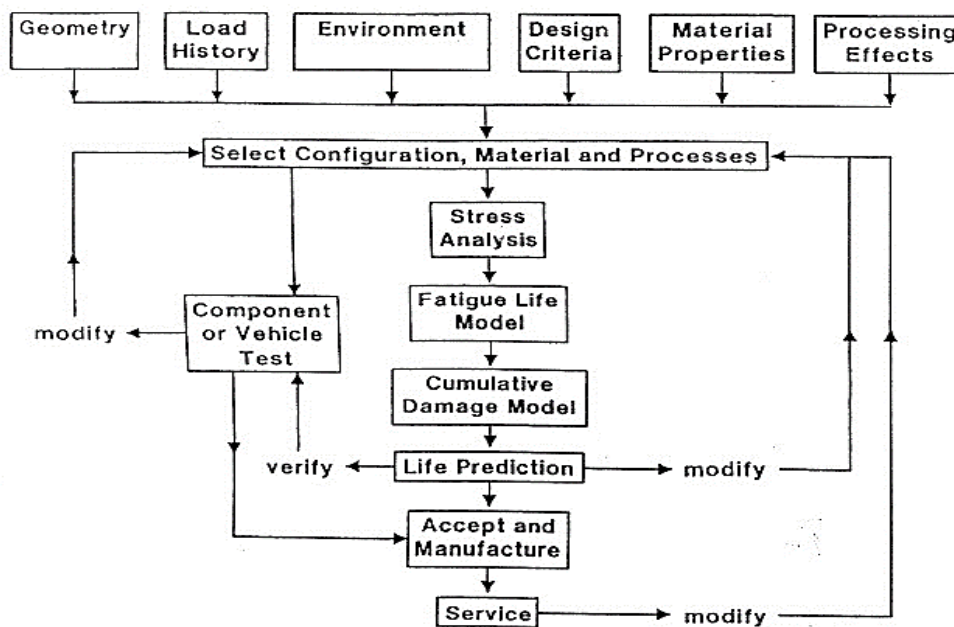


Figure 2.2 Fatigue design flow chart originated by H. S. Reemsnyder from Bethlehem Steel Corp. and slightly modified by H. O. Fuchs. It was created for use by the Society of Automotive Engineers Fatigue Design and Evaluation (SAEFDE) Committee University of Iowa's annual short course on Fatigue Concepts in Design.

Currently there are four fatigue life models, among which selecting the proper one is very important for design engineers:

- 1) The nominal stress-life ( $S-N$ ) model, first formulated between the 1850s and 1870s
- 2) The local strain-life ( $\epsilon-N$ ) model, first formulated in the 1960s.
- 3) The fatigue crack growth ( $da/dN-\Delta K$ ) model, first formulated in the 1960s.
- 4) The two-stage model, which is made of combining models 2 and 3 to join both macroscopic fatigue crack formation (nucleation) and fatigue crack propagation.

As mentioned above the stress-life model has been available for 160 years, while the other methods have been existed since 1960s.

In the  $S-N$  model, the estimation of fatigue life is done by using nominal stresses and relating them to local fatigue strengths in notched and un-notched members. The strain-life method is used directly for local strains and stresses at a notch and several methods are available for determining these local stresses or strains from nominal ones. The fatigue crack growth model uses fracture mechanics concepts and is used to estimate number of cycles required to grow a crack from an existed length to a final length and/or to fracture. The two stage method deals with a crack nucleation life prediction and crack growth life estimation and then adding these two to get a total fatigue life.[15]

### **2.3 Fatigue Loading**

Components and structures in real life are subjected to various loadings. In some cases the loading histories are simple and repetitive and in some others are complex and random, an example of a complex and random one is ground-air-ground cycle of an aircraft shown in Figure 2.3. This figure shows a variable amplitude loading cycle.

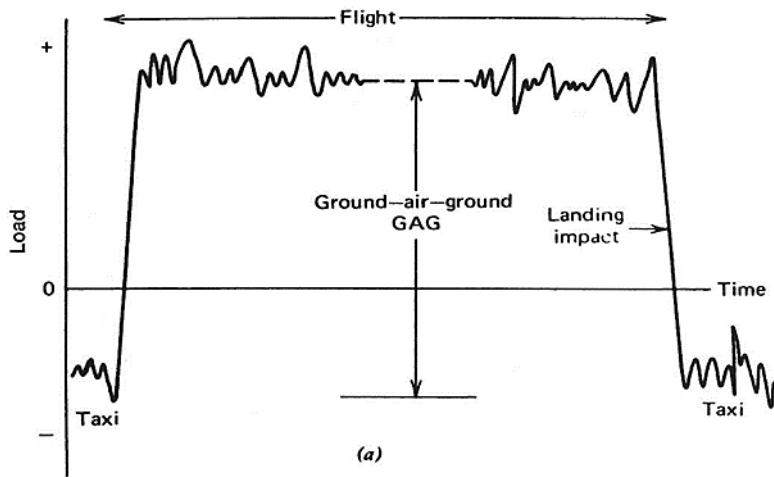


Figure2. 3 Schematic ground-air-ground flight spectrum.

Some of real life loading histories can be modeled as constant amplitude which can also be used to determine the material properties for fatigue design. Stress parameters to characterize constant amplitude cyclic loading are defined below, also a schematic of this loading is shown in figure 2.4.

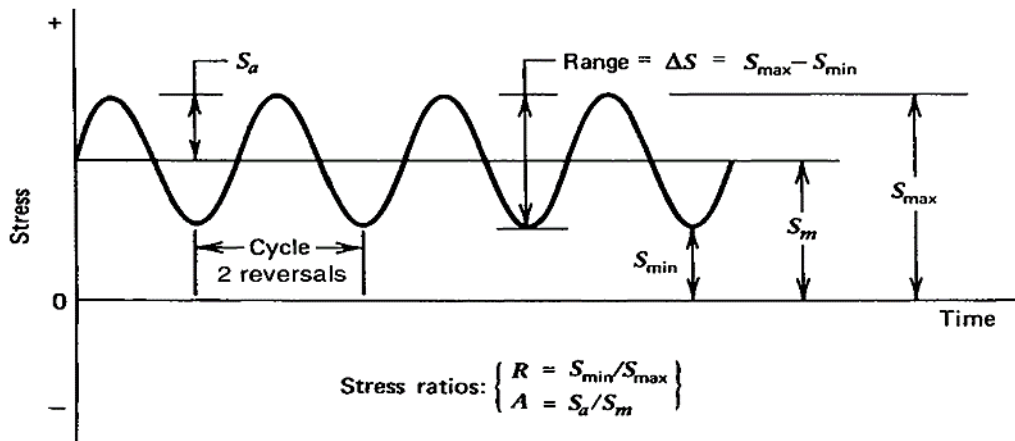


Figure2. 4 Schematic for constant amplitude cyclic loading

$$\text{Stress range: } \Delta S = S_{max} - S_{min} \quad (2.1)$$

$$\text{Stress amplitude: } S_a = \frac{\Delta S}{2} = \frac{S_{max} - S_{min}}{2} \quad (2.2)$$

$$\text{Mean stress: } S_m = \frac{S_{max} + S_{min}}{2} \quad (2.3)$$

$$\text{Stress ratio: } R = \frac{S_{min}}{S_{max}} \quad (2.4)$$

In above equations tensile stresses are taken as positive values and compressive stresses are taken as negative values.  $R=0$  and  $R=-1$  are two common conditions for testing materials to obtain fatigue properties,  $R=-1$  is called fully reversed condition in which  $S_{min} = -S_{max}$ .  $R=0$  (i.e.  $S_{min} = 0$ ) condition is called pulsating tension or released tension. In constant amplitude loading, one cycle is equal to two reversals (in variable amplitude loading, reversals are used). In Figure 2.4 loads also can be used instead of stresses.[15]

## 2.4 Steady State Cyclic Stress-Strain Relation

Bauschinger[19] during the late nineteenth century observed that the stress-strain behavior of a material obtained from a monotonic tension or compression test can be different from the one that is obtained under cyclic loading. In his experiments it was seen that the yield strength of material was reduced after applying an opposite sign load that caused inelastic deformation. In Figure 2.5 it can be seen that the yielding in tension causes a reduction in yield strength in compression. So, the stress-strain behavior of metals can be changed by a single reversal of an inelastic strain.

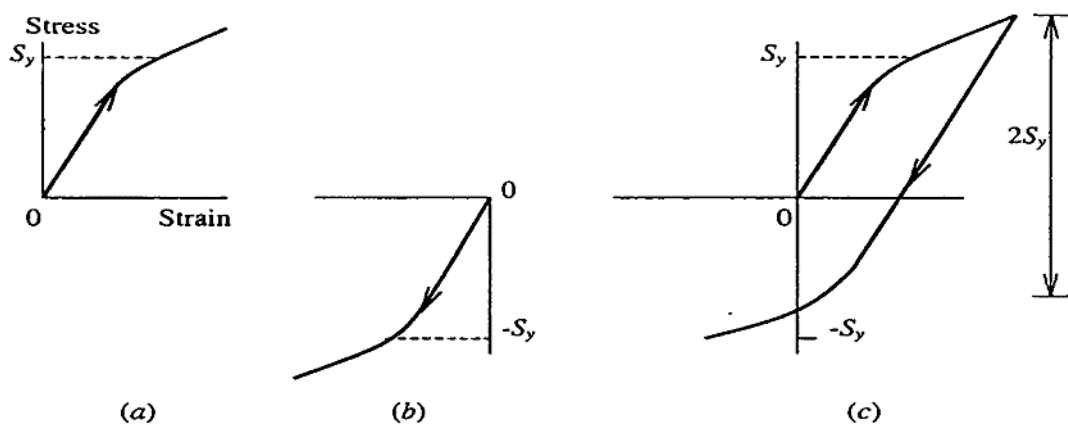


Figure2. 5 Bauschinger effect. (a) Tension loading. (b) Compression loading. (c) Tension loading followed by compression loading.

For most metals in the initial cycles of constant strain-amplitude controlled tests, the stress-strain relation gets stable after rapid softening or hardening (cyclic hardening and softening indicates increased and decreased resistance to deformation, respectively), so fatigue life can be characterized by steady-state behavior. A material cyclically stable stress-strain response which is named as the hysteresis loop is shown in Figure 2.6.

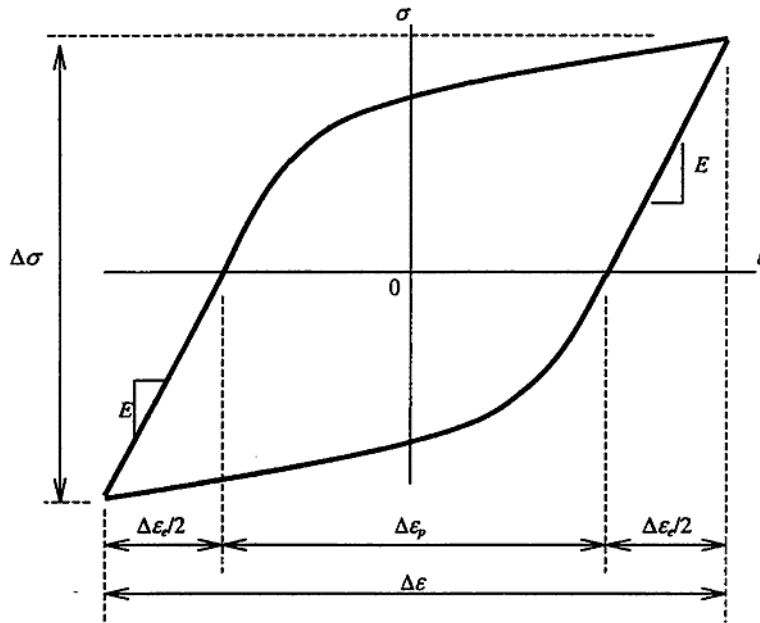


Figure2. 6 Stable cyclic stress-strain hysteresis loop[15]

The elastic work plus plastic work on a material under loading and unloading equals the inside of the hysteresis loop which is defined by the total strain range ( $\Delta\varepsilon$ ) and total stress range ( $\Delta\sigma$ ). The hysteresis loop usually is taken at half of the total fatigue life. The summation of elastic strain component and plastic one ( $\Delta\varepsilon^e$ ,  $\Delta\varepsilon^p$ ) gives the total strain range, which is expressed as follows:[20]

$$\Delta\varepsilon = \Delta\varepsilon^e + \Delta\varepsilon^p = \frac{\Delta\sigma}{E} + \Delta\varepsilon^p \quad (2.5)$$

Where

$E$  = modulus of elasticity

From the hysteresis loops taken from a series of various strain amplitude tests and by plotting the locus of the loop tips on the same  $\sigma$ - $\epsilon$  coordinates one can construct a cyclic stress-strain curve as shown in Figure 2.7 which can be represented by the well-known Ramberg-Osgood equation:

$$\epsilon = \epsilon^e + \epsilon^p = \frac{\sigma}{E} + \left(\frac{\sigma}{K'}\right)^{1/n'} \quad (2.6)$$

Where

$K'$  = the cyclic strength coefficient

$n'$  = the cyclic strain hardening exponent

' (superscript) = the parameters associated with "cyclic behavior" to differentiate them from monotonic behavior parameters

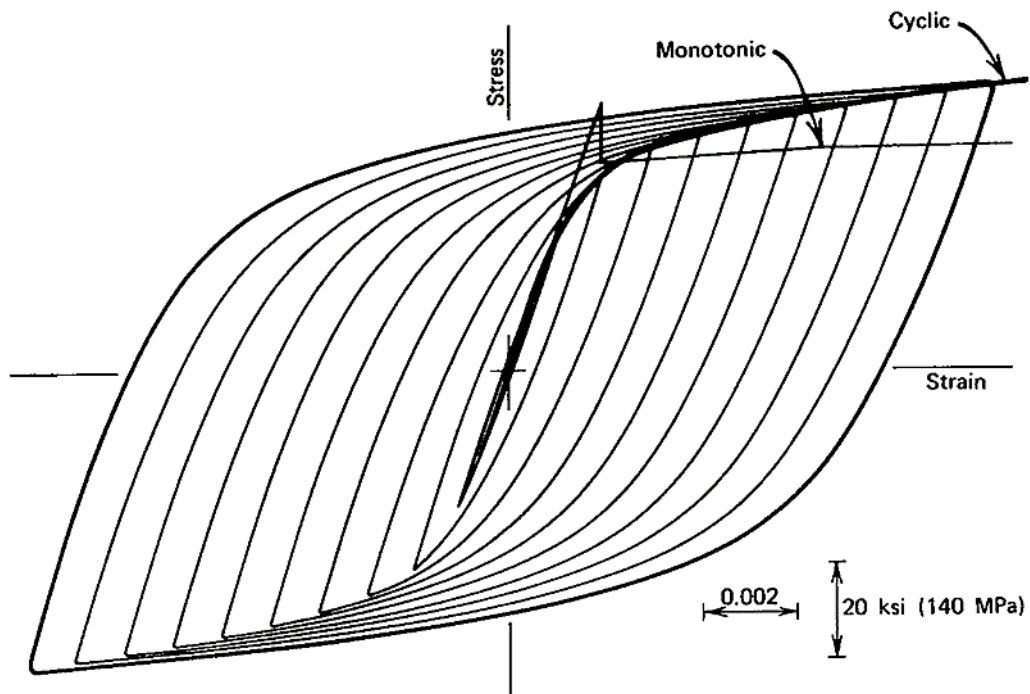


Figure2. 7 Construction of a cyclic stress-strain curve.[15]

There is proposition by Masing[21] which states that the stress amplitude versus strain amplitude curve can also be represented by the expression for cyclic stress-strain curve, this assumption is valid for homogeneous materials:

$$\varepsilon_a = \varepsilon_a^e + \varepsilon_a^p = \frac{\sigma_a}{E} + \left(\frac{\sigma_a}{K'}\right)^{1/n'} \quad (2.7)$$

Where,  $\varepsilon_a^e$  and  $\varepsilon_a^p$  = the elastic and plastic strain amplitudes, respectively.

In terms of strain range ( $\Delta\varepsilon$ ) and stress range ( $\Delta\sigma$ ), the above equation can be rewritten as follows:

$$\frac{\Delta\sigma}{2} = \frac{\Delta\varepsilon^e}{2} + \frac{\Delta\varepsilon^p}{2} = \frac{\Delta\sigma}{2E} + \left(\frac{\Delta\sigma}{2K'}\right)^{1/n'} \quad (2.8)$$

or in a reduced form as follows:

$$\Delta\varepsilon = \frac{\Delta\sigma}{E} + 2\left(\frac{\Delta\sigma}{2K'}\right)^{1/n'} \quad (2.9)$$

## 2.5 Fatigue Life

As mentioned before, there are three stages in fatigue failure process. First phase is the crack initiation, and then crack propagation phase up to a critical size and finally unstable fast crack growth to fracture is the last phase. Stress life ( $S-N$ ) approach is one of the traditional models that put these three stages together and predicts the fatigue life. ( $S-N$ ) approach has a great support of large database and analytical/empirical procedures which have been developed till now. In recent years there is an intense development in considering life prediction of each phase separately by using fracture-mechanics (F-M) approach.[22]

Moreover, in accordance with induced cyclic strains, two cyclic loading domains are identified. If loadings are relatively low then the induced cyclic strains are mostly in the elastic range and a high number of cycles or long lives are reached. This domain is referred to as high-cycle fatigue (HCF). On the other hand, when cyclic loadings are relatively high, during each cycle there are important levels of induced plastic strains. Consequently number of cycles to failure is low and lives are short. This domain is named as low-cycle fatigue (LCF).[22]

Due to low induced plastic strains in high cycle fatigue domain, the stress life ( $S-N$ ) approach is applicable to predict life in this domain, but in low cycle fatigue in accordance with the presence of high levels of plastic strains the stress life method is not suitable. So to predict fatigue life in low cycle fatigue domain, the strain-life ( $\epsilon-N$ ) approach is applicable which will be discussed in next section.

## 2.6 Strain-Life ( $\epsilon-N$ ) Approach

Nowadays strain-based approach to fatigue problems is widely used because strain can be measured and is a good quantity dealing with low-cycle fatigue problems. Notched member fatigue is the most common use of this approach.

The strain-life design method is based on the assumption that the crack initiation life of a notched component is equal to that of a smooth laboratory specimen under the same cyclic strains as the material at the notch root. This concept is shown in Figure 2.8.

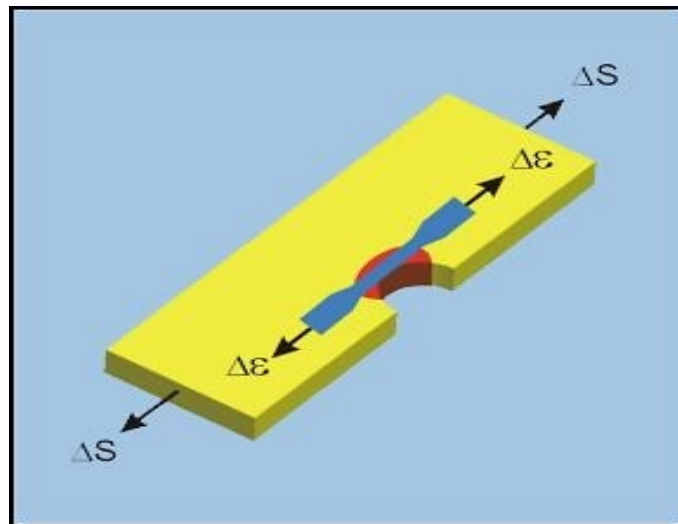


Figure2. 8 Concept of strain-life approach[23]

With the help of this concept, it is possible to calculate the fatigue crack initiation life of a component under cyclic loading, if the strain-time history at the notched root and strain-life fatigue properties of smooth specimen is known. Then using fracture

mechanics concepts it is straight forward to determine the remaining fatigue crack growth life of the component. The strain-based approach is also called local strain approach because fatigue damage calculations are done with direct assessing of local strains.

During most of fatigue life hysteresis loops can predominate and can be reduced elastic strain ranges/amplitudes and plastic ones. Number of cycles to failure can be between 10 and  $10^6$ . The strain life fatigue is also called low cycle fatigue since most life cycles are fewer than about  $10^5$ .

Strain-life fatigue curves illustrated in Figure 2.9 are plotted on log-log scales. In this figure  $N_f$  is the number of cycles to failure and  $2N_f$  is the number of reversals to failure. One of the failure criteria for strain-life curves may be the life to a small detectable crack.

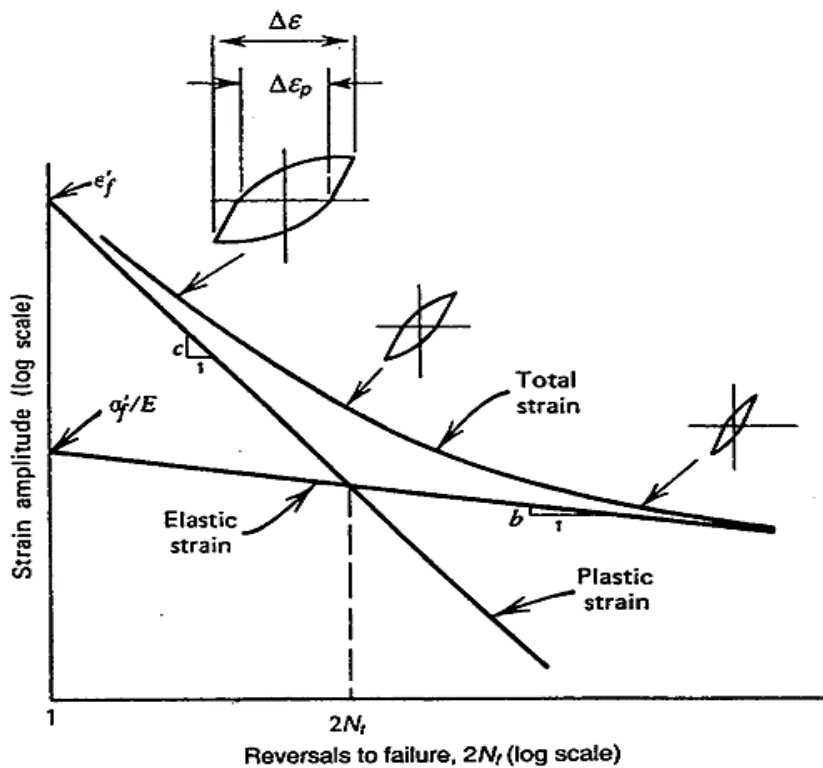


Figure 2.9 Schematic of a total strain-life curve.[15]

From Figure 2.9 it can be seen that the total strain amplitude has been split into elastic and plastic strain components from the steady-state hysteresis loops. It is possible to

approximate both the elastic and plastic curves as straight lines. By summing elastic and plastic strains at a given life ( $N_f$ ), the total strain can be calculated. The plastic strain component is predominant at large strains and short lives (LCF), and the elastic strain component is predominant at small strains and long lives (HCF). From figure 2.9,  $\sigma'_f/E$  and  $\varepsilon'_f$  are the intercepts of the two straight lines at  $2N_f = 1$  for the elastic component and plastic component, respectively.  $b$  and  $c$  are the slopes of the elastic and plastic lines, respectively. Now the equation for strain-life data of small smooth axial specimens can be expressed as:

$$\frac{\Delta\varepsilon}{2} = \varepsilon_a = \frac{\Delta\varepsilon_e}{2} + \frac{\Delta\varepsilon_p}{2} = \frac{\sigma'_f}{E} (2N_f)^b + \varepsilon'_f (2N_f)^c \quad (2.10)$$

Where

$$\frac{\Delta\varepsilon}{2} = \text{total strain amplitude} = \varepsilon_a$$

$$\frac{\Delta\varepsilon_e}{2} = \text{elastic strain amplitude} = \frac{\Delta\sigma}{2E} = \frac{\sigma_a}{E}$$

$$\frac{\Delta\varepsilon_p}{2} = \text{plastic strain amplitude} = \frac{\Delta\varepsilon}{2} - \frac{\Delta\varepsilon_e}{2}$$

$$\varepsilon'_f = \text{fatigue ductility coefficient}$$

$$c = \text{fatigue ductility exponent}$$

$$\sigma'_f = \text{fatigue strength coefficient}$$

$$b = \text{fatigue strength exponent}$$

$$E = \text{modulus of elasticity}$$

$$\frac{\Delta\sigma}{2} = \text{stress amplitude} = \sigma_a$$

The above equation is called the strain-life equation for the zero mean stress situation. Solving this equation for  $N_f$  for a given strain amplitude needs iteration technique or numerical/graphical solutions.

The first part of the Eq. (2.10) which relates life to elastic strain is Basquin's equation[24] as follows:

$$\frac{\Delta\sigma}{2} = \sigma_a = \sigma_f'(2N_f)^b \quad (2.11)$$

And the second part of the Eq. (2.10) is the Manson-Coffin equation[25], [26] which relates life to plastic strain and is expressed as:

$$\frac{\Delta\varepsilon_p}{2} = \varepsilon_f'(2N_f)^c \quad (2.12)$$

The intersection of elastic and plastic strain-life curves is called the transition fatigue life. This life occurs when the elastic and plastic components of strains are equal and is expressed as:

$$2N_t = \left( \frac{\varepsilon_f' E}{\sigma_f'} \right)^{\frac{1}{b-c}} \quad (2.13)$$

The lives less than the transition fatigue life are in the LCF regime where the strains are mainly plastic and the lives larger than  $(2N_t)$  are in the HCF regime where the strains are mainly elastic.

As a conclusion for strain-life testing of un-notched smooth specimens concerning failure criteria is that the fatigue crack length of 0.25 to 5 mm means the life to failure but this range is large so the length of 1 mm fatigue crack can be referred as life to failure.[15]

The strain-based approach covers both LCF and HCF regimes and can be applied for each. In long-life cases where small plastic strains may exist this approach can be used by neglecting the plastic strain term in Eq. (2.10) and in this way the strain-life equation reduces to Basquin's Eq. (2.11).[15]

## 2.7 Estimate of strain-Life fatigue Properties

When there is no data of experimental strain-life fatigue, it is possible to estimate cyclic and fatigue behavior of a material. Using a log-log scale, the intercept and slope of the linear least squares fit to stress amplitude,  $\Delta\sigma/2$ , versus reversals to failure,  $2N_f$ , are the fatigue strength coefficient,  $\sigma'_f$ , and the fatigue strength exponent,  $b$ . Then there should be stress-number of cycles data.

And similar to above estimation, using a log-log scale, the intercept and slope of the linear least squares fit to plastic strain amplitude,  $\Delta\varepsilon_p/2$ , versus reversals to failure,  $2N_f$ , are the fatigue ductility coefficient,  $\varepsilon'_f$ , and the fatigue ductility exponent,  $c$ . determining plastic strain amplitude can be done in two ways, one is to measure it directly from half of the width of stable hysteresis loops at  $\sigma = 0$  and the other more conveniently used is to calculate using following equation:[15]

$$\frac{\Delta\varepsilon_p}{2} = \frac{\Delta\varepsilon}{2} - \frac{\Delta\sigma}{2E} \quad (2.14)$$

Fatigue life is dependent upon the applied strain amplitude and cannot be controlled. Thus, the independent variable treatment of stress and plastic strain amplitudes and dependent variable treatment of fatigue life is needed while fitting the data to determine the four strain-life properties.

To obtain the cyclic strength coefficient,  $K'$ , and the cyclic strain hardening exponent,  $n'$ , the stable stress amplitude versus plastic strain amplitude data are fitted. By using the low-cycle fatigue properties  $K'$  and  $n'$  can be roughly estimated using following equations which are derived from compatibility of strain-life equations:

$$K' = \frac{\sigma'_f}{(\varepsilon'_f)^{\frac{b}{c}}} \quad \text{and} \quad n' = \frac{b}{c} \quad (2.15)$$

In most cases the ranges of fatigue properties are as:

$b$  from about -0.06 to -0.14

$c$  from about -0.4 to -0.7

There is a review and evaluation for existing estimation techniques for cyclic and fatigue properties by Lee and Song[27]. In this review they reach to a conclusion that for a given ultimate tensile strength, the medians method by Meggiolaro & Castro[28] is recommended for aluminum alloys. And also in this review they evaluated most of the models proposed to estimate ultimate tensile strength from hardness and figure out that for both steel and aluminum alloys the Mitchell's equation[29] gives the best results which is expressed as:

$$S_{t,u}(\text{MPa}) = 3.45\text{HB} \quad (2.16)$$

## 2.8 Mean Stress Effects

The discussed fatigue behavior and cyclic strain controlled deformation in previous sections were all in fully reversed condition,  $= \frac{\sigma_{min}}{\sigma_{max}} = -1 = \frac{\epsilon_{min}}{\epsilon_{max}}$ . But in many applications a mean strain\stress effect may exist. There can be a full or partial relaxation of mean stress as shown in Figure 2.10, usually caused by strain controlled cycling with mean strain. Plastic deformation presence is the cause to this relaxation so the rate of it depends on the magnitude of plastic strain amplitude, this means that if the strain amplitude is large, the means stress relaxation is more.[15]

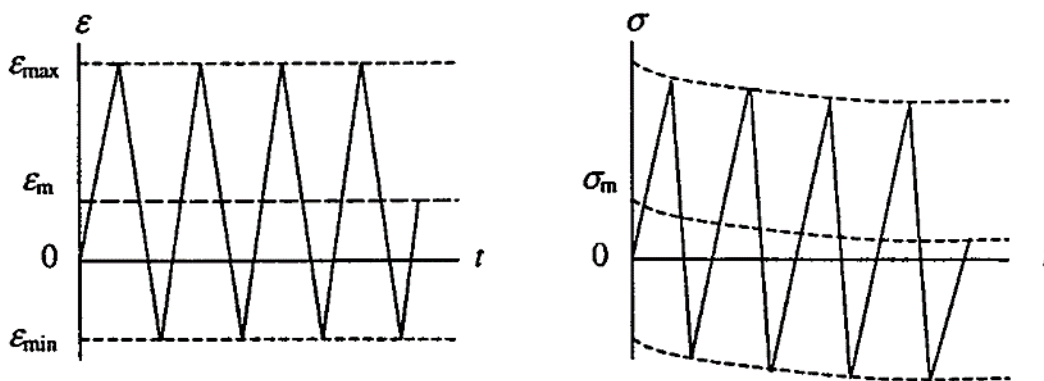


Figure2. 10 Mean stress relaxation under strain-controlled cycling with a mean strain

Mean strain has influence on fatigue behavior when it results in a non-fully relaxed mean stress. In low cycle fatigue region there is more stress relaxation due to large plastic strains at higher strain amplitudes, so mean stress has a smaller effect on fatigue life in low cycle fatigue region than it has in high cycle fatigue region. This behavior for SAE 1045 hardened steel is shown in Figure 2.11.[15]

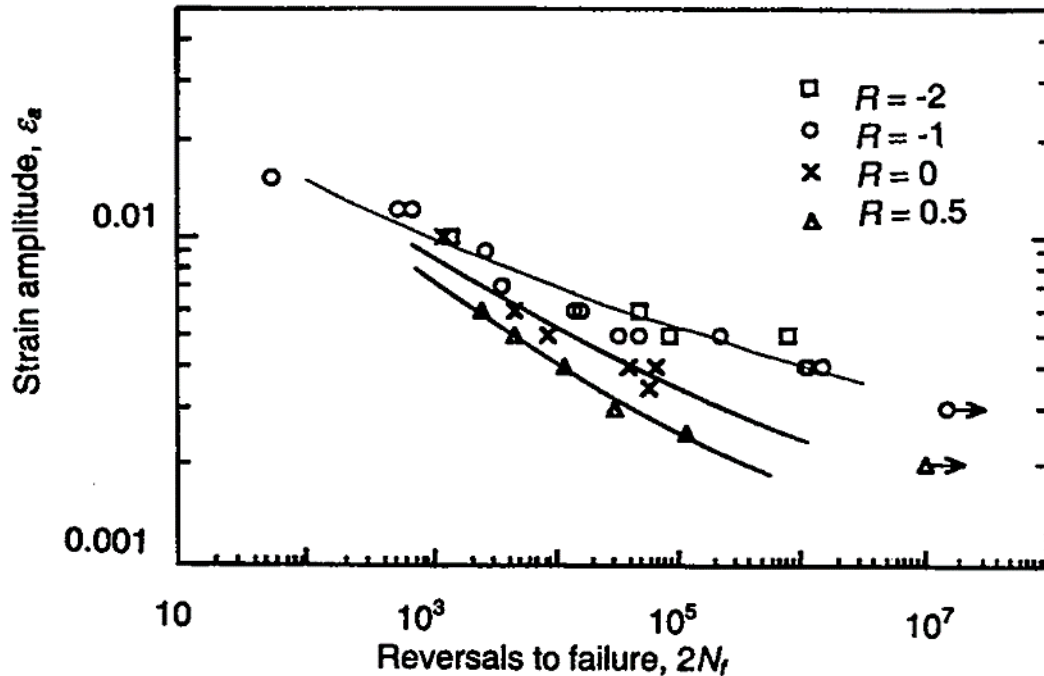


Figure2. 11 Mean stress effect on fatigue life of SAE 1045 hardened steel

To quantify the mean stress effect on fatigue behavior, several mean stress correction models are available dealing with the local strain-life approach. Next, some of them are introduced.

### 2.8.1 Modified Morrow Approach

The original mean stress correction model was presented by Morrow[30] in 1968. Since mean stress is negligible in LCF regime (where the plastic strain has large values) and has a noticeable effect in HCF regime (where the plastic strain has low values), the modified Morrow equation is expressed as:

$$\frac{\Delta\varepsilon}{2} = \varepsilon_a = \frac{\sigma'_f - \sigma_m}{E} (2N_f)^b + \varepsilon'_f (2N_f)^c \quad (2.17)$$

Where

$\sigma_m$  = the mean stress

In equation above for tensile and compressive values,  $\sigma_m$  is taken as positive and negative respectively. From this equation it is predicted that compressive mean stresses are beneficial, and tensile mean stresses are detrimental to fatigue life. More mean stress effect at long lives is predicted using Eq. (2.17) as also can be concluded from Figure 2.11 which is an experimental figure. This equation incorrectly predicts the dependency of elastic to plastic strain ratio on mean stress which is not true since the shape of the stress-strain hysteresis loop is not dependent on the mean stress. The extensive usage of this equation has been for steels and had more success in HCF regime.

### 2.8.2 Manson-Halford Model

An alternative version of Morrow's Mean stress correction model for fatigue life is given by Manson and Halford [31]. In this model to maintain the independence of the elastic-plastic strain ratio from mean stress, they include mean stress parameter in both the elastic and plastic terms of strain-life equation expressed as:

$$\frac{\Delta\varepsilon}{2} = \varepsilon_a = \frac{\sigma'_f - \sigma_m}{E} (2N_f)^b + \varepsilon'_f \left( \frac{\sigma'_f - \sigma_m}{\sigma'_f} \right)^{c/b} (2N_f)^c \quad (2.18)$$

This equation exaggerates mean stress effect at short lives where domination of plastic strains exists and mean stress relaxation occurs.

### 2.8.3 Smith, Watson, and Topper (SWT) Parameter

Another mean stress correction model for strain-based fatigue life is suggested by Smith, Watson, and Topper[32] which is based on strain-life test data with various mean stresses. This model is expressed as:

$$\sigma_{max}\varepsilon_a = \frac{(\sigma'_f)^2}{E} (2N_f)^{2b} + \sigma'_f \varepsilon'_f (2N_f)^{b+c} \quad (2.19)$$

Where

$$\sigma_{max} = \sigma_m + \sigma_a > 0$$

The assumption that for a given life, the product  $\sigma_{max}\sigma_a$  remains constant for different combinations of strain amplitude,  $\varepsilon_a$ , and mean stress,  $\sigma_m$ , is the basis of the SWT equation. Fatigue damage becomes zero and infinite life prediction occurs if the  $\sigma_{max}$  becomes zero or negative (compressive maximum stress), so tension must exist in order to have fatigue fractures. The SWT results are acceptable for a wide range of materials. For steels it is as accurate as Morrow model, and for aluminum alloys it is fairly good. The SWT equation has been successfully applied to precipitation-hardened aluminum alloys in the 2000 and 7000 series by Dowling[33]

### 2.8.4 Walker Mean Stress Equation

The walker Mean stress equation is expressed as[34]:

$$\frac{\Delta\varepsilon}{2} = \varepsilon_a = \frac{\sigma'_f}{E} \left(\frac{1-R}{2}\right)^{(1-\gamma)} (2N_f)^b + \varepsilon'_f \left(\frac{1-R}{2}\right)^{c(1-\gamma)/b} (2N_f)^c \quad (2.20)$$

Where

$\gamma$  = Walker constant

$$R = \frac{\sigma_{min}}{\sigma_{max}}$$

In a case that  $\gamma$  is known, among all the mean stress correction models that discussed, the accuracy of Walker mean stress equation is probably the highest.

## 2.9 Material Response at Notch Tip

One of the key points in fatigue studies is the effect of notches and these have been under consideration for more than 140 years. These geometrical discontinuities exist in most of components and machines like welds on plates, rivet holes in sheets and keyways on shafts. To reduce harmful notch effects, some suitable treatments should be considered.[15]

### 2.9.1 Elastic Stress Concentration Factor

Concentration of stresses and strains occur at notches and as long as  $\sigma/\varepsilon=\text{constant}=E$ , this concentration is characterized by  $K_t$ , and defined as:

$$K_t = \frac{\sigma}{S} = \frac{\varepsilon}{e} \quad (2.21)$$

Where

$\sigma$  and  $\varepsilon$  = local stress and strain at notch

$S$  and  $e$  = nominal stress and strain

Figure 2.12 shows a plate with a hole. The nominal stress is defined as load divided by net area. Net area is the area without considering the notch (the hole in figure 2.12).

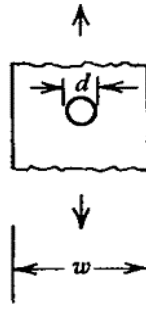


Figure2. 12 A plate with a hole

Some of the ways of obtaining elastic stress concentration factors are mentioned below:

- Theory of elasticity
- Numerical solutions
- Experimental measurements (e.g. photoelasticity and strain gages)

Using numerical solution, the most common and widely used method is finite element method (FEM). A fine mesh around the notch tip is required to have accurate results.

### 2.9.2 The Fatigue Notch Factor $K_f$

Figure 2.13 shows stress-life (S-N) curve of an un-notched and notched specimen, it can be seen that existence of the notches reduces the stress amplitude for a given life, and this reduction should be done by the factor  $K_t$ , but as it can be seen, the actual experimental data lies above estimation done by  $K_t$  factor and this means that the notch has less effect than expected. So, the actual reduction especially for long lives ( $N_f \geq 10^6$ ) is characterized by factor  $K_f$  and it is called fatigue notch factor.  $K_f$  is expressed as below:

$$K_f = \frac{\text{Smooth fatigue strength}}{\text{Notched fatigue strength}} \leq K_t \quad (2.22)$$

As a base  $K_f$  is estimated for zero mean stress cases.

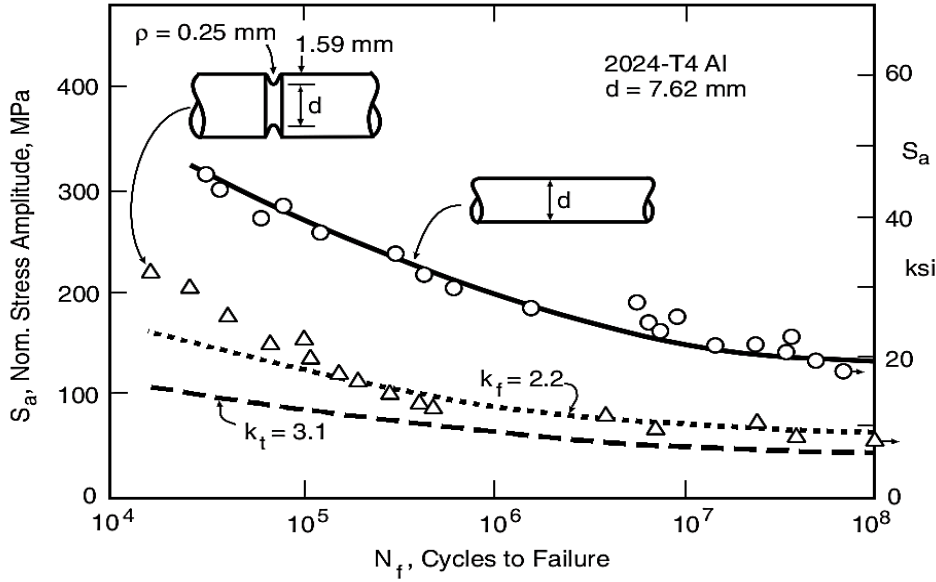


Figure 2.13 Effect of a notch on the rotating bending  $S-N$  behavior of an aluminum alloy, and comparisons with strength reductions using  $K_t$  and  $K_f$ [35]

For large radius of notch tip  $\rho$ , the  $K_f$  value will be equal to  $K_t$  value, but for small notch radius (lower  $K_f$  and longer fatigue initiation life and less damage) the difference will be large. The cause of this difference can be explained through the local yielding behavior or the stress field intensity theory.[36][37][38] The yielding at the notch root caused by cyclic behavior reduces the notch root stress, particularly at shorter lives. This explanation is suggested by the local yielding theory, and the stress field intensity theory assumes that an average stress acting over a finite volume of the material at the notch root controls the fatigue life instead of maximum stress on the surface of the notch root which is calculated using  $K_t$ . This average stress is lower than the maximum surface stress.[15]

### 2.9.3 Notch Sensitivity Factor $q$ and Empirical estimations for $K_f$

Notch sensitivity,  $q$ , can be expressed as:

$$q = \frac{k_f - 1}{k_t - 1} \quad (2.23)$$

The values for  $q$  are between 0 ( $K_f = 1$ , no notch effect) and 1 ( $K_f = 0$ , full notch effect). Peterson[39] suggested an estimated formulation for  $q$  as:

$$q = \frac{1}{1 + \frac{\alpha}{\rho}} \quad (2.24)$$

Where

$\alpha$  = material constant in length dimensions

$\rho$  = radius at the notch root

Figure 2.14 which is also provided by Peterson shows variation of  $q$  with notch radius and material. From this figure a typical value for aluminum alloys can be reached as:

$$\alpha = 0.51 \text{ mm} \quad (\text{aluminum alloys}) \quad (2.25)$$

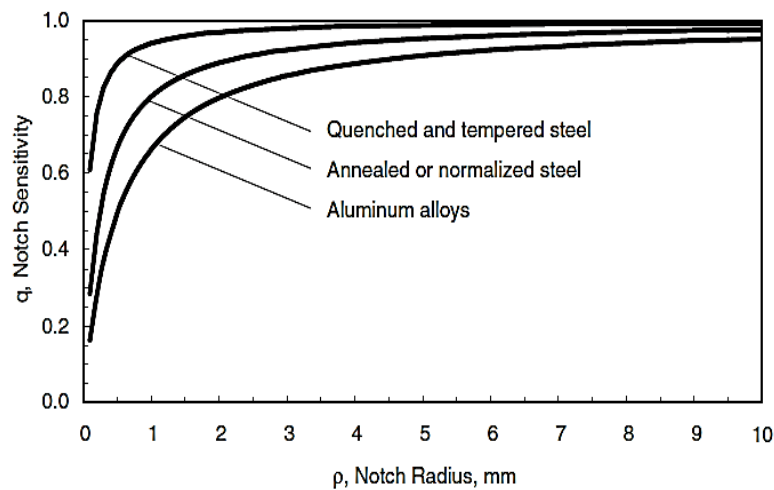


Figure2. 14 Notch sensitivity curves

Combining Equation (2.23) with Equation (2.24) gives a formula to calculate  $K_f$  directly from  $\alpha$ , as:

$$K_f = 1 + \frac{K_t - 1}{1 + \frac{\alpha}{\rho}} \quad (2.26)$$

Another empirical relationship for  $q$  and  $K_f$  is suggested by Neuber:

$$q = \frac{1}{1 + \sqrt{\frac{\beta}{\rho}}} \quad (2.27)$$

$$K_f = 1 + \frac{K_t - 1}{1 + \sqrt{\frac{\beta}{\rho}}} \quad (2.28)$$

Where

$\beta$  = Neuber's material constant

Figure 2.15 shows typical values of  $\beta$  for steels and heat treated aluminum alloys developed by Kuhn. An expression for  $\beta$  by fitting the curve for aluminum one is as follow[34]:

$$\log\beta = -9.402 \times 10^{-9}\sigma_u^3 + 1.422 \times 10^{-5}\sigma_u^2 - 8.249 \times 10^{-3}\sigma_u + 1.451 \quad (2.29)$$

$$\beta, \text{ mm} = 10^{\log\beta} \quad (2.30)$$

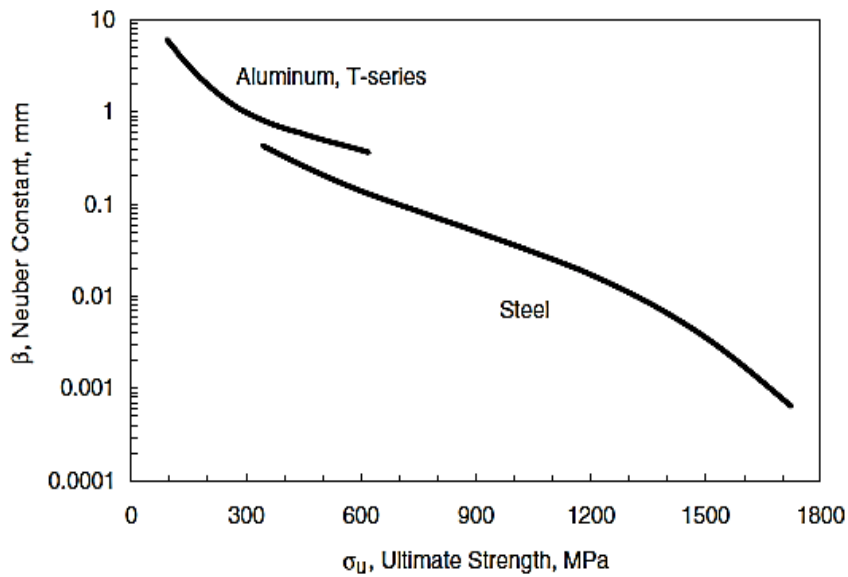


Figure2. 15 Neuber constant curves for steel and T-series aluminum alloys

## 2.9.4 Strain Life Approach in Notched Members

Strain life approach is commonly used in fatigue of notched members, since the deformation in notch root is usually not elastic. In strain-life approach stresses and strains at notch root are employed but in stress-life approach, it is the nominal stresses that have the main role. To use strain-life approach in notched members, two tasks need to be done, first one is to determine local stresses and strains at the notch root and the second one is using these stresses and strains in strain-life equation discussed in previous sections. To obtain the local stress and strains, three ways is discussed in following sections.[15]

For notched members, local stresses and strains and nominal stresses and strains are shown in Figure 2.16.

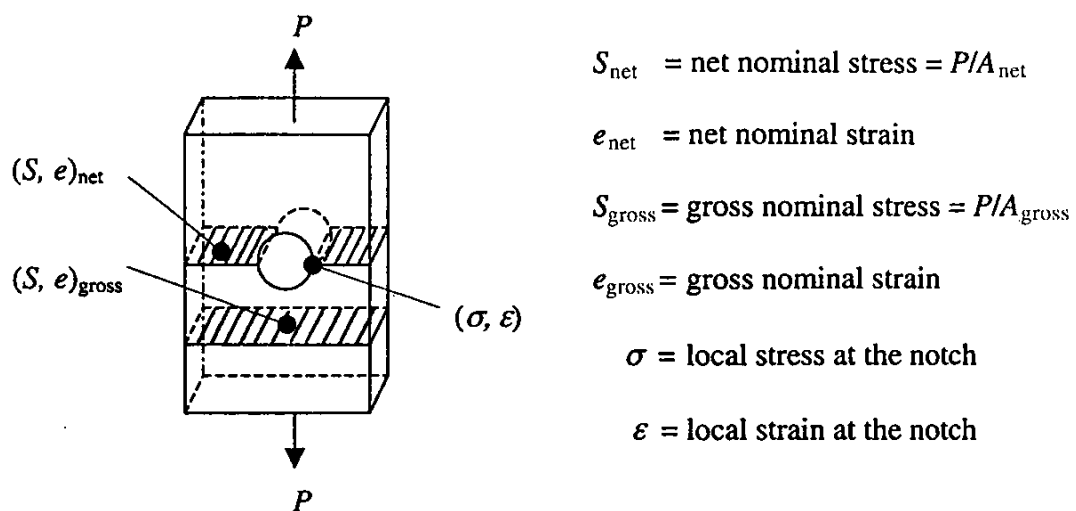


Figure 2. 16 Local and nominal stresses and strains of a notched member[15]

In this thesis net cross-sectional area is used for nominal stress and strain.

For stresses and strains in elastic range following expressions are valid:

$$\sigma = K_t S \quad \epsilon = K_t e \quad (2.31)$$

Commonly local stresses induced by sufficiently high loads are higher than the yield strength and their value will be less than local stress calculated with  $K_t S$ , thus,

relating local stress to nominal stress with  $K_t$  is no longer applicable; and also there is no proportionality between strains and stresses. In this situation, defining stress and strain concentration factors is useful:

$$K_\sigma = \frac{\sigma}{S} \quad (2.32)$$

$$K_\epsilon = \frac{\epsilon}{e} \quad (2.33)$$

In Figure 2.17 variation of strain and stress concentration factors with local stress is schematically shown. From figure it is obvious that when local stress is less than yielding stress, material behaves elastically, strains and stresses are proportional to each other with modulus of elasticity constant  $E$ . With increasing local stress above yielding strength, plastic deformations, reduction of  $K_\sigma$ , increasing of  $K_\epsilon$ , and inelastic behavior occur.

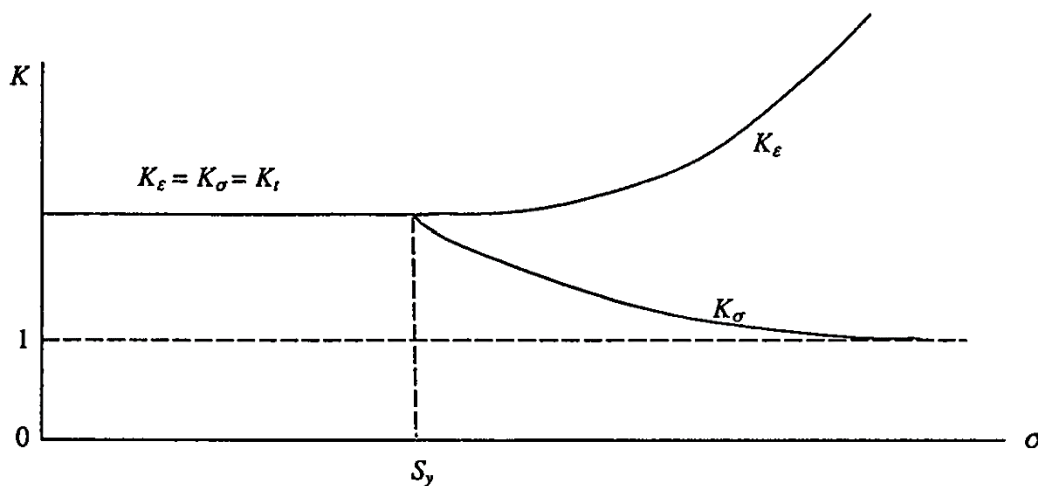


Figure2. 17 Concentration factors variation with local (notch) stress

As discussed in previous section, the monotonic strain-stress curve expressed by Ramberg-Osgood equation relates stress and strain as:

$$\epsilon = \epsilon^e + \epsilon^p = \frac{\sigma}{E} + \left(\frac{\sigma}{K}\right)^{1/n} \quad (2.34)$$

Where

$n$  = monotonic strain hardening exponent

$K$  = monotonic strength coefficient

For a given nominal stress  $S$  or nominal strain  $e$ , local stress or strain can be determined by three ways as:

- Experimental methods
- Finite element methods
- Analytical methods

Finite element method needs a fine mesh and small element size around geometrical discontinuities like notches as well as a good representation for material stress-strain behavior like Ramberg-Osgood equation. For using analytical methods, the value of elastic stress concentration factor is needed. The combination of linear finite element method and analytical method is used for complex geometries where calculating elastic stress concentration factor is difficult. In this approach, the calculated elastic stress concentration factor using FEM is employed along with analytical methods to obtain local stress and strains. The linear rule, Neuber's rule, and Glinka's rule (strain energy density rule) are three analytical methods which will be discussed in next sections.

#### 2.9.4.1 The Linear Rule

The Linear rule[15] is expressed as:

$$K_{\varepsilon} = K_{\sigma} = \frac{\varepsilon}{e} \quad (2.35)$$

For nominal elastic condition, following equation is applicable:

$$e = \frac{S}{E} \quad (2.36)$$

From the two equations above, local strain can be calculated, and for determining local stress Equation (2.34) can be used. In case of cyclic loadings, the range of stresses and strains are used. The linear rule is suitable for extreme plane strain cases.

### 2.9.4.2 Neuber's Rule

Following equation which is a rule for nonlinear material behavior is suggested by Neuber for longitudinal grooved shaft under torsional loading[40]:

$$K_\epsilon K_\sigma = K_t^2 \quad (2.37)$$

By substituting expressions for strain and stress concentration factors:

$$\epsilon \sigma = K_t^2 e S \quad (2.38)$$

From this rule it is found that the elastic stress concentration factor is the geometric mean of the true stress and strain concentration factors.

Simultaneous solution of Neuber's rule and the stress-strain equation is required to determine local strains and stresses. Plotting Equation (2.38) and the stress-strain relation (2.34) on a  $\sigma$ - $\epsilon$  coordinate it can be seen that the intersection of these two curves, which is point A in Figure 2.18 defines the local stress and strain values which is desired.

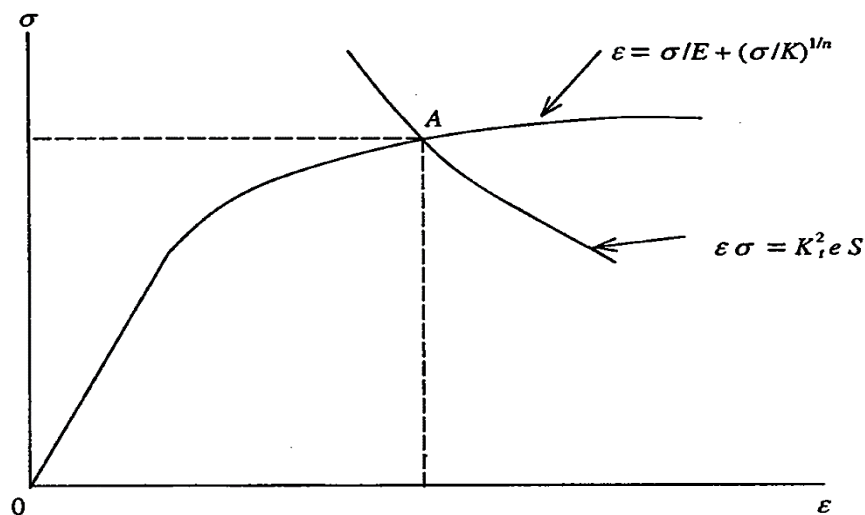


Figure2. 18 Determination of local stress and strain using Neuber's rule

Neuber's rule for nominal elastic behavior can be reduce to following equation by substituting  $e$  as  $S/E$ :

$$\varepsilon\sigma = \frac{(K_t S)^2}{E} \quad (2.39)$$

By combining Equation (2.39) with Equation (2.34), local stress  $\sigma$  can be found by solving following equation using iteration or numerical techniques:

$$\frac{\sigma^2}{E} + \sigma \left( \frac{\sigma}{K} \right)^{1/n} = \frac{(K_t S)^2}{E} \quad (2.40)$$

Replacing stresses and strains with strain and stress ranges and monotonic stress-strain relation with hysteresis one, local stresses and strains for cyclic loading cases can be found. Also for cyclic loading situations, while using Neuber's rule, Topper et al.[4] suggested to use fatigue notch factor  $K_f$  instead of stress concentration factor  $K_t$  since it will give results that are closer to experimental ones (reduction in degree of conservatism). For cyclic loading and nominal elastic behavior following relations are available:

$$\Delta\varepsilon\Delta\sigma = K_f^2 \Delta e \Delta S \quad (2.41)$$

$$\text{for nominal elastic situation: } \Delta e = \frac{\Delta S}{E} \quad (2.42)$$

$$\Delta\varepsilon\Delta\sigma = \frac{(K_f \Delta S)^2}{E} \quad (2.43)$$

$$\frac{(\Delta\sigma)^2}{E} + 2\Delta\sigma \left( \frac{\Delta\sigma}{2K'} \right)^{1/n'} = \frac{(K_f \Delta S)^2}{E} \quad (2.44)$$

$$\Delta\varepsilon = \frac{\Delta\sigma}{E} + 2 \left( \frac{\Delta\sigma}{2K'} \right)^{1/n'} \quad (2.45)$$

After obtaining local stress range from Equation (2.44), it is possible to obtain strain range from hysteresis loop equation (Equation 2.45)). Then maximum stress could

also be obtained. Having these values in hand, calculating notch strain amplitude and notch mean stress can be done using:

$$\varepsilon_a = \frac{\Delta\varepsilon}{2} \quad (2.46)$$

$$\sigma_m = \frac{\sigma_{max} + \sigma_{min}}{2} \quad (2.47)$$

These values are used in fatigue life prediction formulas discussed previously.

### 2.9.4.3 Glinka's Rule

Another notch analysis method has been introduced by Glinka[41]. In this method it is assumed that the factor  $K_t^2$  relates the notch root strain energy density ( $W_e$ ) to the energy density caused by nominal stress and strain ( $W_s$ ):

$$W_e = K_t^2 W_s \quad (2.48)$$

In case of nominally elastic behavior:

$$W_s = \frac{1}{2} \frac{S^2}{E} \quad (2.49)$$

$$W_e = \frac{\sigma^2}{2E} + \frac{\sigma}{1+n} \left(\frac{\sigma}{K}\right)^{1/n} \quad (2.50)$$

Resulting in:

$$\frac{\sigma^2}{E} + \frac{2\sigma}{1+n} \left(\frac{\sigma}{K}\right)^{1/n} = \frac{(K_t S)^2}{E} \quad (2.51)$$

Equation is the well-known Glinka's rule or strain energy density formula, physical interpretation of this rule is shown in Figure 2.19.

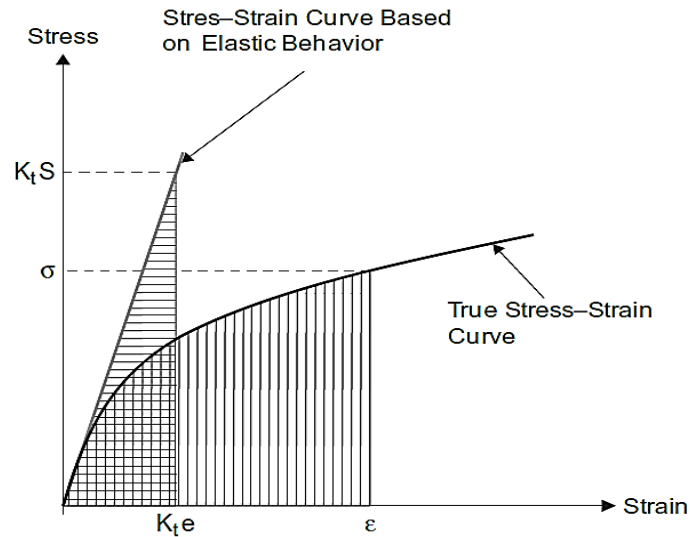


Figure 2.19 Strain energy density method

The only difference between using Neuber's rule and Glinka's rule (Equations (2.40) and (2.51)) is the term  $2/(1+n)$ . By applying Glinka's rule, longer fatigue life is predicted since smaller notch strain and stress is predicted, so application of Neuber's rule is a more conservative way of fatigue life prediction.

Again in the case of cyclic loading, stresses and strains should be replaced with corresponding ranges, and monotonic stress-strain loop equation should be replaced with hysteresis one ( using  $K'$  and  $n'$ , instead of  $K$  and  $n$ ):

$$\frac{(\Delta\sigma)^2}{E} + \frac{4\Delta\sigma}{1+n'} \left( \frac{\Delta\sigma}{2K'} \right)^{1/n'} = \frac{(K_t \Delta S)^2}{E} \quad (2.52)$$

Among these three notch analysis methods, the least conservative fatigue life results can be obtained by using the Linear rule, and the most conservative one can be obtained by Neuber's rule, and using Glinka's rule, results will be between the Linear rule results and Neuber's rule results.

## 2.10 Review of Linear Elastic Fracture Mechanics (LEFM)

The existence of a crack in an engineering component or structure can significantly reduce its strength and life. The total life of a component can be divided into crack initiation life and crack growth life as follows:

$$N_{total} = N_{initiation} + N_{growth}$$

↓

*S-N*

$\epsilon-N$

↓

LEFM

$N_{initiation}$  may range from zero to almost the entire life

$N_{growth}$  can be very small or nearly the entire life

There has been a heavy use of fracture mechanics in aerospace, ship, nuclear and ground vehicle (recently) industries. Using Fracture mechanics concepts, the strength of a component which has a crack or flaw can be assessed. For materials that behave mostly elastic during the fatigue process, LEFM concepts are used.

### 2.10.1 Loading Modes

There are three modes by which a crack can extend, these three modes are shown in Figure 2.20. Since cracks tend to grow on the maximum tensile stress plane, the most common mode in fatigue is mode I.

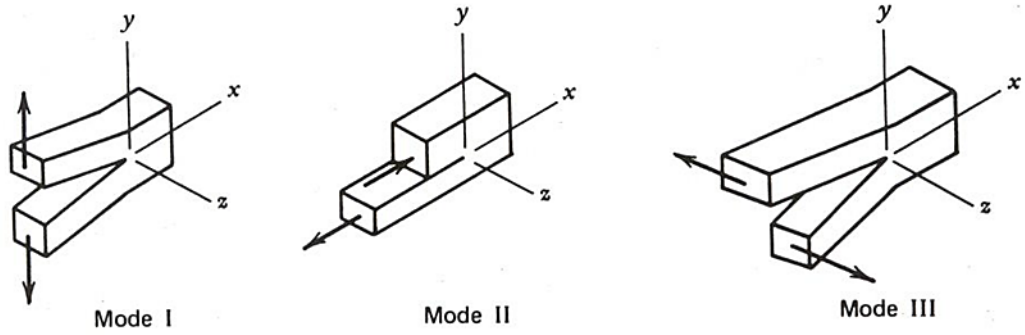


Figure2. 20 Three modes of crack extension

### 2.10.2 Stress Intensity Factor

The basic work done for development of stress intensity factor was done by Griffith[42] nearly a century ago. Later, using Griffith's theory, Irwin[43] quantified the crack tip driving force as stress intensity factor  $K$ :

$$G = \frac{K^2}{E} \quad \text{for plane stress} \quad (2.53)$$

$$G = \frac{K^2}{E} (1 - \nu^2) \quad \text{for plane strain} \quad (2.54)$$

Where

$G$  = Energy release rate (required elastic energy per unit crack surface area for crack extension)

The determination of  $K$  values can be done by analytical and computational calculations by using theory of elasticity and experimental methods like photo-elasticity. The dependence of  $K$  on the combination of crack length, loading, and geometry can be expressed as:

$$K = S\sqrt{\pi a} f\left(\frac{a}{W}\right) \quad \text{or} \quad K = S\sqrt{a} Y \quad (2.55)$$

Where

$a$  = the crack length

$S$  = the nominal stress (assuming the crack did not exist)

$f\left(\frac{a}{w}\right)$ , and  $Y$  = dimensionless geometry parameters

$W$  = a width dimension

The common unit for  $K$  is  $\text{MPa}\sqrt{\text{m}}$

For a single edge notched beam (SENB) in bending shown in Figure 2.21, the  $K$  value is calculated in one of the following forms:

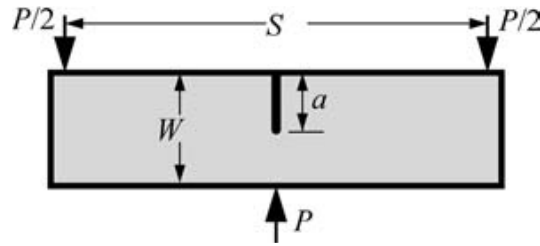


Figure 2. 21 SENB in bending

$$K_I = \sigma_{nom} \sqrt{\pi a} \left[ \begin{array}{l} 1.106 - 1.552 \left(\frac{a}{w}\right) + 7.71 \left(\frac{a}{w}\right)^2 - 13.53 \left(\frac{a}{w}\right)^3 \\ + 14.23 \left(\frac{a}{w}\right)^4 \end{array} \right] \quad (2.56)$$

Equation (2.56) is suitable for  $S = 8W$

$$K_I = \sigma_{nom} \sqrt{a} \frac{1.99 - \frac{a}{W} \left(1 - \frac{a}{W}\right) \left(2.15 - 3.93 \frac{a}{W} + 2.7 \left(\frac{a}{W}\right)^2\right)}{\left(1 + 2 \frac{a}{W}\right) \left(1 - \frac{a}{W}\right)^{3/2}} \quad (2.57)$$

Where

$$\sigma_{nom} = \frac{Mc}{I} = \frac{6M}{BW^2} = \frac{3PS}{2BW^2} \quad \text{and} \quad B = \text{Thickness} \quad (2.58)$$

Equation (2.57) is suitable for a specimen with  $S=4W$

An alternative expression for  $K$  in terms of applied load  $P$  is given as:

$$K_I = \frac{P}{B\sqrt{W}} f\left(\frac{a}{W}\right) \quad (2.59)$$

Where,

$$f\left(\frac{a}{W}\right) = \frac{3 \frac{S}{W} \sqrt{\frac{a}{W}}}{2 \left(1 + 2 \frac{a}{W}\right) \left(1 - \frac{a}{W}\right)^{3/2}} \left[ \begin{array}{c} 1.99 - \frac{a}{W} \left(1 - \frac{a}{W}\right) \\ \left\{ 2.15 - 3.93 \left(\frac{a}{W}\right) + 2.7 \left(\frac{a}{W}\right)^2 \right\} \end{array} \right] \quad (2.60)$$

Here,  $S$  = span length

### 2.10.3 Monotonic and Cyclic Plastic Zone

In order to use LEFM theory, the region of yielding at the crack tip which is called the plastic zone, needs to be not very large. For calculating the plastic zone size under monotonic and cyclic loading following expressions are used:

$$2r_y = \frac{1}{\pi} \left(\frac{K}{S_y}\right)^2 \quad \text{for plane stress} \quad (2.61)$$

$$2r'_y \cong \frac{1}{4\pi} \left(\frac{\Delta K}{S_y}\right)^2 \quad \text{for plane stress} \quad (2.62)$$

$$2r_y \cong \frac{1}{3\pi} \left(\frac{K}{S_y}\right)^2 \quad \text{for plane strain} \quad (2.63)$$

$$2r'_y \cong \frac{1}{12\pi} \left(\frac{\Delta K}{S_y}\right)^2 \quad \text{for plane strain} \quad (2.64)$$

Where,

$2r_y$  = monotonic plastic zone size

$S_y$  = yield strength

$2r'_y$  = cyclic plastic zone size

There is an approximate limitation suggestion to use LEFM concepts under monotonic loading as:

$$r_y \leq \frac{a}{8} \quad (2.65)$$

## 2.11 Fatigue Crack Growth (FCG)

The initial existence of a crack with a dangerous size (Having a critical size which would cause immediate unstable fracture upon loading) is unusual, so, for brittle fracture to occur, a cyclic loading is required to make the crack to grow and reach a critical size. This process is called fatigue crack growth.

The crack length,  $a$ , versus number of cycles,  $N$ , for three identical specimens under different cyclic loadings are shown in Figure 2.22.

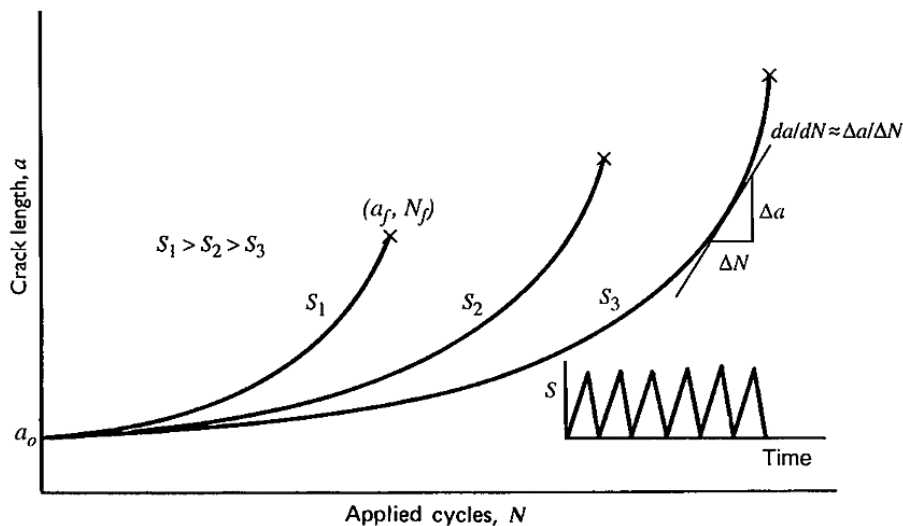


Figure2. 22 Fatigue crack length versus number of cycles to fracture

As seen in Figure 2.22, FCG life and fracture crack length gets shorter as cyclic stresses gets larger. And also the crack growth rates are higher at larger stresses. The slope at a point on an  $a$ - $N$  curve equals the rate of the crack growth,  $da/dN$  or  $(\Delta a / \Delta N)$ .

For fatigue crack growth under constant amplitude cyclic loading, following expression are used:

$$\Delta\sigma_{nom} = \sigma_{nom_{max}} - \sigma_{nom_{min}} \quad (2.66)$$

$$\Delta K = \Delta\sigma_{nom}\sqrt{\pi a} f\left(\frac{a}{W}\right) \quad (2.67)$$

$$K_{max} = \sigma_{nom_{max}}\sqrt{\pi a} f\left(\frac{a}{W}\right) \quad (2.68)$$

$$K_{min} = \sigma_{nom_{min}}\sqrt{\pi a} f\left(\frac{a}{W}\right) \quad (2.69)$$

$$\Delta K = K_{max} - K_{min} \quad (2.70)$$

$$\Delta K = \frac{\Delta P}{B\sqrt{W}} f\left(\frac{a}{W}\right) \quad (2.71)$$

$$R = \frac{P_{min}}{P_{max}} = \frac{\sigma_{nom_{min}}}{\sigma_{nom_{max}}} = \frac{K_{min}}{K_{max}} \quad (2.72)$$

Where

$\sigma_{nom}$  = nominal stress

In case that  $\sigma_{nom_{min}}$  is compressive,  $K_{min}$  will be taken as zero because stress intensity factor is undefined in compression.

For expressing fatigue crack growth, the convenient form is as follows:

$$\frac{da}{dN} = f(\Delta K, R) \quad (2.73)$$

The crack growth rate versus stress intensity factor range curve can be obtained by applying LEFM theory. The log-log scale of a  $da/dN$  vs stress intensity factor range is shown in Figure 2.23. This curve consists of three regions. At Region II where  $\Delta K$  values are in intermediate level, the curve is linear. In region I and III where  $\Delta K$  values are low and high respectively, the crack growth rate deviates from linearity. A crack will not grow below a threshold value of  $\Delta K$  available in region I. The rate

of the crack growth is very high and unstable at region III till it reaches a critical value of  $K$  at which fracture occurs.

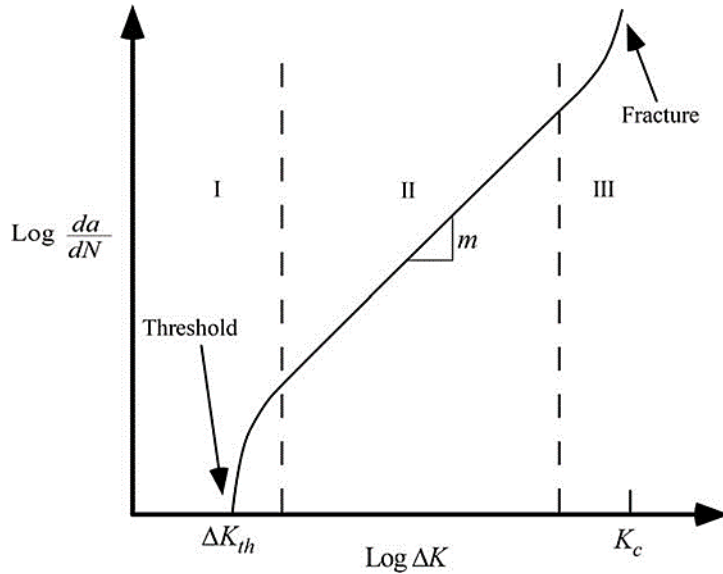


Figure2. 23 Fatigue crack growth rate, a schematic sigmoidal behavior

The linear part of the curve which is related to stable macroscopic crack growth can be represented by the following power law relationship as suggested by Paris and Erdogan[44]:

$$\frac{da}{dN} = C \Delta K^m \quad (2.74)$$

In above relation named as Paris Law,  $C$  and  $m$  are the material constants determined experimentally and named as Paris constants. Paris equation is used mostly for  $R = 0$  loading. Since integrating Paris Law gives conservative FCG lives, it can be used for three regions in most cases.

Stress-life ( $S-N$ ) or strain-life ( $\epsilon-N$ ) equations are usually based on fully reversed stress or strain situations, but FCG data are usually based on pulsating tension situation with  $R = 0$ .

### 2.11.1 Mean Stress Effects for FCG

For a given  $\Delta K$ , by increasing  $R$  ratio crack growth rate also increase, this effect is stronger for brittle materials and weak for ductile materials.  $R$  ratio also has less effect in region II than regions I and III. These effects are shown schematically in Figure 2.24.

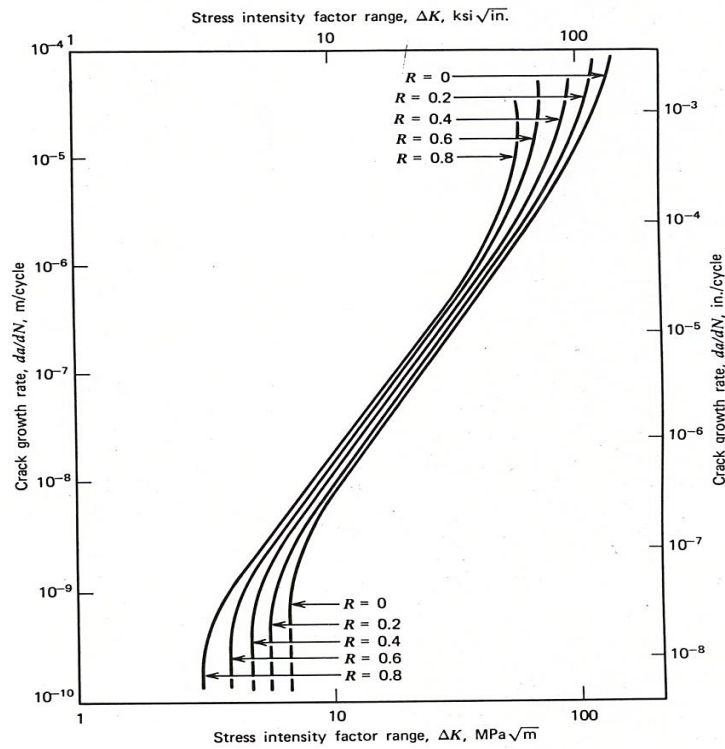


Figure2. 24 schematic mean stress effect on FCG

#### 2.11.1.1 The Walker Equation for FCG

One of the empirical relationships for describing mean stress effects with  $R \geq 0$  can be expressed by applying Walker relationship to stress intensity factor range as follows:

$$\frac{da}{dN} = \frac{C_0}{(1-R)^{m(1-\gamma)}} (\Delta K)^m = C'(\Delta K)^m \quad (2.75)$$

Where  $C_0$  and  $m$  are the Paris Coefficients and slope for  $R = 0$  condition and  $\gamma$  is the Walker constant which is a material constant, The slope of the curve  $m$  is not effected by  $R$ , but  $C'$  (the Walker equation coefficient) is expressed as:

$$C' = \frac{C_0}{(1-R)^{m(1-\gamma)}} \quad (2.76)$$

## 2.12 Fracture Toughness Testing

To measure the resistance of a material to crack growth is named fracture toughness test. ASTM is one of the organizations that publish standardized procedures for fracture toughness measurements.

### 2.12.1 Specimen Configurations

ASTM standards allows five types of specimens to characterize fracture initiation and crack growth which are:

- The compact specimen
- The single edge notched bend SE(B) geometry
- The arc-shaped specimen
- The disk specimen
- The middle tension (MT) panel

These five specimen are shown in Figure 2.25.

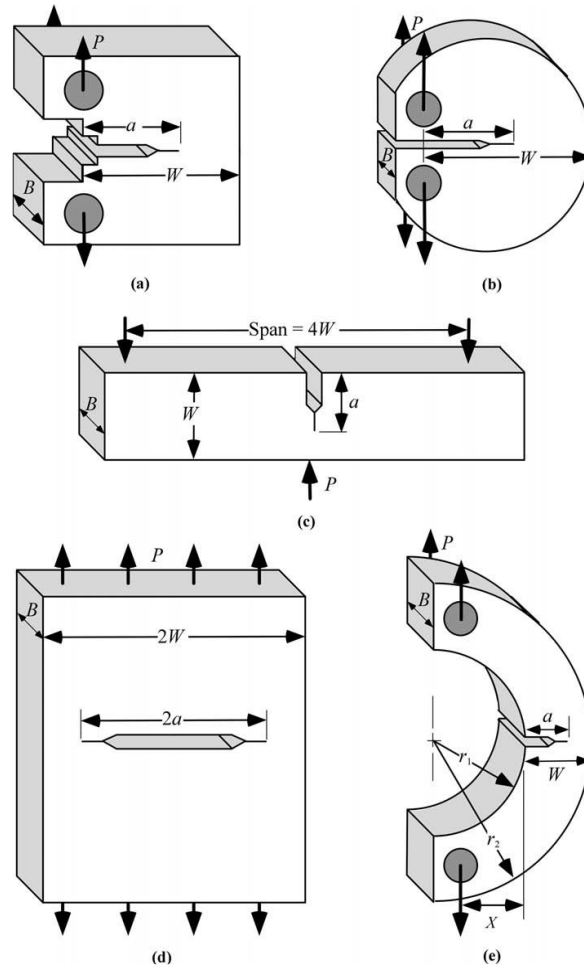


Figure 2.25 Standardized test specimens: (a) compact specimen, (b) disk-shaped compact specimen, (c) single-edge-notched bend SE(B) specimen, (d) middle tension (MT) specimen, and (e) arc-shaped specimen.[45]

The crack length ( $a$ ), the thickness ( $B$ ), and width ( $W$ ) are three important characteristic dimensions of each specimen. In general  $W=2B$  and  $a/W \approx 0.5$ . The flexibility of SE(B) specimen is more with respect to size. Although, the standard length for loading span is  $4W$ , with a single fixture wide range of SE(B) specimens can be tested because the loading span can be adjusted continuously to any value that is in its range of capacity if the fixture design is proper. The Figure 2.26 shows an apparatus for three-point bend testing.[45]

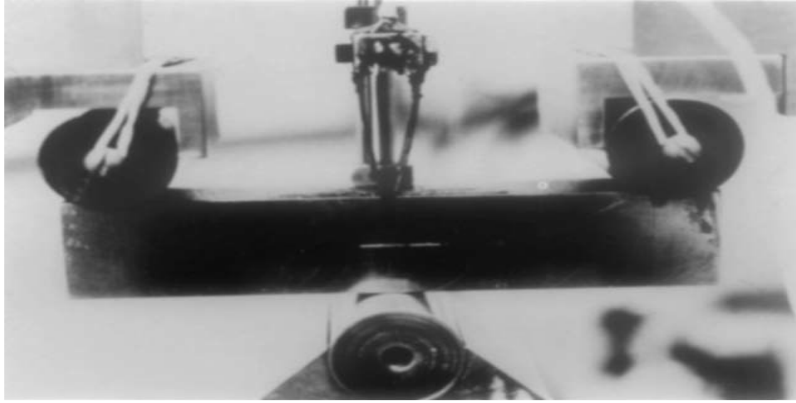


Figure2. 26 Three-point bending apparatus for testing SE(B) specimens

### 2.12.2 Fatigue Pre-cracking

In order to use fracture mechanics theory, infinitely sharp cracks are needed prior to loading. In spite of the fact that specimens that are used in laboratory are away from this ideal, it is possible to produce adequately sharp cracks using cyclic loading. The pre-cracking procedure in a typical specimen is shown in Figure 2.27.

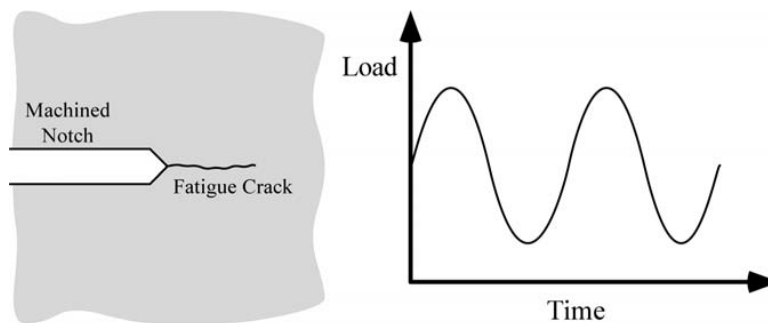


Figure2. 27 Fatigue pre-cracking of a typical specimen, a fatigue crack is initiated at the notch tip through cyclic loading

It can be seen that a fatigue crack is initiated at tip of the machined notch and by careful control of cyclic loads it propagates to the desired length.

Nowadays modern servo-hydraulic test machines can be programmed to produce sinusoidal loading and other wave forms loadings.

The production of initiated fatigue crack must be in such a way that it does not have an unwanted influence on the toughness value which will be measured. To measure precise fracture toughness the fatigue crack must meet the following conditions:

- The radius of crack tip at failure must be much larger than the radius of initiated fatigue crack.
- The plastic zone which is produced during fatigue cracking must be smaller than the plastic zone at fracture.[45]

### 2.12.3 Measurement Tools

During any fracture toughness test, measuring the applied load and a characteristic displacement on the test specimen is a minimum need. In order to measure applied loads, the load cells are needed and nearly all test machines are equipped with them.

The most common equipment to measure displacements in fracture mechanics tests is the clip gage which is shown in Figure 2.28. The clip gage attaches to the mouth of the crack; it is made of four resistance-strain gages bonded to a pair of cantilever beams. When beams deflects a change of voltage across the strain gages occur, this voltage change varies linearly with displacement. There should be attached or machined sharp knife edges into the specimen to enable the clip gages to be attached into them to ensure free rotation of each beam ends.[45]

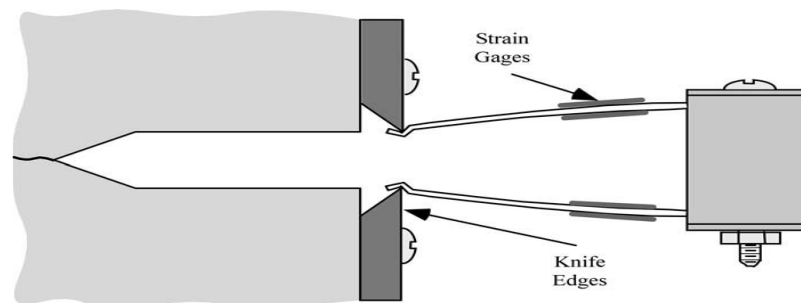


Figure2. 28 Measurement of the crack-mouth-opening displacement with a clip gage.

### 2.12.4 $K_{Ic}$ Testing

$K_{Ic}$  is the critical value of mode I stress intensity factor which can be used as a proper fracture parameter in a material that acts linearly elastic prior to failure, such that the produced plastic zone is small enough compared to specimen dimensions. In 1970, the first standardized  $K_{Ic}$  testing method, ASTM E 399[46], was published. In ASTM E 399,  $K_{Ic}$  is referred to as “plain strain fracture toughness”.

Much of early fracture toughness testing was performed on thin sections and it was shown that  $K_c$  which is a thickness-dependent apparent toughness might not be a single valued material property. On the other hand, when the specimen is sufficiently thick, (i.e. plane strain conditions prevail) then  $K_{Ic}$  is thickness independent. Hence it is called plane strain fracture toughness and it is a material property. Thus tests were shifted from thin sections to thick sections in order to develop testing methods for  $K_{Ic}$  determination.

#### 2.12.4.1 ASTM E 399

Specimen configurations that are permitted by E 399 are: the compact, SE(B), arc-shaped, and disk-shaped specimens. They are usually fabricated with  $W=2B$ . To produce a sharp crack, fatigue pre-cracking is required for all test specimens. The ratio of allowed crack size to width ( $a/W$ ) in E 399 is between 0.45 and 0.55. If the technician follows all the procedure outlined in the standard, almost all the mechanical tests including fracture toughness test lead to valid results. However,  $K_{Ic}$  test may produce invalid result if the plastic zone at fracture is too large.

Due to strict size necessities, E 399 recommends to check the below size requirements for a valid  $K_{Ic}$ :

$$B, a \geq 2.5 \left( \frac{K_{Ic}}{\sigma_{YS}} \right)^2 \quad (2.77)$$

$$0.45 \leq a/W \leq 0.55 \quad (2.78)$$

Although by increasing strength there is a tendency to decrease toughness, there is not a specific relationship between  $K_{Ic}$  and  $\sigma_{YS}$  in metals, so strength-thickness table in E 399 should be used when a better data is not available. According to ASTM E-399 for fatigue pre-cracking,  $K_{max}$  should be no larger than  $0.8 K_{Ic}$ . At the final size of the crack  $K_{max}$  should be less than  $0.6 K_{Ic}$  and also during fatigue  $K_{max}$  should always be less than  $K_{Ic}$  to avoid failure of the specimen.

To select proper loads the user needs to know anticipated  $K_{Ic}$  value. If he or she acts in conservative way and selects low loads, pre-cracking time may be too long or otherwise by selecting high loads the results may be invalid.

Testing pre-cracked specimens according to E 399 requires to monitor and record applied loads and crack opening displacements. Three typical types of load-displacement curves with critical load  $P_Q$  which is defined for each type of curve are shown in Figure 2.29.

In the 5% method, the  $P_5$  is found by contracting a line from origin that has a slope 5% less than the recorded slope so for the type I case the load-displacement curve is smooth and it deviates slightly from linearity before reaching a maximum load  $P_{max}$ . So for type I curve,  $P_Q = P_5$ . For type I case where a small amount of unstable crack growth (i.e. a pop-in) occurs before the curve deviates from linearity by 5%. So for type II curve  $P_Q$  is defined at the pop-in. Type III failures are those in which failure proceeds across the entire remaining ligament without hesitation and in this case  $P_Q = P_{max}$ .

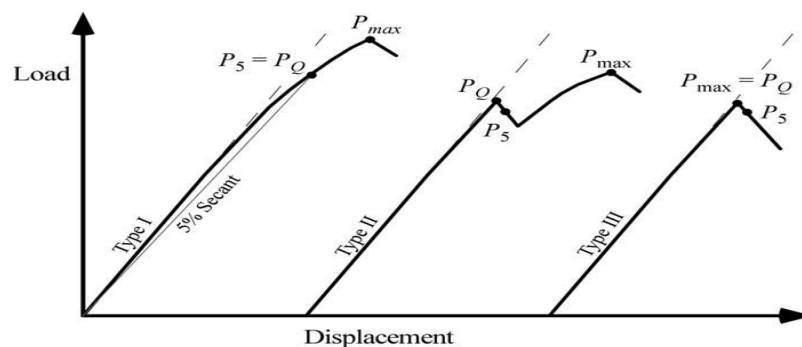


Figure2. 29 Three types of load-displacement behavior in a  $K_{Ic}$  test.

From the  $P_Q$  value and measured crack length, provisional fracture toughness  $K_Q$  can be calculated from the following relationship:

$$K_Q = \frac{P_Q}{B\sqrt{W}} f\left(\frac{a}{W}\right) \quad (2.79)$$

Where  $f(a/W)$  is a dimensionless function of  $a/W$  which is given in E 399 for four types of specimens. The calculated  $K_Q$  value is a valid  $K_{Ic}$  result only if all the validity requirements in the standard are met including:

$$0.45 \leq a/W \leq 0.55 \quad (2.80)$$

$$B, a \geq 2.5 \left(\frac{K_Q}{\sigma_{YS}}\right)^2 \quad (2.81)$$

$$P_{max} \leq 1.10P_Q \quad (2.82)$$

If all the requirements of ASTM E 399 are met by the test, then  $K_Q = K_{Ic}$ .

## CHAPTER III

### LIFE PREDICTIONS

In this chapter, through the application of strain-life method (using corresponding formulas by Morrow, SWT, Manson-Halford and Walker), along with FEM simulations, fatigue crack initiation life under a specific cyclic loading is determined; and then fatigue crack propagation life up to a desired crack length is calculated applying LEFM approach with the help of Walker and Paris equations.

#### 3.1 Geometry, Loading and Boundary Conditions of Problem

A single edge notched bend (SENB) specimen of rectangular cross section was analyzed in this thesis. The geometry and dimensions of this specimen are drawn using SOLIDWORKS software which is shown in Figure 3.1. The dimensions are in [mm] and are selected according to ASTM E399 standard described in section 2.12 of chapter II. The specimen is loaded in three point bending condition. A schematic of loading and supports is illustrated in Figure 3.2. The specimen is under cyclic loading; its maximum and minimum values are 8 [KN] and 0.8 [KN] respectively ( $R=0.1$  suggested by ASTM E399). The maximum loading value is selected according to ASTM E399 standard suggestion (80% of limiting load). During fatigue pre-cracking  $K_{max}$  should be less than 80% of  $K_{Ic}$ . The span length (distance between supports) is 120 [mm] =  $4W$ . For  $K_{Ic}=29$  MPa[10] and for a crack length of 14.4 [mm], the limiting load is calculated using Equation (2.59),  $P_{lim}=10000$  [N].

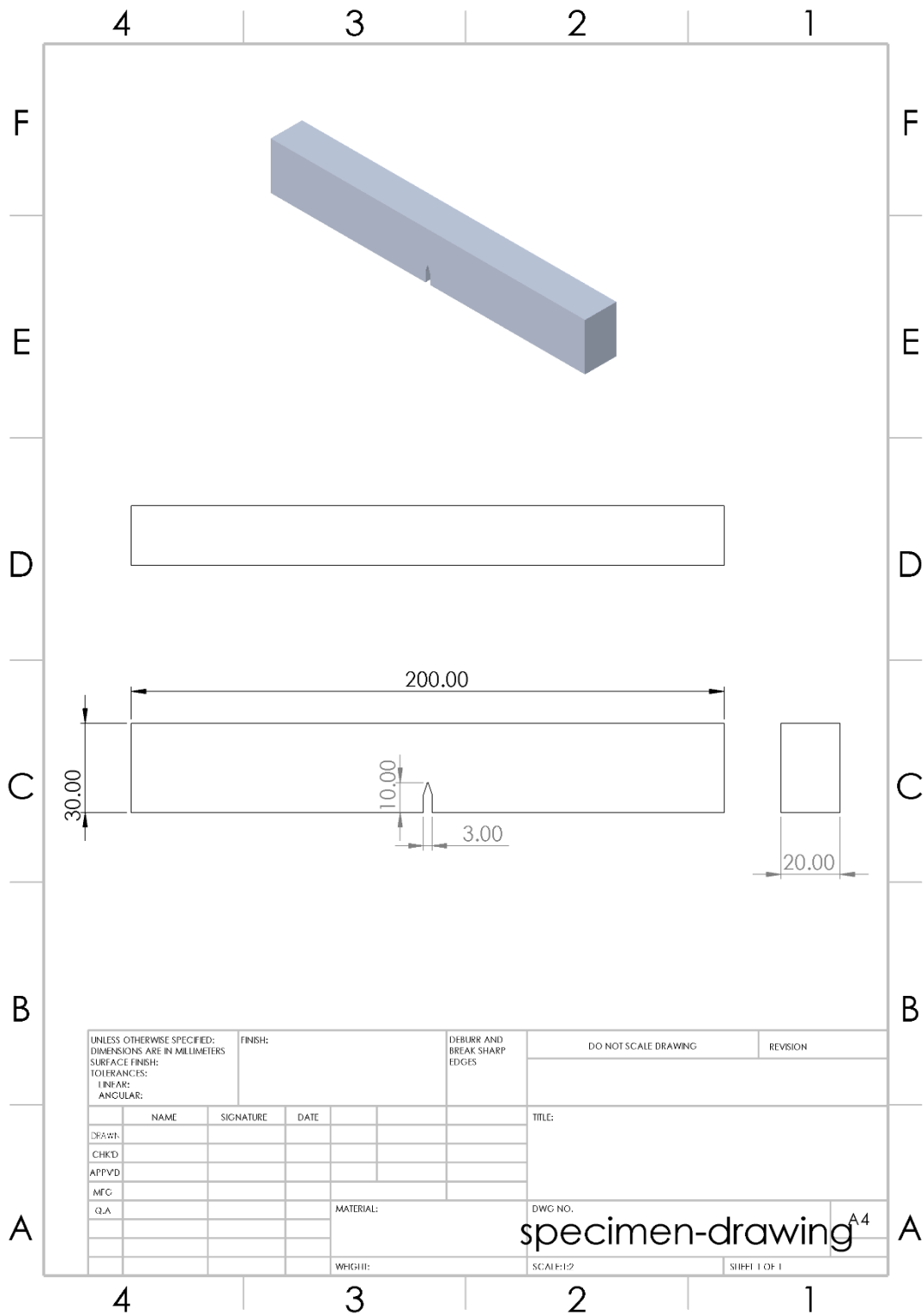


Figure3. 1 Geometry and dimensions of SENB specimen drawn by SOLIDWORKS software. Dimensions are in [mm]

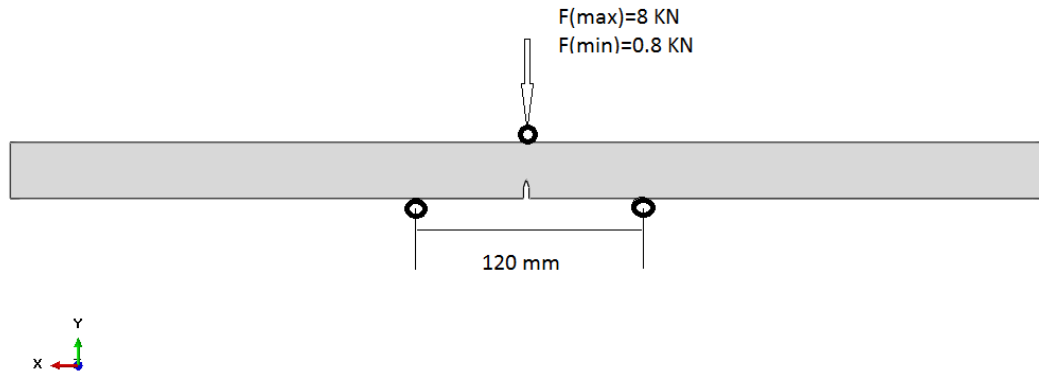


Figure3. 2 Schematic of specimen loading and boundary conditions

### 3.2 Material of the Specimen

The specimens analyzed and tested in this study are made of aluminum alloy 6082 T651. The major alloying ingredients of 6xxx-series aluminum alloys are magnesium and silicon. These series of aluminum alloys are mostly used in automotive, aerospace and ship industries as structural materials because of their various and attractive combinations of properties such as medium and high strength, formability, fatigue resistance and low cost. Among these series, 6082 has the highest strength but it has relatively low ductility so it has been chosen. Al 6082 is heat treatable and has a high corrosion resistance. To have the aluminum alloy 6082 furnished in T651 temper, metal is solution heat-treated, stress relieved by stretching, and then artificially aged.

The chemical composition of al 6082 is shown in Table 3.1, and the physical/mechanical properties of al 6082 T651 is shown in Table 3.2.

Table3.1: Chemical composition of al 6082

Chemical element	Silicon (Si)	Magnesium (Mg)	Manganese (Mn)	Iron (Fe)	Chromium (Cr)	Zinc (Zn)	Titanium (Ti)	Copper (Cu)	Aluminum (Al)
%Present	0.7-1.3	0.6-1.2	0.4-1.0	0-0.5	0-0.25	0-0.2	0-0.1	0-0.1	Balance

Table3. 2: Physical and mechanical properties of al 6082 T651

Density	Modulus of Elasticity (E)	Poisson's Ratio	Yield Tensile Strength (YTS)	Ultimate Tensile Strength (UTS)
2.7 g/cm <sup>3</sup>	70 GPa	0.33	280 MPa	320 MPa

### 3.3 Stress Analysis of Specimen in Abaqus®

In order to predict fatigue crack initiation life using strain-life formulas, elastic stress concentration factor at the notched part of the specimen is required. For this purpose maximum stress at the notch tip of the specimen under the described loading is determined using Abaqus software.

To analyze stress in the specimen using Abaqus, a two dimensional half model (with plane stress\plane strain assumption) and a three dimensional quarter model are created. Since specimen is symmetric in x and z directions it is suitable to model half of the specimen for 2-D analysis and quarter of the specimen for 3-D analysis to reduce the processing time of analyzes. The created models are shown in Figure 3.3. The notch radius was taken as 0.25 [mm]. (This value is an estimate based on the enlarged photographs of a notch produced by a particular cutter in the same material, in an earlier study [14]).

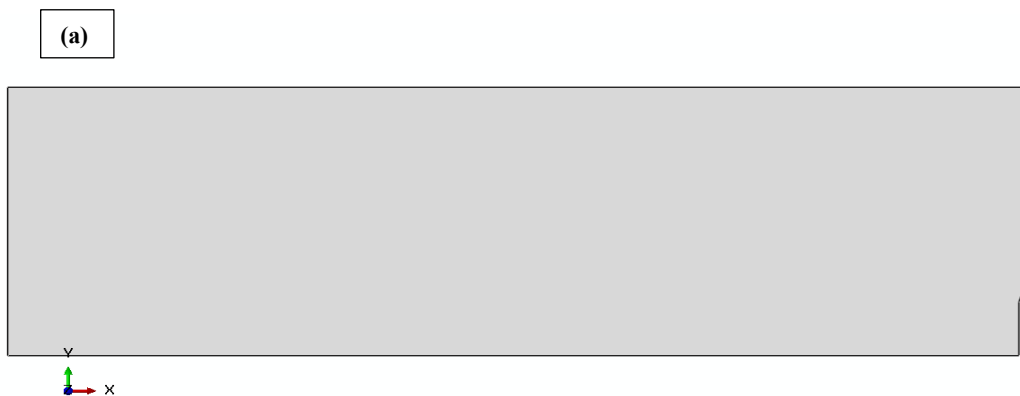


Figure 3.3 (continued in next page)

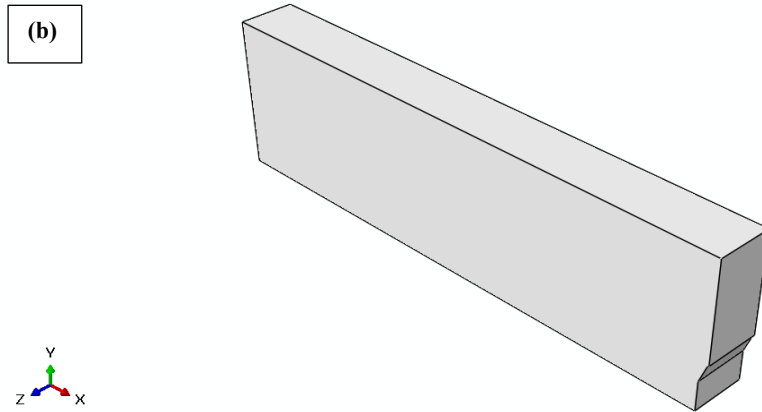


Figure3. 3 (a): 2-D half model created by Abaqus. (b): 3-D quarter model created by Abaqus

The loading and boundary conditions were defined after defining material properties and completing assembly and step parts in Abaqus. Figure 3.4 shows the loading and boundary conditions defined on the specimen in Abaqus.

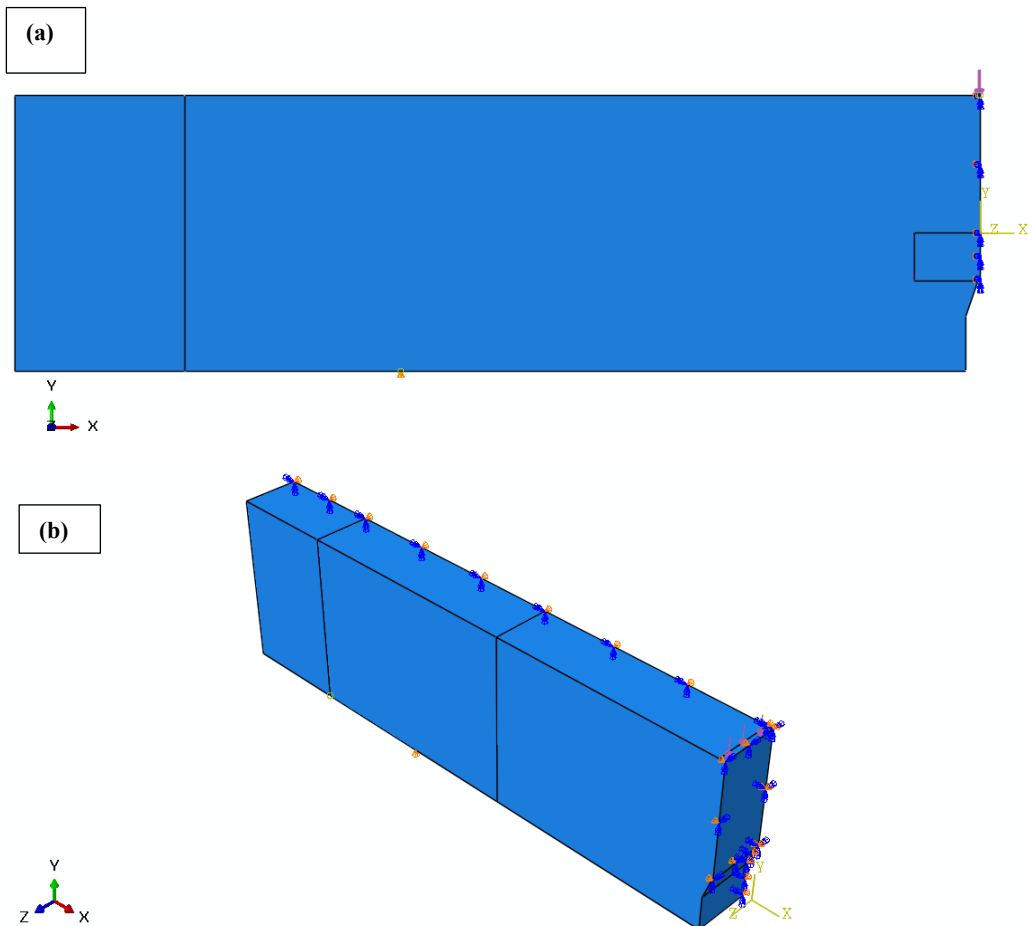


Figure3. 4 Loading and boundary conditions defined in Abaqus, (a): 2-D model, (b): 3-D model

The loading segments in above figure is magnified in Figure 3.5. It can be seen that loading is taken as pressure load on a very small area through defining a partition.

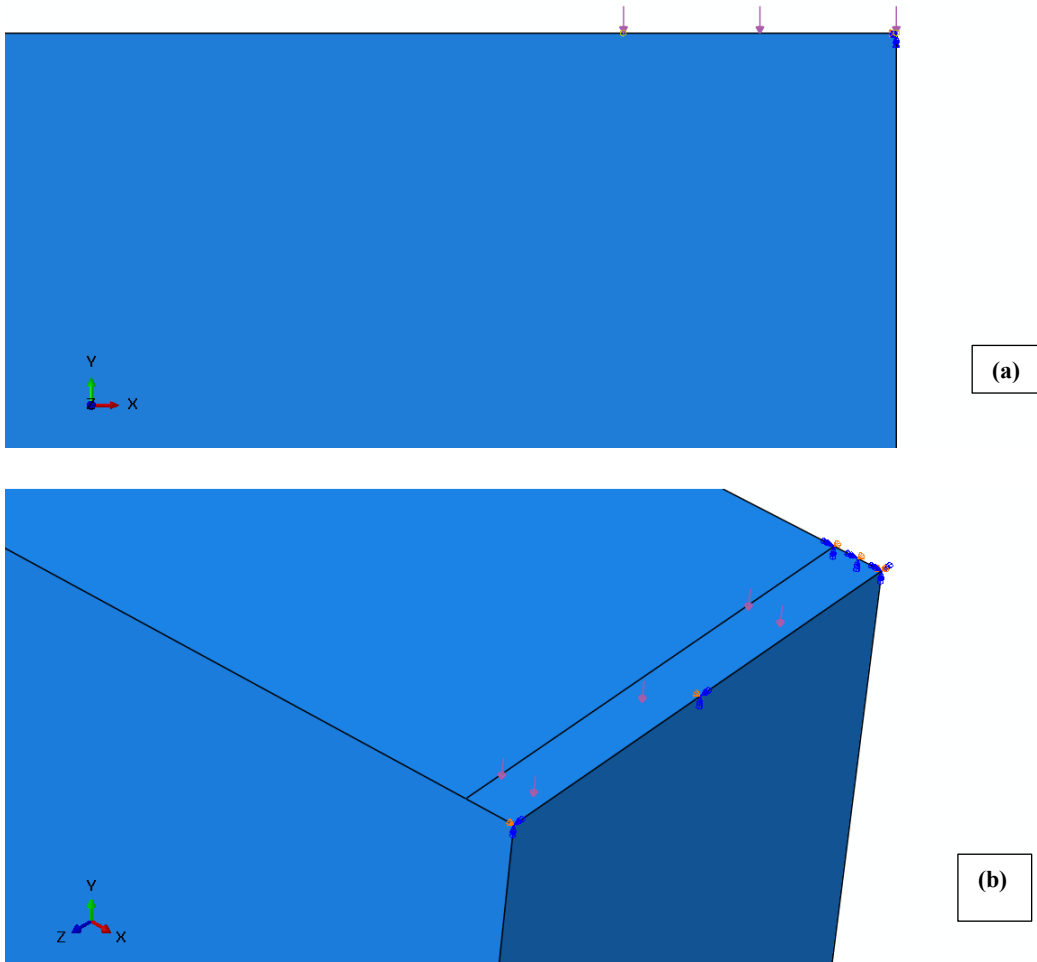


Figure3. 5 Applied loading as a pressure load over a very small area. (a): 2-D model, (b): 3-D model

One of the defined boundary conditions in Figure 3.4 is support boundary condition and the others are x-symmetry and z-symmetry boundary conditions as shown in Figure3.6 and 3.7.

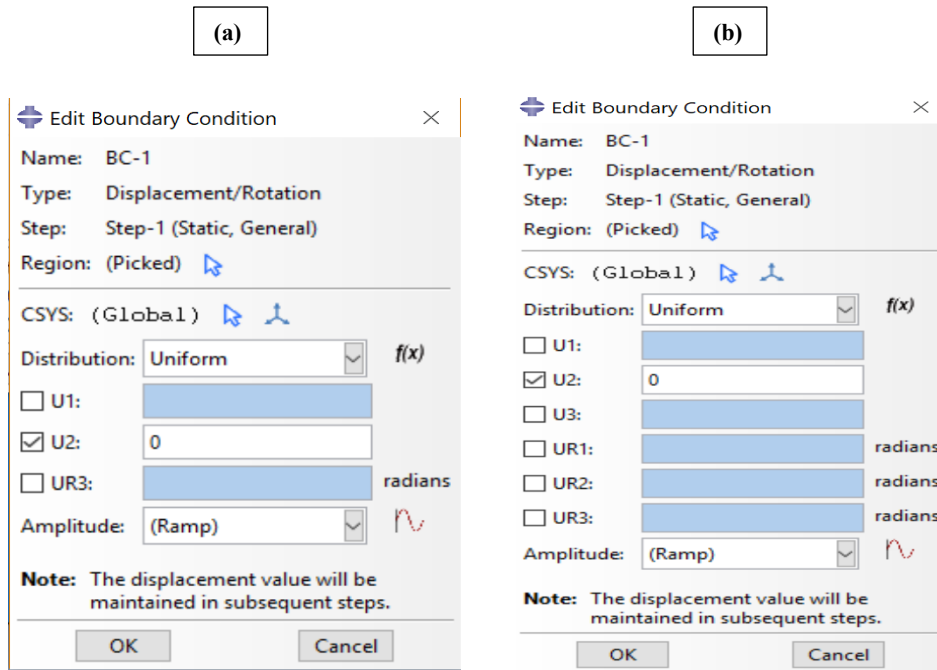


Figure3. 6 Support boundary condition. (a): 2-D model, (b): 3-D model

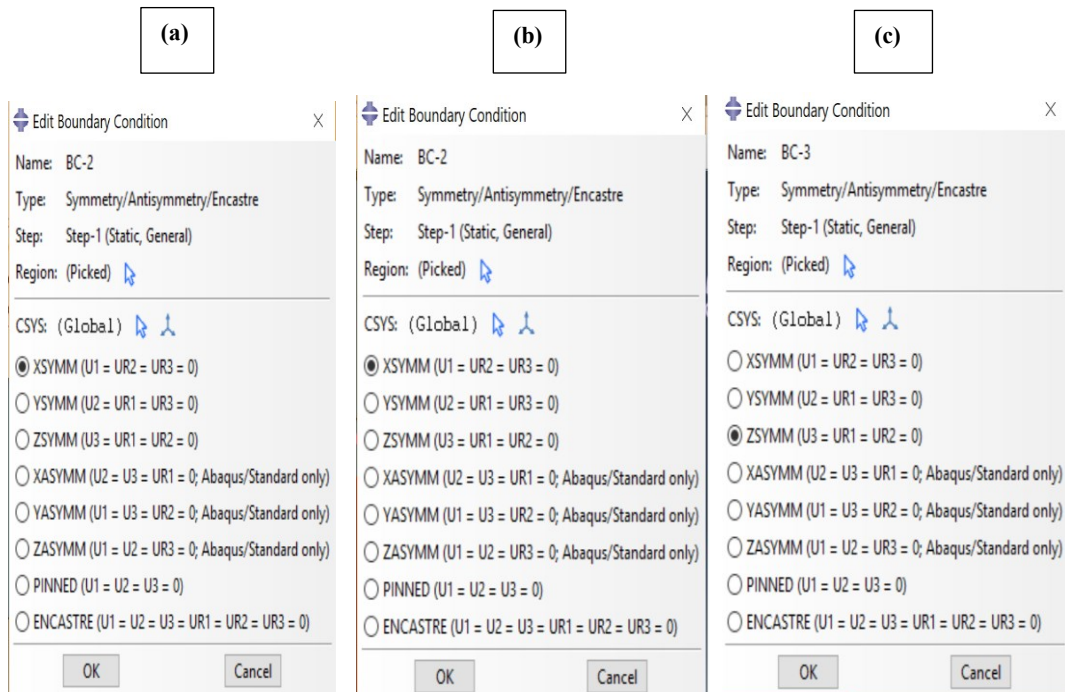


Figure3. 7 (a): x-symmetry boundary condition for 2-D model. (b) & (c): x-symmetry & z-symmetry BC for 3-D model

After defining load and boundary conditions as discussed above, meshing should be considered. Because of notch geometry and importance of analysis accuracy around notch tip, fine meshing should be done around the notch tip. After many meshing iterations (by choosing different meshing techniques and element shapes), the best meshing technique and element shape reached as shown in Figure 3.8. This was done with the help of defining partitions which allows to apply different meshing techniques and seedings for each partition. Each color shows a different meshing technique which is structured for green parts, free for pink part and sweep for yellow part. Element shapes are quadratic in both green and pink parts for 2-D model and hexahedral in both green and yellow parts for 3-D model. Algorithm used in free meshing of pink part is advancing front with mapped meshing everywhere appropriate and medial axis for yellow part with minimize the mesh transition selected.

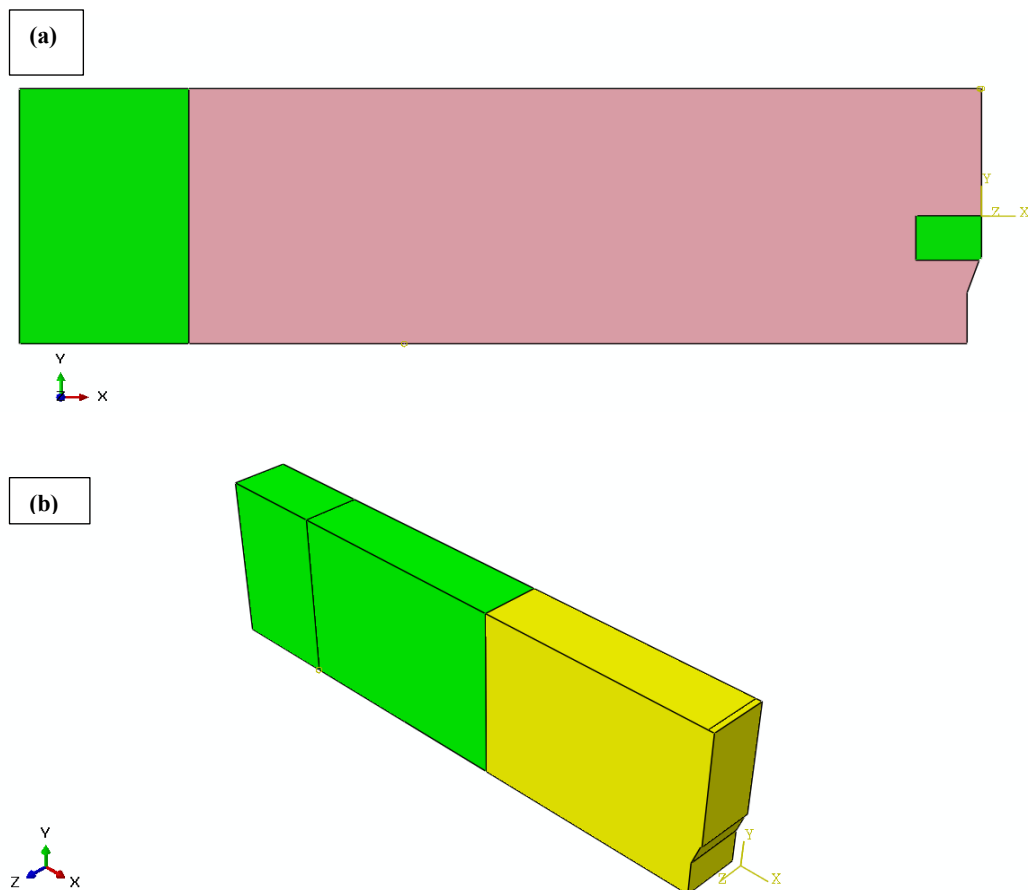


Figure3. 8 Meshing controls of specimen model in Abaqus. (a): 2-D model, (b): 3-D model

After defining meshing controls, seeding of edges were done with a lot of various combinations of edge seeds reaching to appropriate seeding combination. Initial analysis for 2-D model was done with linear elements (CPE4R), but convergence of results was not reached. Because of this, element type is changed to quadrilateral to have a more accurate stress analysis. Element type used for this specimen model is CPE8R (an 8-node biquadratic plane strain quadrilateral, reduced integration). A convergence study were done and the final mesh of the specimen model is obtained with a total number of 113345 quadratic quadrilateral elements of type CPE8R. And for 3-D model meshing was done by using element type of C3D8 (an 8-node linear brick) and a total number of 125334 elements. Meshing patterns for both models are shown in Figure 3.9.

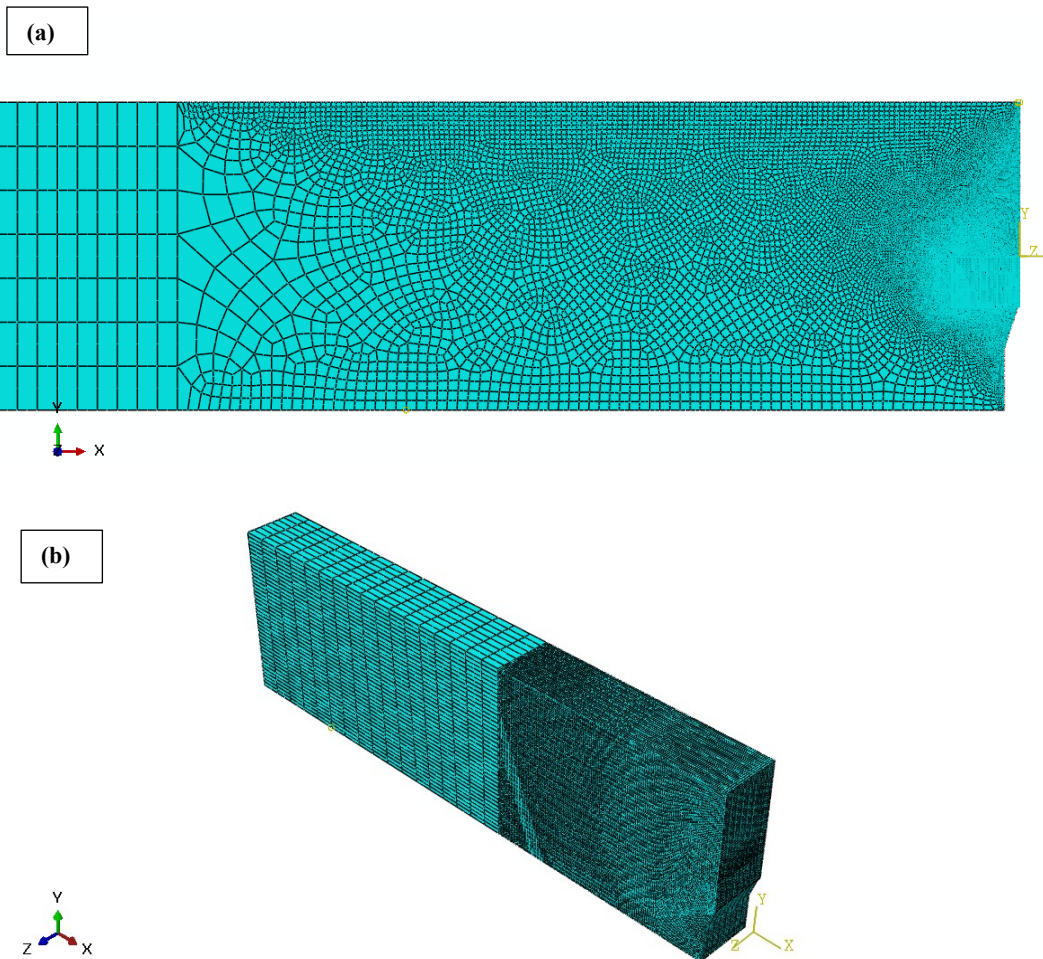


Figure3. 9 Meshing pattern of specimen model in Abaqus. (a): 2-Dmodel, (b): 3-D model

In the above figure, fine mesh around notch tip is magnified in Figure 3.10 for 2-D model and Figure 3.11 for 3-D model.

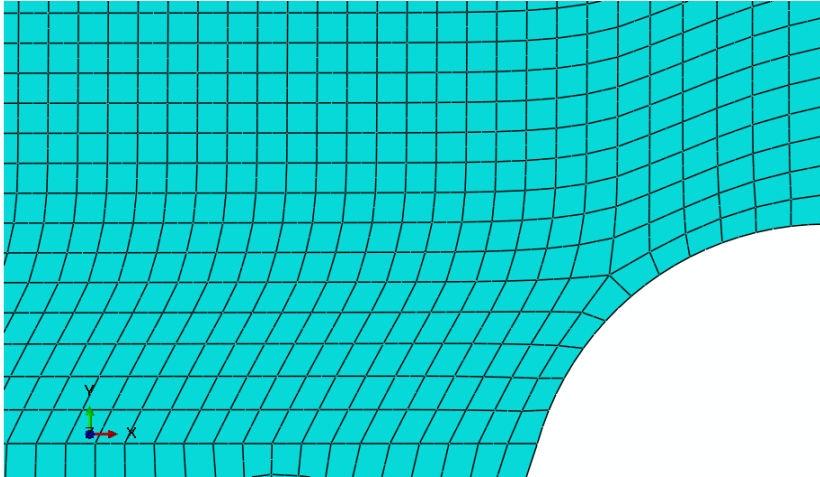


Figure3. 10 Fine mesh around notch of specimen 2-D model in Abaqus

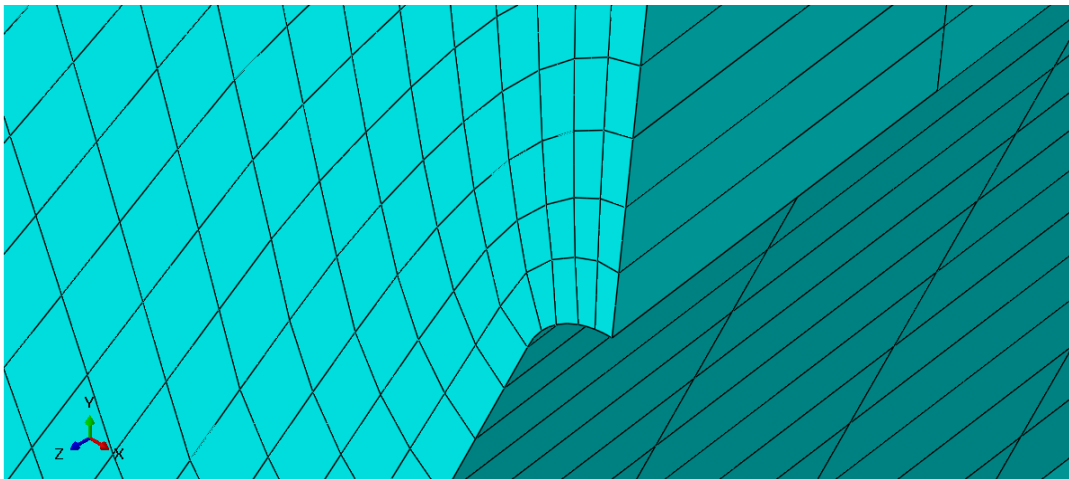


Figure3. 11 Fine mesh around notch tip of specimen 3-D model in Abaqus

Next task was creating jobs and submitting models to analyze. Figure 3.12 shows the result of linear elastic analysis as stress distribution around the notch tip of the specimen. Red colored regions have the highest stress magnitudes. The maximum value for stress in the notch tip (applied load is  $P=800$  [N]) is:

$$\begin{array}{llll}
 \sigma_{max} = 116.798 & \text{MPa} & \text{2-D model} & \\
 \sigma_{max} = 80.776 & \text{MPa} & \text{3-D model} & (3.1)
 \end{array}$$

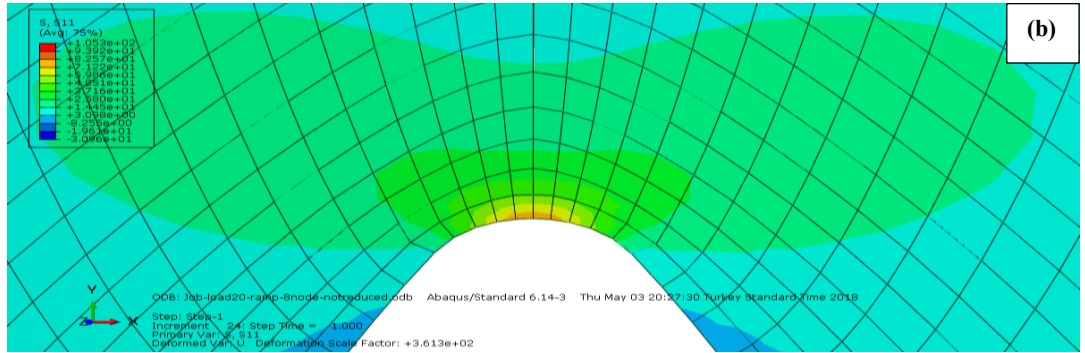
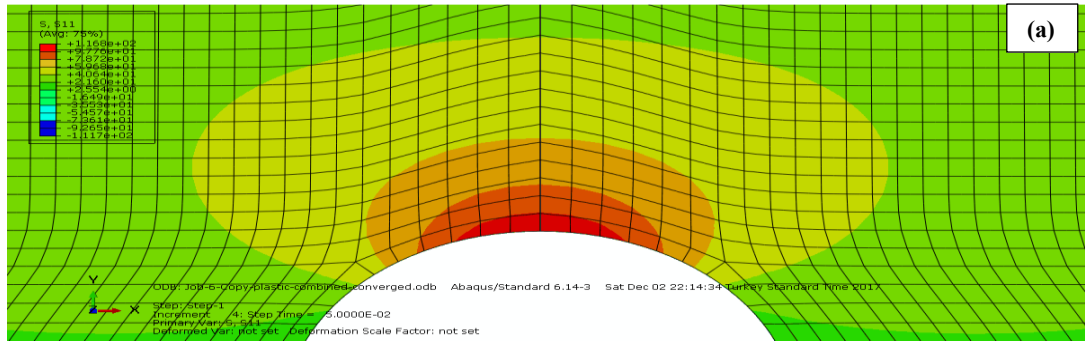


Figure3. 12 Stress distribution around notch tip analyzed by Abaqus. (a): 2-D model, (b): 3-D model  
Stress distribution extending from notch root to surface where the loading is applied is also shown in Figure 3.13.

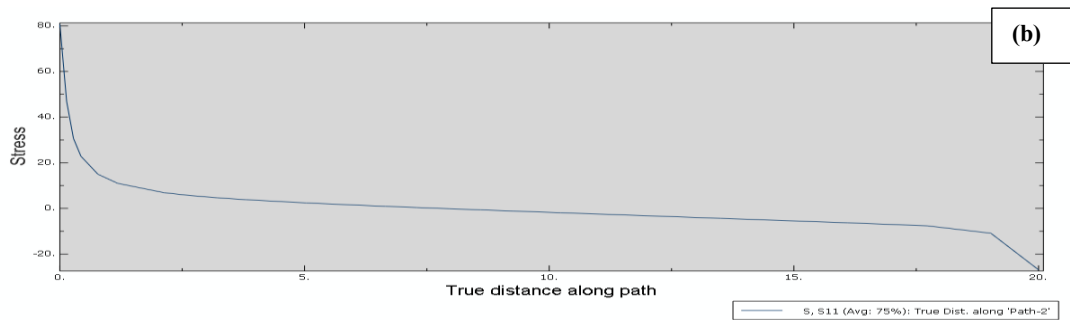
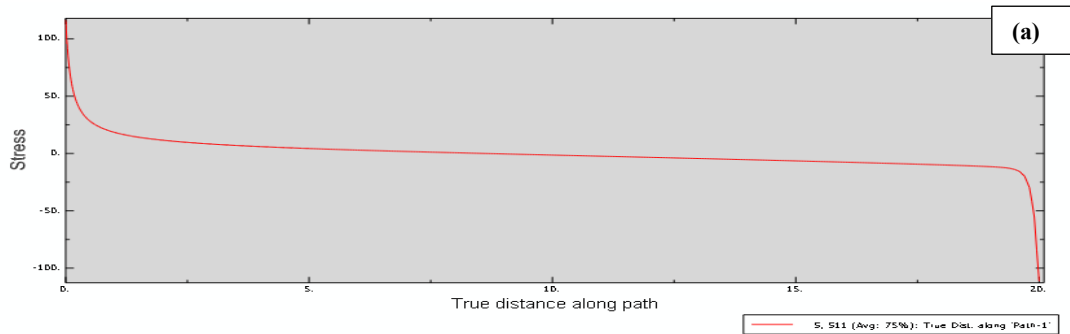


Figure3. 13 Stress distribution extending from notch root to surface where the loading is applied.

Also a stress analysis was done with 3D quarter model with plane strain boundary condition to check 2-D stress analysis availability. The result of analysis as stress around the notch and also stress distribution of the notch tip through thickness of model is shown in figure 3.14.

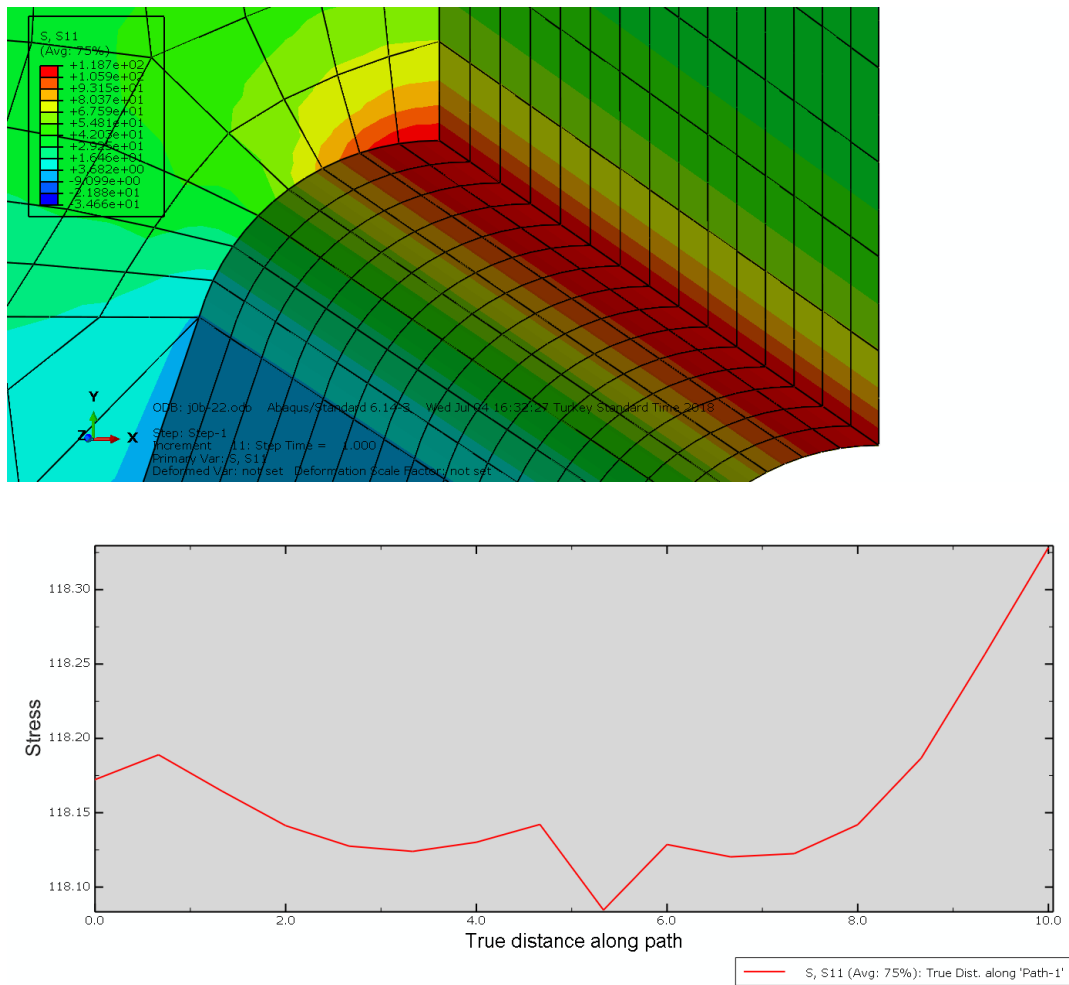


Figure3. 14 (a) 3-D quarter model stress analysis with plane strain boundary condition. (b) stress distribution of notch tip through thickness of model

From figure 3.14 it is concluded that both 2-D and 3-D analyses with plane strain boundary condition give same stress results.

### 3.4 Calculation of Elastic and Fatigue Stress Concentration Factor, $K_t$ and $K_f$

In order to obtain elastic stress concentration factor,  $K_t$ , net sectional nominal stress of the notch tip,  $\sigma_{nom}$ , is also required and it is calculated using following formula:

$$\sigma_{nom} = \frac{Mc}{I} \quad (3.2)$$

Where,

$\sigma_{nom}$  = nominal stress

M = bending moment

c = distance from neutral axis to extreme fiber

I = moment of inertia

With maximum stress and net sectional nominal stress of notch tip in hand now it is possible to obtain elastic stress concentration factor of the notch using following formula:

$$K_t = \frac{\sigma_{max}}{\sigma_{nom}} \quad (3.3)$$

Applied load and obtained results for stress and stress concentration factor are summarized in Table 3.3.

Table3. 3: Applied load and corresponding  $\sigma_{max}$ ,  $\sigma_{nom}$ , and  $K_t$

Applied Load [N]	M [N.m]	C [m]	I [M <sup>4</sup> ]	Maximum Stress at Notch Tip $\sigma_{max}$ [MPa]		Nominal Stress $\sigma_{nom}$ [MPa]	Elastic Stress Concentration Factor $K_t$	
				2-D	3-D		2-D	3-D
800	24	0.01	(4/3)(10 <sup>-8</sup> )	116.798	80.776	18	6.4887	4.487

Topper et al.[4] suggested to use fatigue stress concentration factor,  $K_f$ , instead of elastic stress concentration factor  $K_t$ , since the predicted fatigue lives using  $K_f$  fits better to actual experimental results.

As discussed in section 9.3 of chapter II, there are two formulas for obtaining fatigue stress concentration factor, one is suggested by Neuber and the other is suggested by Peterson as:

$$K_{f_{neuber}} = 1 + \frac{K_t - 1}{1 + \sqrt{\frac{\beta}{\rho}}} \quad (3.4)$$

$$K_{f_{Peterson}} = 1 + \frac{K_t - 1}{1 + \frac{\alpha}{\rho}} \quad (3.5)$$

Where

$\rho$  = notch radius

$\beta$  = Neuber's material constant

$\alpha$  = Peterson's material constant

For obtaining Neuber's material constant following formula can be used which is developed by fitting the curve that Kuhn provided[34]:

$$\log \beta = -9.402 \times 10^{-9} \sigma_u^3 + 1.422 \times 10^{-5} \sigma_u^2 - 8.249 \times 10^{-3} \sigma_u + 1.451 \quad (3.6)$$

$$\beta, \text{ mm} = 10^{\log \beta} \quad (3.7)$$

And for aluminum alloys the suggested value for Peterson's material constant in reference[15] is:

$$\alpha = 0.51 \text{ mm} \quad (3.8)$$

Table 3.4 provides the corresponding results for fatigue stress concentration factor calculated by Neuber's and Peterson's formula.

Table3. 4: fatigue stress concentration factor

Peterson's material constant $\alpha$	Neuber's material constant $\beta$	$K_{f_{neuber}}$		$K_{f_{peterson}}$	
		2-D	3-D	2-D	3-D
0.51 mm	0.9107	2.8871	2.198	2.8055	2.147

As seen in Table 3.4, value of  $K_f$  calculated using Neuber formula is higher than that calculated using Peterson formula. So with Neuber formula for elastic stress concentration factor, predicted lives are more conservative than that with Peterson formula.

### 3.5 Cyclic Material Properties and Calculation of Cyclic Local Stresses and Strains

With  $K_f$  value and cyclic material properties in hand it is possible to obtain cyclic local stresses and strains and ranges of them using Neuber's rule discussed in section 9.4.2 of chapter II. The cyclic properties of al 6082 T6 is obtained from two difference references[47][48] with slightly different values and are summarized in Table 3.5.

Table3. 5: Strain-life and cyclic properties of 6082 T6 aluminum alloy

Properties	Reference[47]	Reference[48]
Cyclic hardening exponent, $n'$	0.064	0.064
Cyclic hardening coefficient, $K'$ [MPa]	443	444
Fatigue strength exponent, b	-0.0695	-0.07
Fatigue strength coefficient, $\sigma'_f$ [MPa]	485	487
Fatigue ductility exponent, c	-0.827	-0.593
Fatigue ductility coefficient, $\epsilon'_f$	0.773	0.209

The corresponding formulas to obtain cyclic local stresses and strains are summarized below:

$$\varepsilon_{max}\sigma_{max} = \frac{(K_f S_{max})^2}{E} \quad (3.9)$$

$$\varepsilon_{max} = \frac{\sigma_{max}}{E} + \left(\frac{\sigma_{max}}{K'}\right)^{1/n'} \quad (3.10)$$

$$\frac{\sigma_{max}^2}{E} + \sigma_{max} \left(\frac{\sigma_{max}}{K'}\right)^{1/n'} = \frac{(K_f S_{max})^2}{E} \quad (3.11)$$

$$\Delta\varepsilon\Delta\sigma = \frac{(K_f \Delta S)^2}{E} \quad (3.12)$$

$$\Delta\varepsilon = \frac{\Delta\sigma}{E} + 2 \left(\frac{\Delta\sigma}{2K'}\right)^{1/n'} \quad (3.13)$$

$$\frac{(\Delta\sigma)^2}{E} + 2\Delta\sigma \left(\frac{\Delta\sigma}{2K'}\right)^{1/n'} = \frac{(K_f \Delta S)^2}{E} \quad (3.14)$$

$$\sigma_{min} = \sigma_{max} - \Delta\sigma \quad (3.15)$$

$$\sigma_m = \frac{\sigma_{max} + \sigma_{min}}{2} \quad (3.16)$$

Cyclic local stresses and strains and corresponding ranges were calculated using Equations (3.9)-(3.16) for each one of the cyclic material properties given in Table 3.5. These calculations were done for elastic stress concentration factor,  $K_t$ , and also for both Neuber and Peterson fatigue stress concentration factors,  $K_f$ , separately. The results are presented in Table 3.6 and Figure 3.15. As an example the calculation process considering material properties of reference[47] and  $K_{f_{neuber}}$  obtained from 2-D analysis are described below:

To obtain  $\sigma_{max}$ , the equations (3.9) and (3.10) were combined and a code in matlab[49] was written. With some iterations the  $\sigma_{max}$  value was obtained. Iterations are done by assuming a trial value then comparing the values of left and right side of

equation, when they match, the assumed trial value will be the answer. Matlab code is as following:

```
smax=180
smin=18
Δs=162 MPa
kt=2.8871
E=70000
kprime=443
nprime=0.064
sigmamax=323.37
(((kt*smax)^2)/E)
(((sigmamax)^2)/E)+((sigmamax)*((sigmamax/kprime)^(1/nprime)))
```

Next  $\Delta\sigma$  was obtained through combining Equations (3.12) and (3.13). Again with a code written in matlab and with some iterations the corresponding value for  $\Delta\sigma$  was obtained. The matlab code is as follows:

```
smax=180
smin=18
deltas=162
kt=2.8871
E=70000
kprime=443
nprime=0.064
deltastigma=464.781
(((kt*deltas)^2)/E)
(((deltastigma)^2)/E)+(2*(deltastigma)*((deltastigma/(2*kprime)^(1/nprime))))
```

Next corresponding values for  $\sigma_{\min}$ ,  $\sigma_m$ ,  $\epsilon_{\max}$ , and  $\Delta\epsilon$  are obtained through a code written in matlab as follows:

```
kt=2.8871
smax=180
E=70000
sigmamax=323.37
deltastigma=464.781
sigmamin=sigmamax-deltastigma
sigmam=(sigmamax+sigmamin)/2
epsilonmax=((kt*smax)^2)/(E*sigmamax)
deltaepsilon=((kt*deltas)^2)/(E*deltastigma)
```

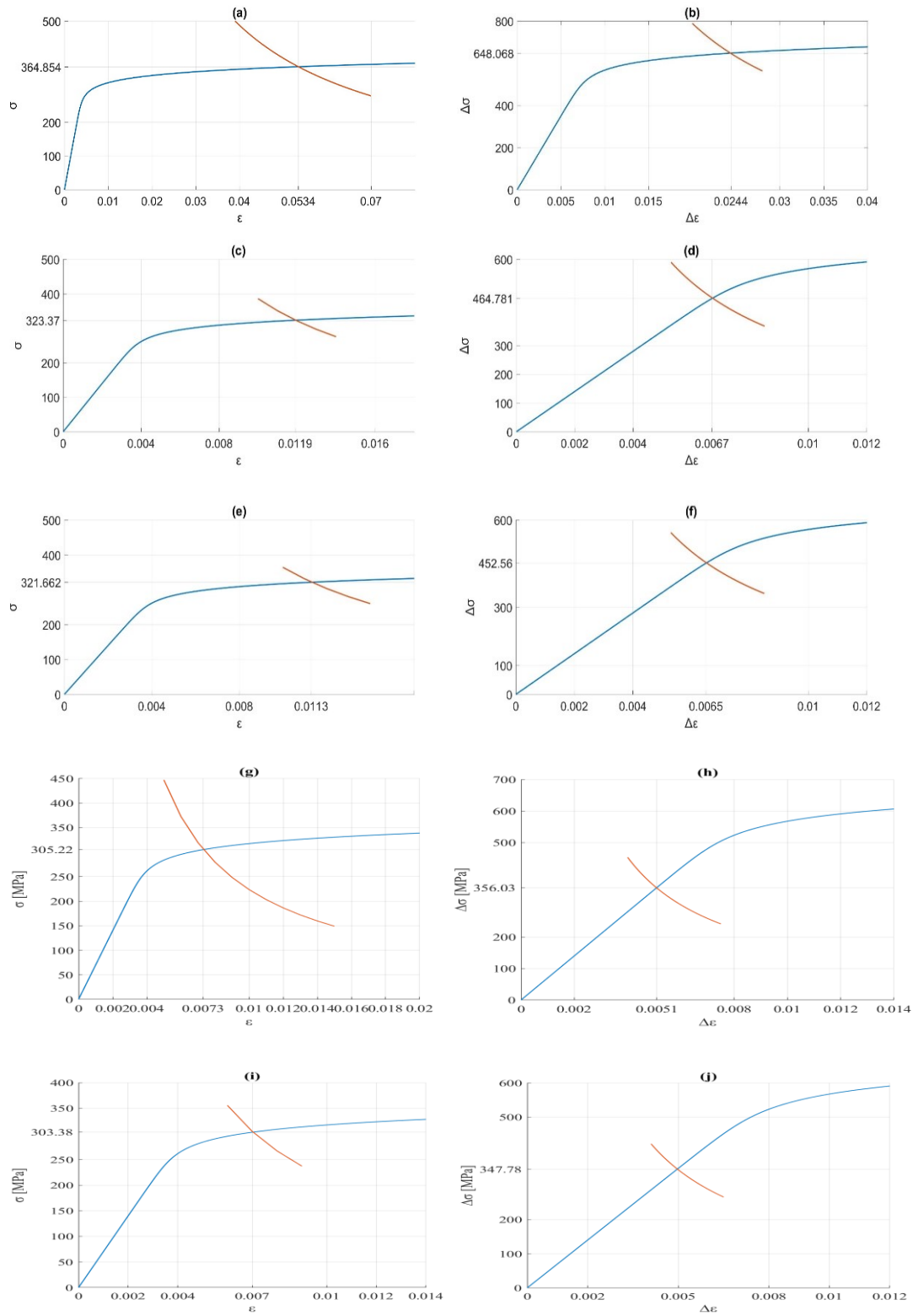


Figure3. 15 Determination of cyclic local stresses and strains and their ranges using Neuber's rule for material reference[47]. (a) & (b) using  $K_t$ ; (c) & (d) using  $K_{f_{neuber}}$ ; (e) & (f) using  $K_{f_{peterson}}$ . All by 2-D model result. And by 3-D model result: (g) & (h) using  $K_{f_{neuber}}$ ; (i) & (j) using  $K_{f_{peterson}}$

Table3. 6: Cyclic local stresses and strains

	Material Reference[47]					Material Reference[48]				
	2-D			3-D		2-D			3-D	
	$K_t$ 6.4887	$K_{f_{neuber}}$ 2.8871	$K_{f_{Peterson}}$ 2.8055	$K_{f_{neuber}}$ 2.8055	$K_{f_{Peterson}}$ 2.147	$K_t$ 6.4887	$K_{f_{neuber}}$ 2.8871	$K_{f_{Peterson}}$ 2.198	$K_{f_{neuber}}$ 2.8055	$K_{f_{Peterson}}$ 2.147
$\sigma_{max}$ [MPa]	364.85	323.37	321.66	305.22	303.38	365.61	324.00	322.29	305.77	303.92
$\Delta\sigma$ [MPa]	648.06	464.78	452.56	356.03	347.78	649.34	464.87	452.62	356.03	347.78
$\sigma_{min}$ [MPa]	-283.21	-141.41	-130.89	-50.81	-44.4	-283.7	-140.86	-130.33	-50.26	-43.86
$\sigma_m$ [MPa]	40.82	90.979	95.382	127.20	129.49	40.944	91.570	95.981	127.75	130.03
$\varepsilon_{max}$	0.0534	0.0119	0.0113	0.0073	0.0070	0.0533	0.0119	0.0113	0.0073	0.0070
$\Delta\varepsilon$	0.0244	0.0067	0.0065	0.0051	0.0050	0.0243	0.0067	0.0065	0.0051	0.0050

In above results it is seen that minimum cyclic stress is negative while R=0.1. The negative cyclic minimum stress comes from residual stresses induced by cyclic loadings.[15]

Beside calculated local stresses and strains using Neuber's rule summarized in Table 3.6, 2-D and 3-D elasto-plastic analysis was done for ten cycles in Abaqus software to obtain local stress and strains at the notch tip of specimen. The loading and boundaries are in three point bending condition as in previous analyses. The specimen material stress-strain data shown in figure 3.16(a), was defined for Abaqus by filling a table to perform elasto-plastic analysis. Cyclic loading was applied through defining an amplitude for ten cycles. The defined amplitude is shown in Figure 3.16(b). The amplitude value of 1 is maximum applied load (8KN) and the amplitude value of .1 is the minimum applied load (0.8KN). For 3-D analysis a mesh with total number of 151140 linear hexahedral elements of type C3D8R is used.

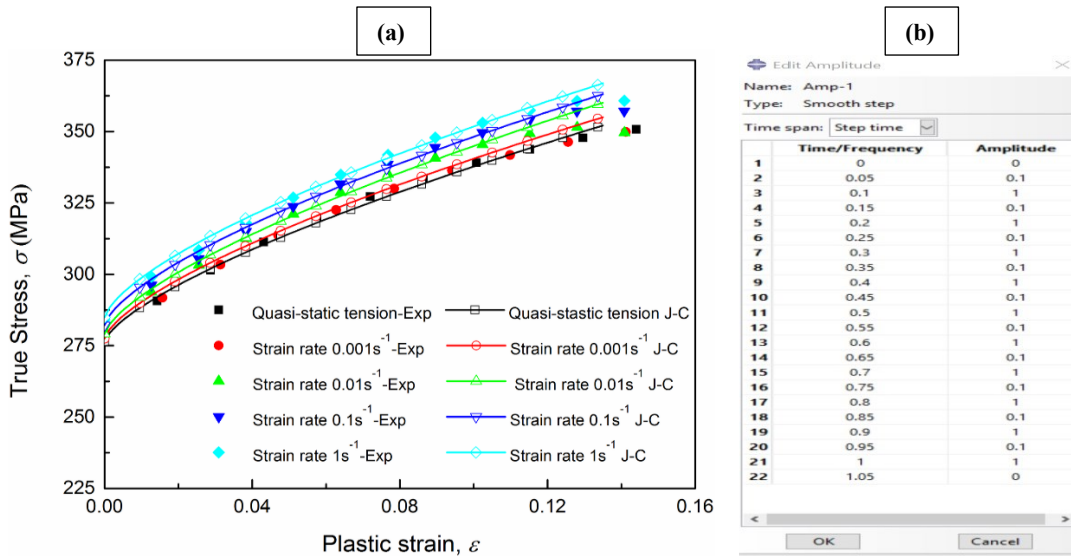


Figure 3.16 (a): Al 6082 T6 stress-strain plot[50] (b): Defined Amplitude in Abaqus for ten cycles

Figure 3.17 shows the stress results of 2-D and 3-D elasto-plastic analysis. In abaqus there is no such an option as selecting just plane stress or plain strain, instead both of them can be selected and then a depth of model is asked which in our model is 20 [mm].

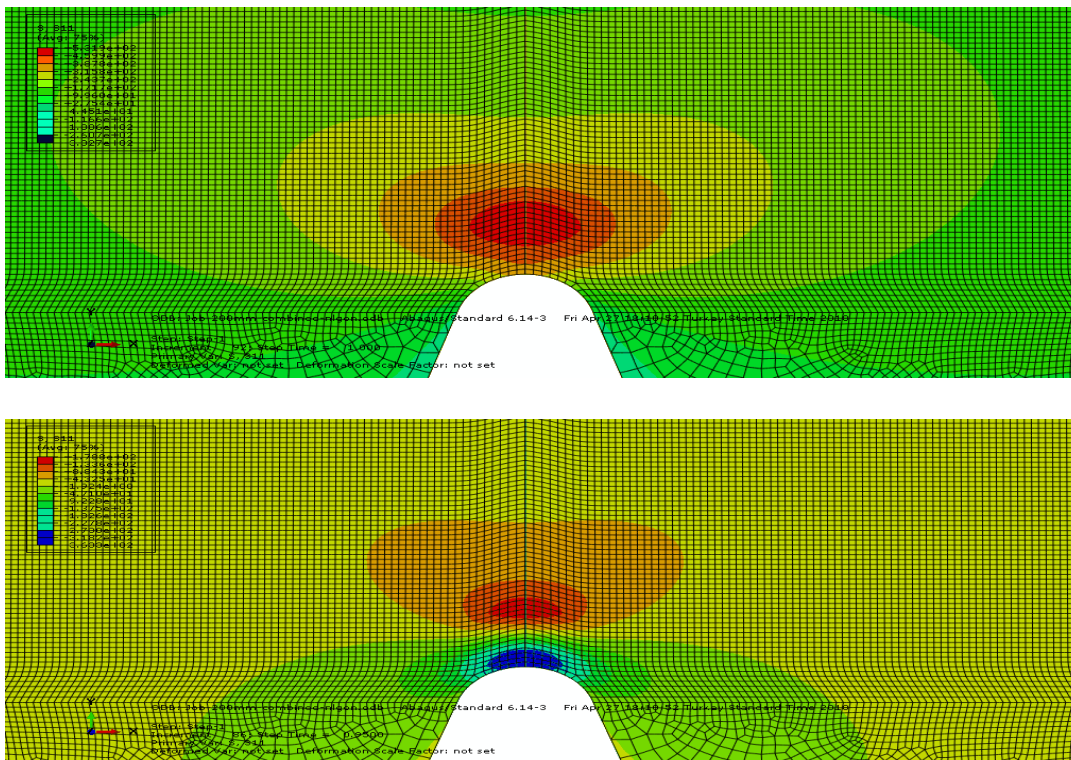


Figure 3.17 (continued in next page)

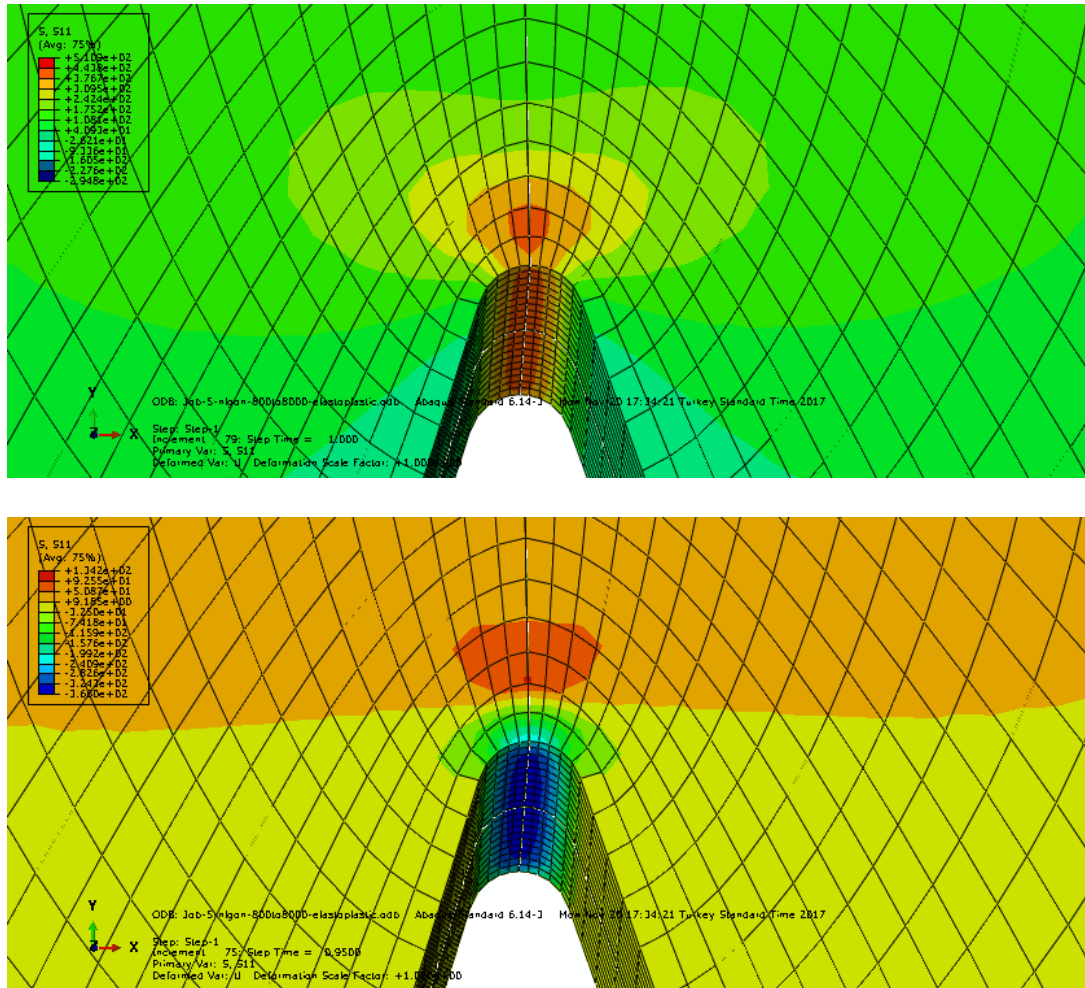


Figure3. 17 maximum and minimum local stresses after ten cycles. (a) and (b) for 2-D analysis and (c) and (d) for 3-D analysis

With examining Abaqus analysis results, small reduction in maximum stress magnitude and small increase of residual stress in after each cycle was observed. Local stresses and strains (in x-direction) of the notch tip at the end of ten cycles from each 2-D and 3-D analysis are summarized in Table 3.7.

Table3. 7: local stresses and strains at the end of ten cycles obtained from 2-D and 3-D analysis in Abaqus. (E) is total strain. (LE) is the logarithmic strain which is true strain.

	2-D	3-D
$\sigma_{max}$ [MPa]	335.16	368.7
$\sigma_{min}$ [MPa]	-320.217	-237.9
$\Delta\sigma$ [MPa]	655.87	606.6
$\sigma_m$ [MPa]	7.765	65.4
$\varepsilon_{max}$	0.02656 (LE) 0.02621 (E)	0.01473 (LE) 0.01462 (E)
$\varepsilon_{min}$	0.01086(LE) 0.01080 (E)	0.00704 (LE) 0.00701 (E)
$\Delta\varepsilon$	0.0157 (LE) 0.0155	0.00769 (LE) 0.00761 (E)

The difference between 2-D and 3-D analysis results may arise from the plane stress/strain assumption applied in 2-D model. But 3-D analysis results are more close to Neuber rule results calculated using stress concentration factor acquired using 2-D analysis. The little difference may be due to lack of applied cycles which here are ten. To get more accurate results, it is required that elasto-plastic analysis should be done for approximately half of specimen life cycles (it requires powerful and expensive computers and it is time consuming).

### 3.6 Fatigue Crack Initiation Life Prediction

After obtaining cyclic material properties and cyclic local stresses and strains presented in Table 3.5 and (3.6-3.7) respectively, next step was prediction of fatigue

crack initiation life using strain-life formula described in section 6 of chapter II.  $N_f$  is the life (number of cycles) to be calculated not  $(2N_f)$  which is reversals. This formula is as follows:

$$\frac{\Delta\varepsilon}{2} = \varepsilon_a = \frac{\Delta\varepsilon_e}{2} + \frac{\Delta\varepsilon_p}{2} = \frac{\sigma'_f}{E} (2N_f)^b + \varepsilon'_f (2N_f)^c \quad (3.17)$$

As observable in Table 3.6, a considerable cyclic local mean stress exists, so it is useful to apply strain-life formulas which are modified considering mean stress effect. These formulas are described in section 8 of chapter II and are summarized as follows:

Modified Morrow Equation

$$\frac{\Delta\varepsilon}{2} = \frac{\sigma'_f - \sigma_m}{E} (2N_f)^b + \varepsilon'_f (2N_f)^c \quad (3.18)$$

Manson-Halford Equation

$$\frac{\Delta\varepsilon}{2} = \frac{\sigma'_f - \sigma_m}{E} (2N_f)^b + \varepsilon'_f \left( \frac{\sigma'_f - \sigma_m}{\sigma'_f} \right)^{c/b} (2N_f)^c \quad (3.19)$$

SWT Equation

$$\sigma_{max} \varepsilon_a = \frac{(\sigma'_f)^2}{E} (2N_f)^{2b} + \sigma'_f \varepsilon'_f (2N_f)^{b+c} \quad (3.20)$$

Walker Equation ( $R = \frac{\sigma_{min}}{\sigma_{max}}$ )

$$\frac{\Delta\varepsilon}{2} = \frac{\sigma'_f}{E} \left( \frac{1-R}{2} \right)^{(1-\gamma)} (2N_f)^b + \varepsilon'_f \left( \frac{1-R}{2} \right)^{c(1-\gamma)/b} (2N_f)^c \quad (3.21)$$

Using Equations (3.17) to (3.21), fatigue crack initiation life was calculated for each  $K_{f_{neuber}}$  and  $K_{f_{Peterson}}$  and for each set of material properties presented in Table 3.5. Also by using local stresses and strains obtained by 3-D elasto-plastic analysis, fatigue crack initiation life was calculated. The results are presented in Table 3.8.

Table3. 8: Fatigue crack initiation life predictions

	Material Reference[47]					Material Reference[48]				
	$K_{f_{neuber}}$		$K_{f_{peterson}}$		3-D FEA	$K_{f_{neuber}}$		$K_{f_{peterson}}$		3-D FEA
	2-D	3-D	2-D	3-D		2-D	3-D	2-D	3-D	
Strain-Life Equation [cycles]	19400	-	37200	-	7100	36500	-	64500	-	14900
Modified Morrow [cycles]	4160	15500	5700	21000	3050	9350	33000	12900	43000	6650
SWT [cycles]	3984	23400	4690	27500	1462	6620	33500	7745	38500	2410
Walker [cycles]	3510	33000	6040	52000	2600	6650	40000	10450	60000	5450
Manson-Halford [cycles]	980	7000	1600	11000	900	1870	8300	2800	12500	1900

With inspecting Table 3.8, it is observable that in general, the modified Morrow and walker formulas give highest life for 2-D and 3-D respectively, and the Manson-Halford formula gives the least life.

To illustrate the procedure of calculating fatigue crack initiation life by using material properties in reference[47] and Neuber fatigue stress concentration factor  $K_{f_{neuber}}$ , a code is presented below:

In this matlab code of, fatigue crack initiation life formulas corresponding to various estimation approaches are written and lives are found by iterations:

Strain-Life Equation:

$\Delta\epsilon = 0.0067$

$\sigma' = 485$

$b = -0.0695$

$c = -0.827$

$\epsilon' = 0.773$

$E = 70000$

$N_i = 19400$

$\Delta\epsilon / 2$

$$\left( \frac{\sigma'}{E} \right)^2 \left( 2N_i \right)^b + \left( \epsilon' \right)^c \left( 2N_i \right)^c$$

Modified Morrow:

$\sigma_m = 90.979$

$\Delta\epsilon = 0.0067$

$\sigma' = 485$

$b = -0.0695$

$c = -0.827$

$\epsilon' = 0.773$

$E = 70000$

$N_i = 4160$

$\Delta\epsilon / 2$

$$\left( \frac{\sigma' - \sigma_m}{E} \right)^2 \left( 2N_i \right)^b + \left( \epsilon' \right)^c \left( 2N_i \right)^c$$

SWT:

$\sigma_{max} = 323.37$

$\Delta\epsilon = 0.0067$

$\sigma' = 485$

$b = -0.0695$

$c = -0.827$

$\epsilon' = 0.773$

$N_i = 3984$

$E = 70000$

$\sigma_{max} \left( \Delta\epsilon / 2 \right)$

$$\left( \frac{\sigma'}{\sigma_{max}} \right)^2 \left( 2N_i \right)^{2b} + \left( \epsilon' \right)^c \left( 2N_i \right)^{b+c}$$

Walker:

R=-0.4319

gamma=0.641

deltaepsilon=0.0067

sigmafprime=485

b=-0.0695

c=-0.827

epsilonfprime=0.773

E=70000

Ni=3510

deltaepsilon/2

$$\left(\frac{\sigma_f'}{E}\right)^{\frac{1-R}{2}} (1-\gamma)^{\frac{1-\gamma}{2}} (2N_i)^b + \epsilon_f' \left(\frac{1-R}{2}\right)^{\frac{c}{2}} (1-\gamma)^{\frac{c}{2}} (2N_i)^c$$

Manson-Halford:

sigmam=90.979

deltaepsilon=0.0067

sigmafprime=485

b=-0.0695

c=-0.827

epsilonfprime=0.773

Ni=980

deltaepsilon/2

$$\left(\frac{\sigma_f' - \sigma_m}{E}\right)^{\frac{1-R}{2}} (2N_i)^b + \epsilon_f' \left(\frac{\sigma_f' - \sigma_m}{\sigma_f'}\right)^{\frac{c}{2}} (2N_i)^c$$

### 3.7 Fatigue Crack Growth Life Prediction

Here an initial crack size of 1 [mm] is assumed. In order to apply LEFM concepts it is also necessary that the crack length emanating from the notch root should be long enough so that it extends beyond the plastic zone around the notch tip. This length in general is about 1 mm. The next step is to calculate the number of cycles to grow the nucleated crack to a desired length. This goal is accomplished by using Paris law and Walker equation for FCG. The main parameter in FCG equations is Stress intensity

factor range,  $\Delta K$ , as described in section 10.2 of chapter II. The formulas for calculation of  $\Delta K$  are summarized as follows:

$$\Delta K = \Delta\sigma_{nom}\sqrt{\pi a}f\left(\frac{a}{W}\right) \quad (3.21)$$

For three point bending configuration:

$$\Delta K = \frac{3\Delta PS}{2BW^2}\sqrt{a}\frac{1.99 - \frac{a}{W}\left(1 - \frac{a}{W}\right)\left(2.15 - 3.93\frac{a}{W} + 2.7\left(\frac{a}{W}\right)^2\right)}{\left(1 + 2\frac{a}{W}\right)\left(1 - \frac{a}{W}\right)^{\frac{3}{2}}} \quad (3.22)$$

where

$S$  = span length

$\Delta P$  = applied load range ( $P_{\max} - P_{\min}$ )

$B$  = thickness of specimen

$W$  = specimen height

$a$  = crack length

General form of FCG relation is as follows:

$$\frac{da}{dN} = f(\Delta K, R) \quad (3.23)$$

And some of FCG equations are also summarized as follows:

Paris equation:

$$\frac{da}{dN} = C\Delta K^m \quad (3.24)$$

where  $C$  and  $m$  are Paris constants.

Walker equation:

$$\frac{da}{dN} = \frac{C_0}{(1-R)^{m(1-\gamma)}} (\Delta K)^m \quad (3.25)$$

Where  $C_0$  and  $m$  are Paris constant for  $R = 0$  condition and  $\gamma$  is Walker constant.

To calculate the required number of cycles to grow a crack from an initial length,  $a_i$ , to a final length,  $a_f$ , integration of one of the FCG equations can be done. Since  $f(a/W)$  is changing as the crack grows, closed form integration is not possible. With numerical integration from one of FCG equations, it is possible to obtain FCG life. For this purpose equation (3.24) is discretize in  $n$  intervals within the range of initial value,  $a_i$ , and final value,  $a_f$ , of the crack size  $a$ , as follows:

$$\Delta a_j = a_{j+1} - a_j \quad (j = 1.2. \dots, n) \quad (3.26)$$

Then the initial integral is substituted by a summation as follows:

$$N = \int_{a_i}^{a_f} \left( \frac{dN}{da} \right) da = \sum_i^f \Delta N_j = \sum_i^f \frac{\Delta a_j}{f(\Delta K, R)} \quad (3.27)$$

The material data required for FCG is presented in Table 3.9 as follows:

Table3. 9: FCG material data[10],[51],[52]

Fatigue crack growth threshold $\Delta K_{th}$ [MPa $\sqrt{m}$ ]	Fracture toughness $K_{Ic}$ [MPa $\sqrt{m}$ ]	Paris constant C [mm/cycle/MPa $\sqrt{m}$ ]	Paris constant m	Walker equation constant $\gamma$
3	29	$2.71 \times 10^{-8}$	3.7	0.641
-	-	$1.8 \times 10^{-8}$	3.8	-
-	-	$6.1 \times 10^{-9}$	4.2	-
-	-	$3.31 \times 10^{-7}$	2.629	-

For the crack to grow it is needed that  $\Delta K$  be larger than its threshold value,  $\Delta K_{th}$ , and lower than critical value,  $K_{Ic}$ . In this study, at the minimum crack length (11 mm which is the notch depth plus the assumed initial crack size):

$$\Delta K = 15.049 \text{ MPa} > \Delta K_{th} = 3 \text{ MPa}$$

Calculation of above result was done in matlab using following code:

```
a=11
Pmax=8000
Pmin=800
B=20
W=30
S=120
KImax=10^(-3/2)*(Pmax/(B*sqrt(W)))*[(3*(S/W)*sqrt(a/W))/(2*(1+2*(a/W))*(1-(a/W))^(3/2))]*[1.99-
(a/W)*(1-(a/W))*(2.15-3.93*(a/W)+2.7*(a/W)^2)]
KImin=10^(-3/2)*(Pmin/(B*sqrt(W)))*[(3*(S/W)*sqrt(a/W))/(2*(1+2*(a/W))*(1-(a/W))^(3/2))]*[1.99-
(a/W)*(1-(a/W))*(2.15-3.93*(a/W)+2.7*(a/W)^2)]
deltaKI=KImax-KImin
```

A code with the knowledge described in section 3.7 was written in Matlab[49] software for the calculation of number of cycles to grow an initiated crack of 11 mm length to a 16.4 mm length (including the notch length which is 10 mm). The results are plotted as  $a$  versus  $N$ ,  $\Delta K$  versus  $N$ , and  $K_{\max}$  versus  $N$  shown in Figure 3.18. It is seen from the figures that Walker equation gives more conservative life estimations than Paris equation.

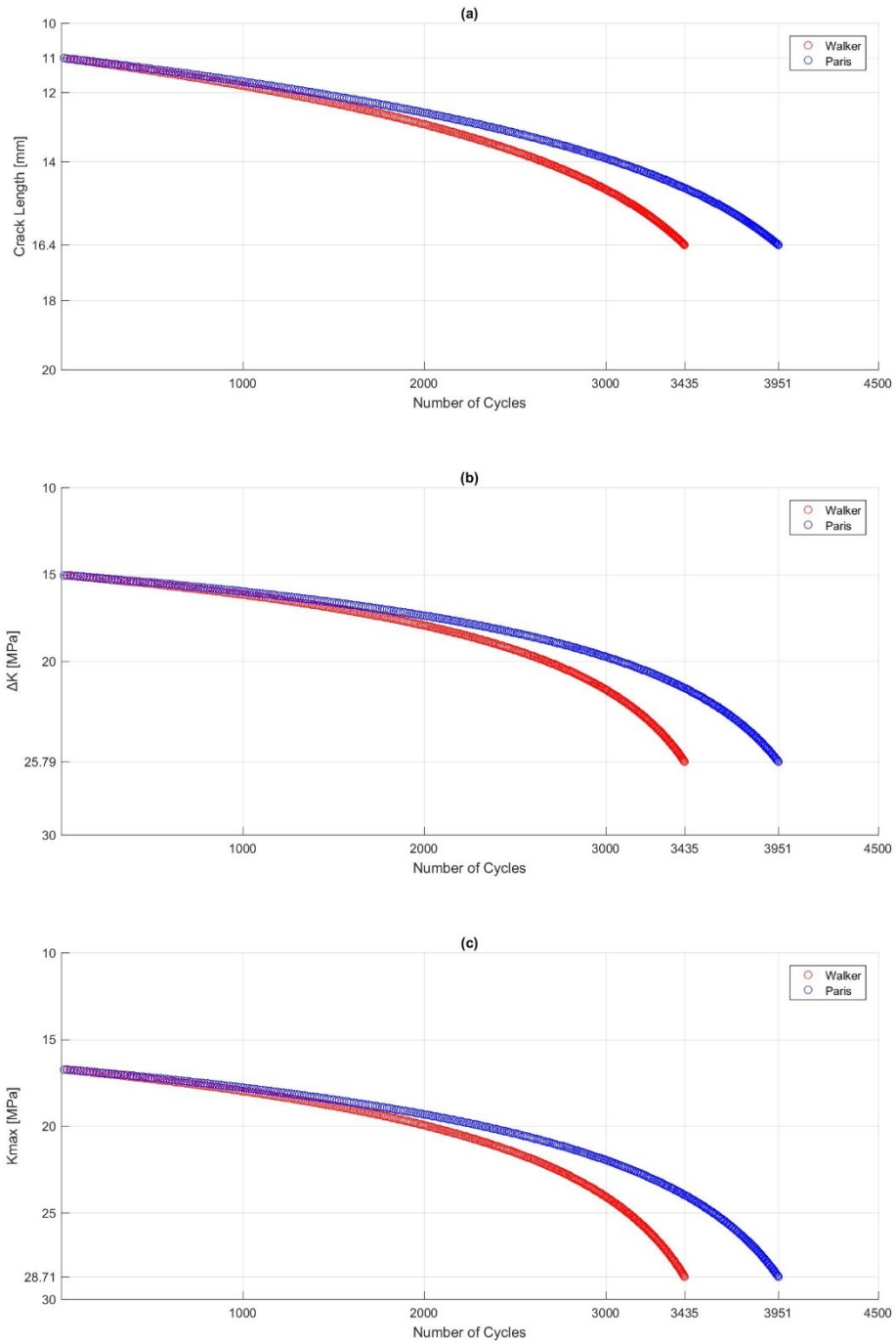


Figure3. 18 FCG life prediction using Walker equation for the initiated crack to grow from 1 [mm] length to 6.5 [mm] length. (a) Crack length versus Number of cycles; (b)  $\Delta K$  versus Number of cycles; (c)  $K_{max}$  versus Number of cycles

### 3.8 Total Fatigue Life

After calculation of fatigue crack initiation life in section 3.6 and crack propagation life up to desired length (16.4 mm), now it is time to add these two lives to get total life. For FCG, the life calculated using Walker equation is used. The results are presented in Table 3.10 as follows:

Table3. 10 Total fatigue life up to crack length of 16.4 mm

Total Fatigue Life up to 16.4 [mm]	Material Reference[47]					Material Reference[48]				
	$K_{f_{neuber}}$		$K_{f_{peterson}}$		3-D FEA	$K_{f_{neuber}}$		$K_{f_{peterson}}$		3-D FEA
	2-D	3-D	2-D	3-D		2-D	3-D	2-D	3-D	
Strain-Life Equation + FCG [cycles]	22835	-	40635	-	10535	39935	-	67935	-	18335
Modified Morrow + FCG[cycles]	7595	18935	9135	24435	6485	12785	36435	16335	46435	10085
SWT + FCG [cycles]	7419	26835	8125	30935	4897	10055	36935	11180	41935	5845
Walker + FCG [cycles]	6945	36435	9475	55435	6035	10085	43435	13885	15935	8885
Manson-Halford + FCG [cycles]	4415	10435	5035	14435	4335	5305	11735	6235	63435	5335



## CHAPTER IV

### EXPERIMENTAL ANALYSES

Three test were done under constant amplitude cyclic loadings. First test was done with a SEN (B) specimen with identical notch dimensions to simulated one in previous chapter. The width, thickness and length of specimen are 20 [mm], 30 [mm] and 550 [mm] respectively. This test was done as a pilot experiment in four point bending condition. In order to track crack growth in as many ways as possible, two gages were attached to the specimen. One was a strain gage attached to back face of the specimen to measure the strains and the other was a crack propagation gage (Vishay Micro-Measurements, TK-09-CPB02-005/DP). The pattern of crack propagation gage consists of 10 resistor strands of different length connected in parallel. It is bonded to the specimen over the crack propagation area. When the crack grows through the gage pattern it causes successive open-circuiting of the strands which results in an increase in total resistance. This produces stepped increases in resistance with successive open-circuiting as shown in figure 4.1. The distance between each strand is known, so it is possible to record the propagation of crack as each strands breaks. The specimen with bonded gages are shown in figure 4.2.

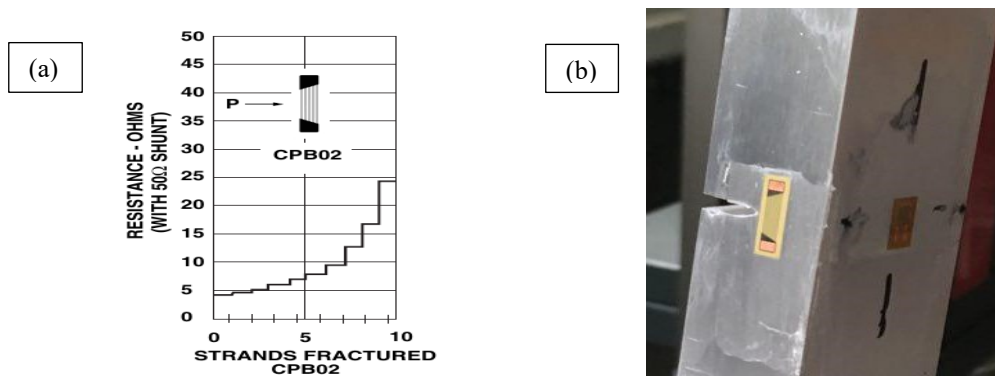


Figure 4. 1 (a): Gage resistance chart, (b): Specimen with bonded gages

In order to accelerate crack growth in this pilot test, it is decided to induce some tensile residual stresses at the notch root. For producing these residual stresses the specimen was under cyclic loading for 5 minutes in four point bending condition, such that the notch root is compressed. Then it was under cyclic loading with maximum value of 15 [kN] and minimum value of 1.5 [kN] at 10 [Hz]. Load values are selected according to ASTM E399 Standard. The cyclic loading was produced with DARTEC 9500 servo-hydraulic universal testing machine shown in figure 4.3.

After 8 minutes of cyclic loading the specimen fractured as shown in figure 4.4.



Figure 4. 2 (a): DARTEC machine, (b): Fractured specimen

By doing pilot test we concluded that

- Our data acquisition device worked well and we could collect all five data (Time, Force, Displacement, Crack length, Strain at the back side of the notch) successfully.
- The crack grew almost perfectly up to fracture that is there was no deviation in crack direction and the crack is quite straight without a zigzag pattern. Post fracture examination of crack surface visually indicated that the crack front is also quite straight, the parts near the boundary just slightly behind the part in the middle,

The results of this pilot test as various plots are shown in figure4.5.

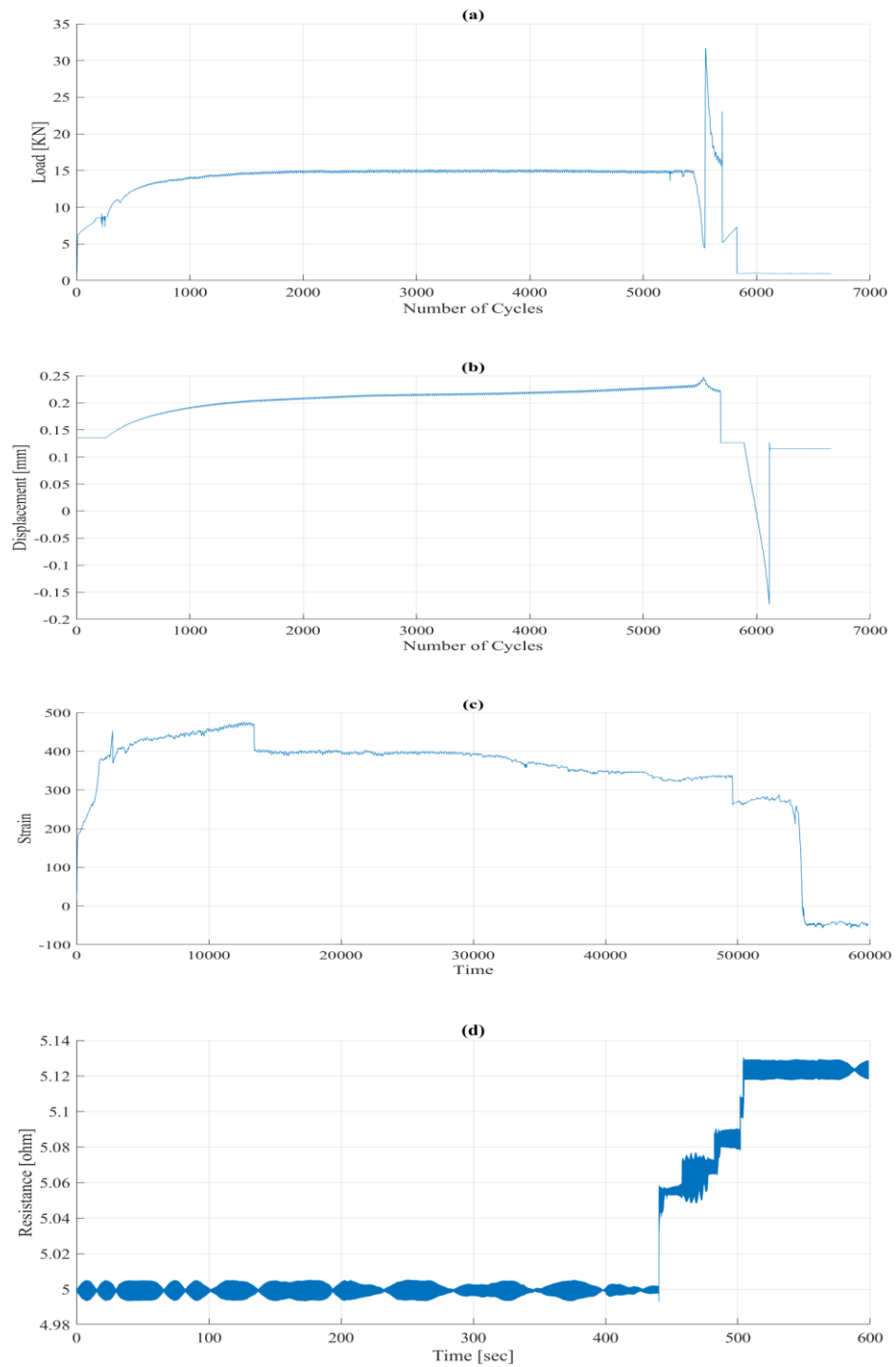


Figure 4. 3 Pilot test results as: (a) load-N, (b) displacement-N, (c) & (d) displacement-N & stiffness-N between 2000 cycles and 5500 cycles, and (e) crack propagation gage resistance-time. From (b), it can be seen that a small increase in displacement from 2000 cycles to 5500 cycles is due to crack growth.

The other two main tests were done with 2 identical specimens with the same dimensions of specimen simulated in previous chapter. For each specimen, one crack propagation gage (Vishay Micro-Measurements, TK-09-CPB02-005/DP) is bonded to one side of the notch, and a foil type gage (KRAK GAGE) is bonded to the other side of the notch. Photographs of specimen 1 with bonded gages are shown in figure 4.6 and photographs of specimen 2 with bonded gages are shown in figure 4.7.

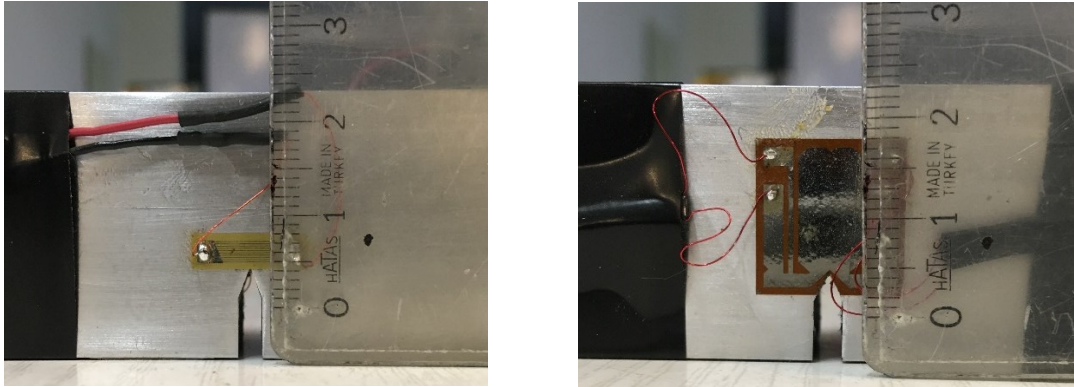


Figure 4. 4 Photographs of specimen 1 with bonded gages

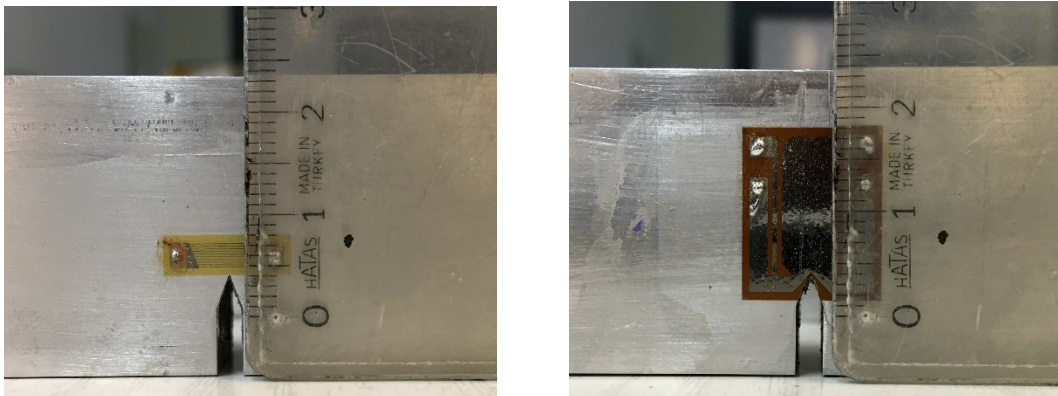


Figure 4. 5 Photographs of specimen 2 with bonded gages

The crack length foil (KRAK GAGE) serves as a transducer. The KRAK GAGE-structure consists of a conducting layer on an electrically insulating backing. The KRAK GAGE's are bonded, similar to the strain gage technique, onto the specimen and then connected to the FRACTOMAT. The crack length measuring system FRACTOMAT is based on the indirect potential drop method and continuously indicates the measuring values.[53]

The testing setup with the specimen is shown in figure 4.8.

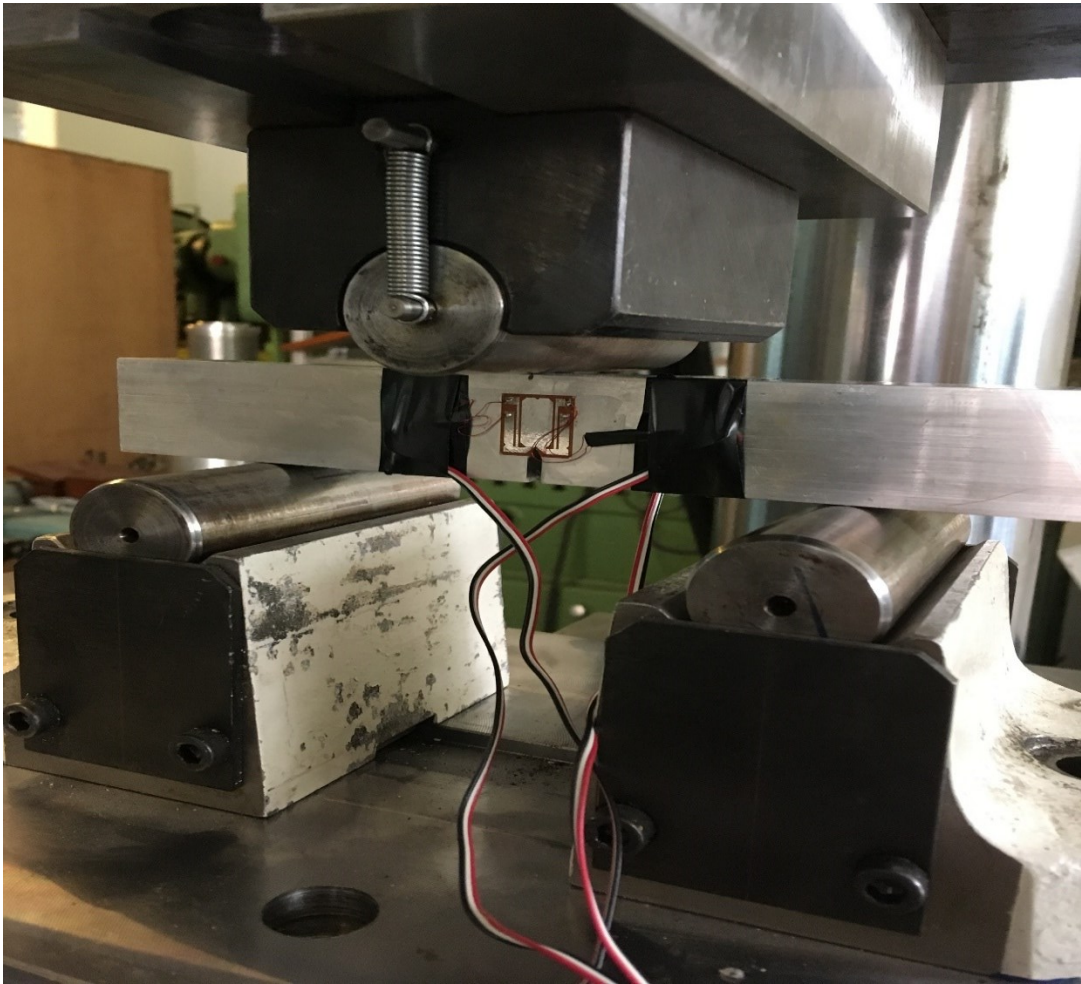


Figure 4. 6 The testing setup with specimen

The first specimen was loaded cyclically in opposite direction under four point bending condition for about 6 minutes with maximum and minimum load magnitudes of 8 KN and 1.2 KN to produce crack accelerating residual stresses in the specimen. Then for each specimen an identical test was done in three point bending condition.

For each test the loading inputs were 8 [KN] as maximum load and 0.8 [KN] as minimum load with a frequency of 10 [Hz]. These load values are based on the estimated  $K_{Ic}$  of the specimens and recommendations of ASTM E399 standard for fracture toughness test specimens. First test was done for the specimen with tensile residual stresses and the second test was done for the specimen without any residual stresses.

After test photographs of the specimen with residual and the specimen without residual stresses are shown in figure 4.9 and 4.10 respectively.

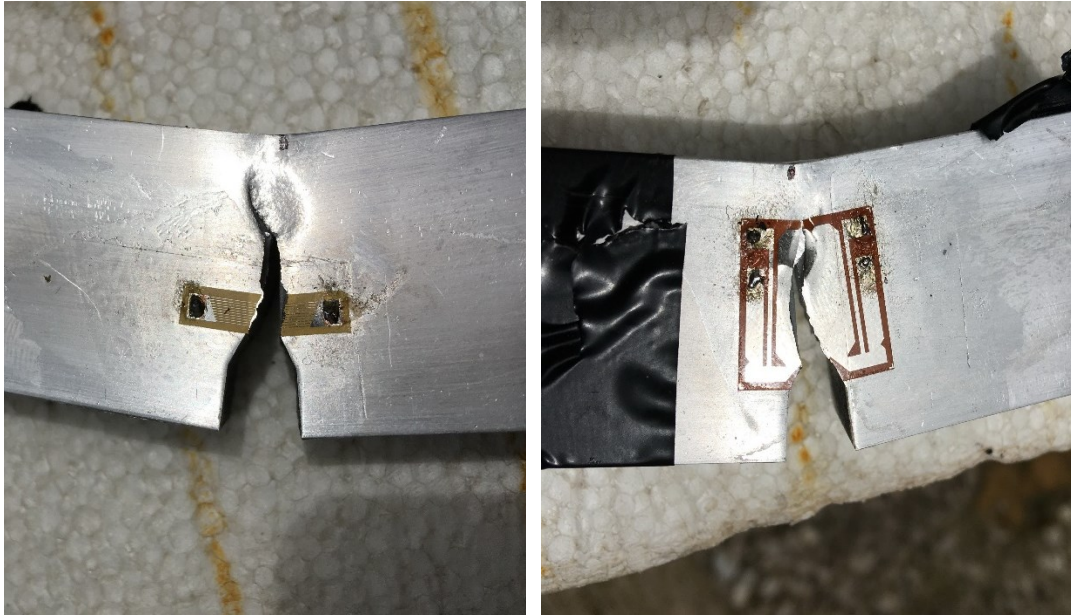


Figure 4. 7 After test photographs of specimen with residual stresses

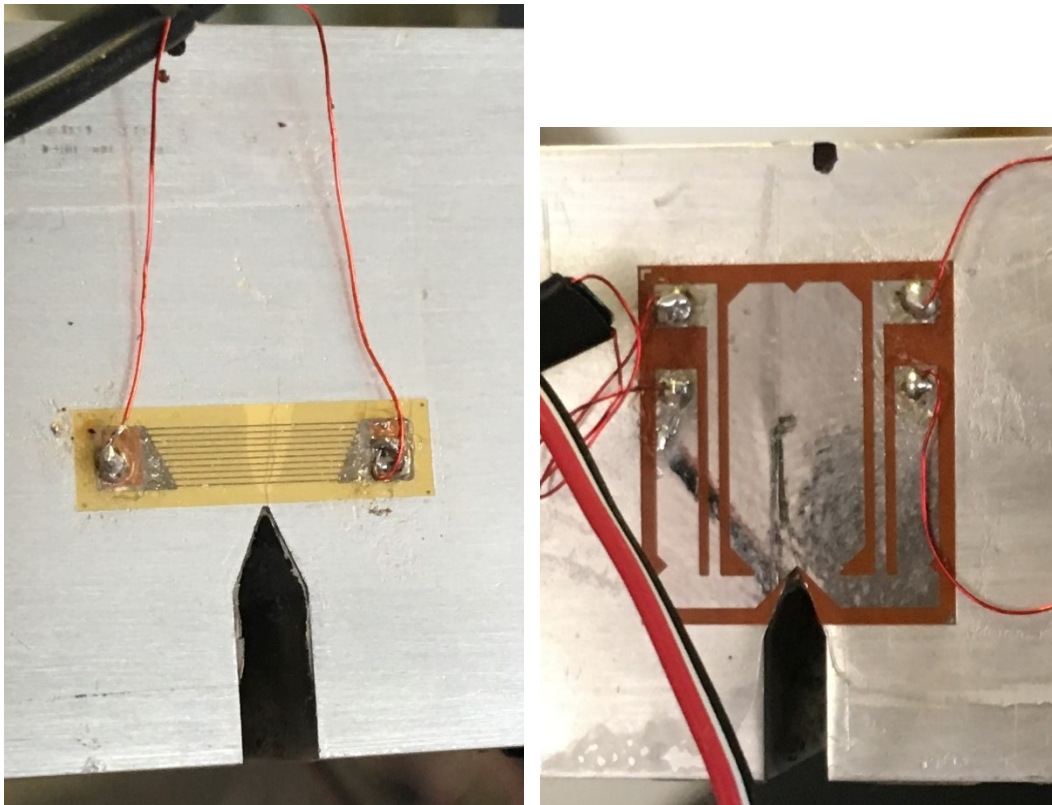


Figure 4. 8 After test photographs of specimen without residual stresses

Tests Data was acquired at a sampling rate of 100 [Hz]. Then acquired data was analyzed with Matlab software. The result of data analyzes for test one (specimen with residual stresses) and test two (specimen without residual stresses) are shown in figure 4.11 and 4.12 respectively. The load line displacement data were acquired in the tests for calculating the crack length by using the formula which is provided by [10]. But there was an error in data acquisition device resulting in incorrect displacements values, so this approach was not used in this study.

By inspecting figure 4.11(a) and 4.12 (a), it is observable that maximum and minimum load values are converged about 2000 cycles.

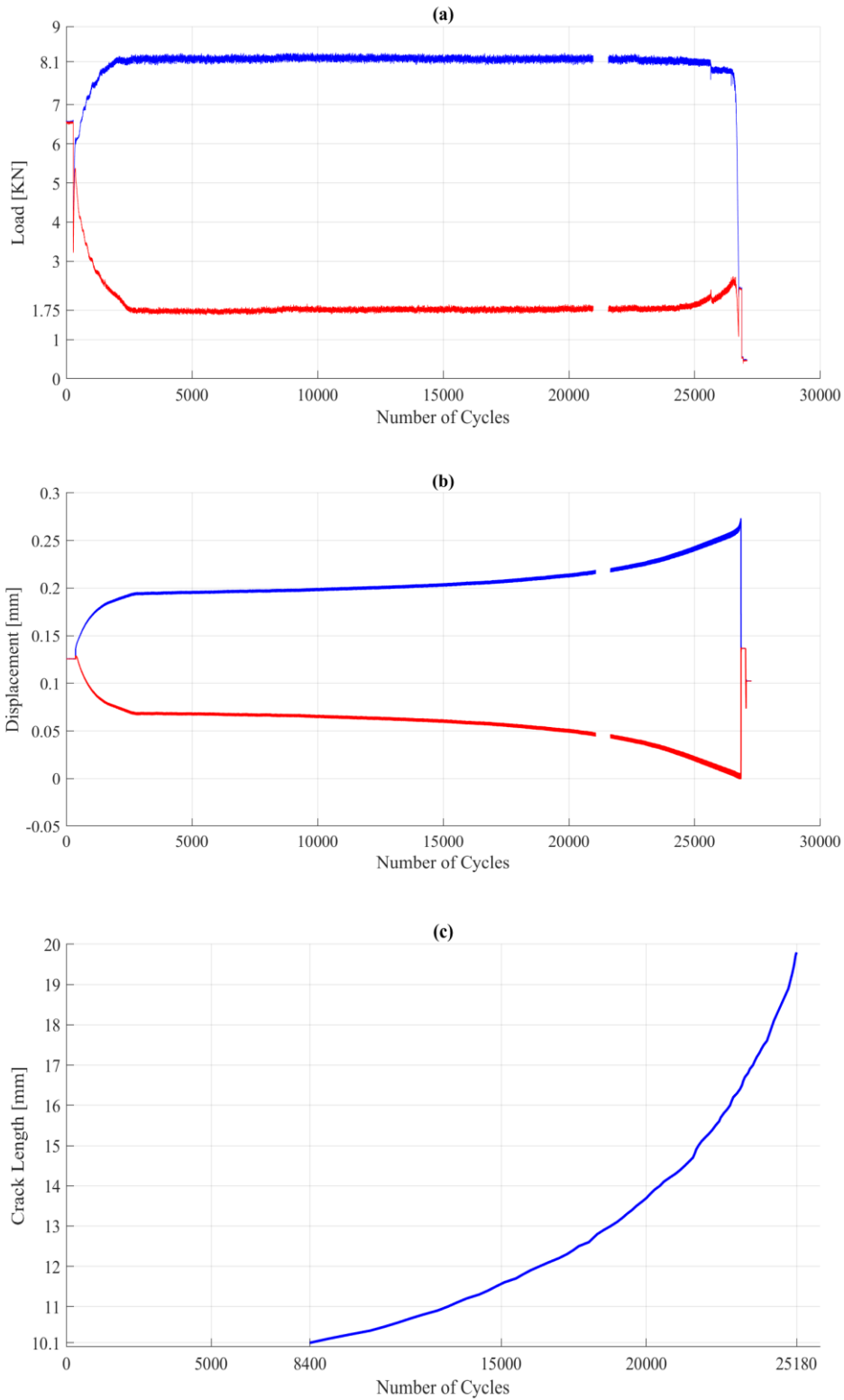


Figure 4. 9 Test one results. (a): maximum and minimum magnitudes of load versus N. (b): maximum and minimum values of displacement versus N. (c): crack length (acquired using krak gage) versus N. It should be noted that notch depth is included in crack length.

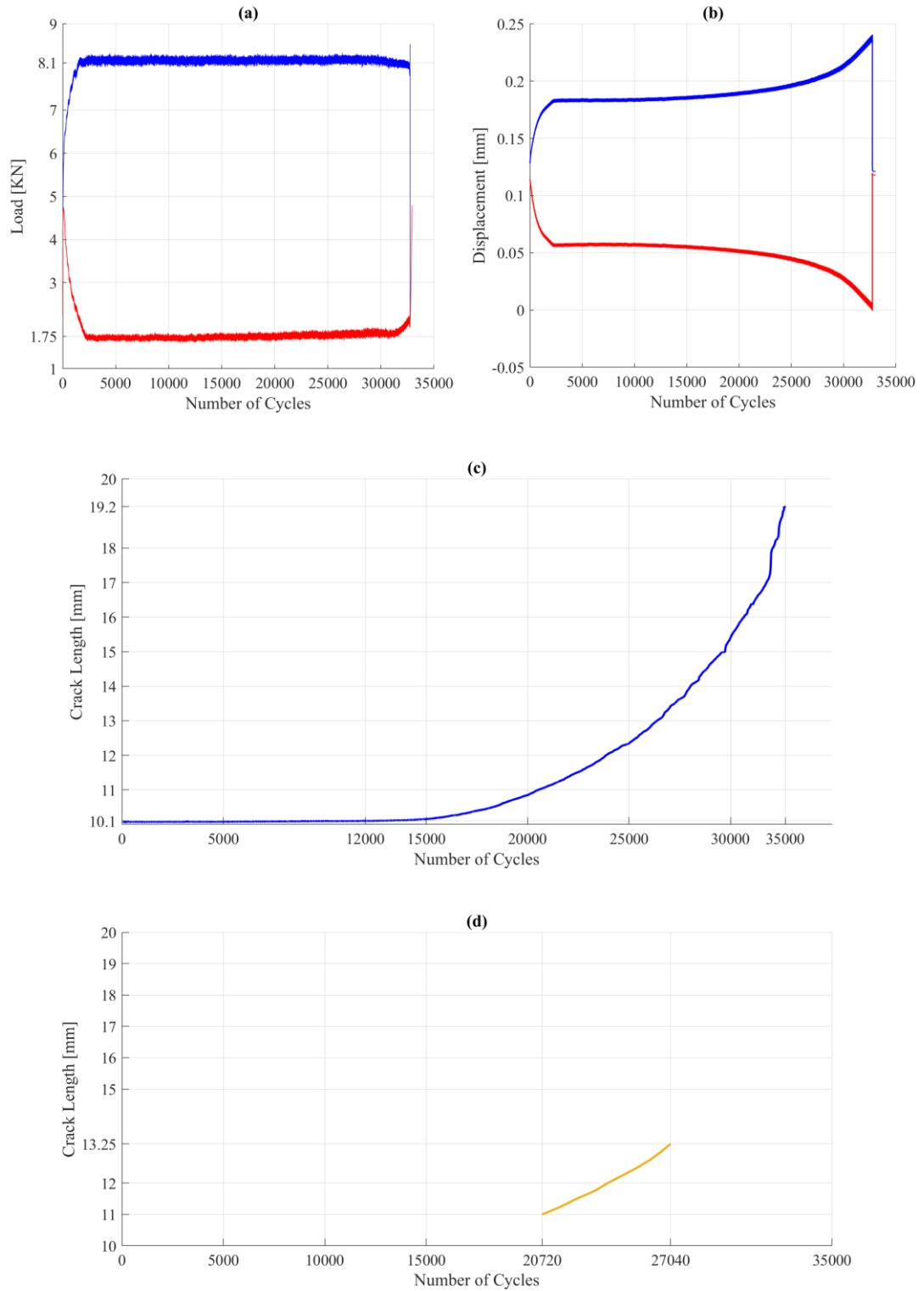


Figure 4. 10 Test two results. (a): maximum and minimum magnitudes of load versus N. (b): maximum and minimum values of displacement versus N. (c): crack length (acquired using krak gage) versus N. (d): crack length (acquired using crack propagation gage) versus N.



## CHAPTER V

### COMPARISONS, CONCLUSION AND FUTURE WORK

In this study, in chapter III, fatigue crack initiation life for cracked beam specimen was estimated then the life for propagating the initiated crack to a desired length was also calculated. Then tests were done for the simulated geometry on two specimens to determine the fatigue crack initiation life and the life required to propagate it to a desired length in reality. One of the tests was with a specimen with residual stresses and the other was with a specimen without residual stresses.

To compare the predicted fatigue crack initiation life with the experimental one (specimen without residual stresses), first an initiated crack length should be assumed. In literature a crack size in order of 1 mm is suggested to be taken as initiated fatigue crack length [15]. However this is an approximation. In this study predicted lives are compared with 0.1 mm and 1 mm crack length as initiated fatigue crack size. The comparison is shown in table 5.1. 0.1 mm corresponds to the smallest crack which could be detected by FRACTOMAT device.

By inspecting table 5.1, it is seen that for a crack length of 0.1 mm as initiated crack size, the lives predicted by Morrow and Walker approach by using Peterson stress concentration factor obtained by 2-D stress analysis and material cyclic properties of [48] are close to the life obtained by experiment. On the other hand, assuming initiated crack length as 1 mm, the life predicted by Morrow by using Peterson stress concentration factor obtained by 3-D stress analysis and material cyclic properties of [47] well agree with the life obtained by experiment.

Table 5. 1 Fatigue crack initiation life (numerical & experimental)

		Material Reference[47]					Material Reference[48]				
		$K_{f_{neuber}}$		$K_{f_{Peterson}}$		3-D FEA	$K_{f_{neuber}}$		$K_{f_{Peterson}}$		3-D FEA
		2-D	3-D	2-D	3-D		2-D	3-D	2-D	3-D	
Strain-Life Equation [cycles]		19400	-	37200	-	7100	36500	-	64500	-	14900
Modified Morrow [cycles]		4160	15500	5700	21000	3050	9350	33000	12900	43000	6650
SWT [cycles]		3984	23400	4690	27500	1462	6620	33500	7745	38500	2410
Walker [cycles]		3510	33000	6040	52000	2600	6650	40000	10450	60000	5450
Manson-Halford [cycles]		980	7000	1600	11000	900	1870	8300	2800	12500	1900
Experiment [cycles]	Initiated crack length 0.1 [mm]	12000									
	Initiated crack length 1 [mm]	20720									

Fatigue crack initiation and propagation versus number of cycles obtained by numerical calculations and experiment for specimen without residual stresses are shown in figure 5.1.

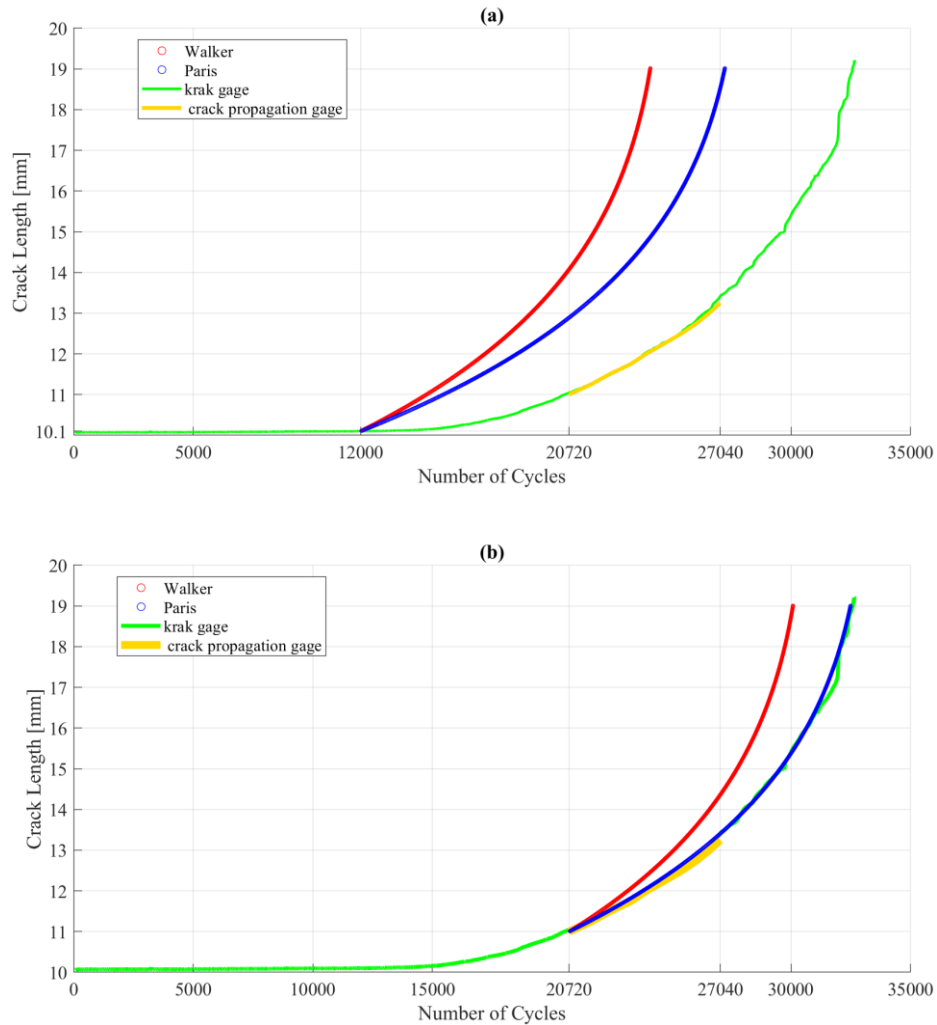


Figure 5. 1 Fatigue crack initiation and propagation life. (These are obtained by both numerical and experimental analyses for specimen without residual stresses.) (a): 0.1 mm assumed initiated crack length. (b): 1 mm assumed crack initiation length

It is observable from above plots that assuming crack initiation length as 1 mm gives better results in FCG predictions.

To monitor the influence of residual stresses on fatigue crack initiation and propagation the results of data analyses of two specimens are plotted together in figure 5.2.

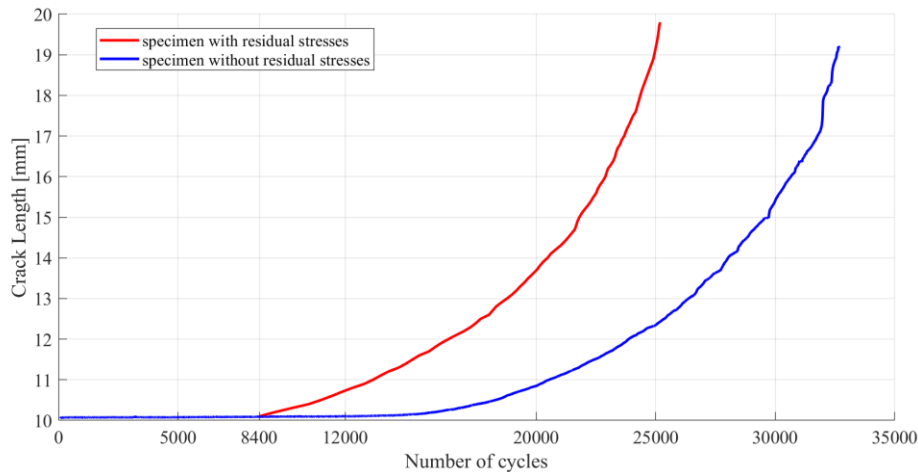


Figure 5. 2 Crack initiation and propagation life of specimens with and without residual stresses

It is clearly observable that residual stresses induced to the specimen accelerated the initiation and propagation of fatigue crack.

The little differences between numerical predictions and experimental results may arise from errors that are mentioned below as:

- Material cyclic and strength properties which were not provided by producer of specimens.
- The notch tip may not have the exact dimensions of the simulated one in Abaqus.
- The adhesive used was not the one suggested by gage manufacturers.
- Some errors may be induced by loading machine and data acquisition device.

At the bottom line with the procedure presented in this study, and during the experiments, the specimens prepared

- Did not break due to an unstable crack growth during the tests (except the pilot one which was not simulated).
- Did not undergo a macroscopic plastic deformation.
- A crack of desired length grew in a reasonable time (about 56 minutes for specimen without residual stresses and about 42 minutes for specimen with residual stresses).

- Inducing tensile residual stresses significantly accelerate crack initiation and growth.
- Crack growth could be successfully monitored by using different means which produce consistent results.

Therefore it is concluded that the procedure applied in this thesis could be a useful approach to predict the crack initiation and propagation lives of cracked beam test specimens. By using this approach and trying different notch geometries (depth and tip radius) as well as load levels, one can find appropriate values of these parameters and minimize the time required to prepare many cracked beam test specimens.

As some future work followings can be considered:

- More refined crack initiation models can be employed.
- Matching theory and experiment for mixed-mode crack initiation and propagation can be considered for broader applications.
- Quantifying the effects of residual stress by simulations and experiments can be accomplished.
- Quantifying the effect of residual stressing on fracture toughness can be investigated.



## REFERENCES

- [1] B. L. Braglia, "Crack initiation and propagation in VAN-80 steel . by," Lehigh University, 1978.
- [2] M. Benachour, M. Benguediab, and N. Benachour, "Notch Fatigue Crack Initiation and Propagation Life under Constant Amplitude Loading Through Residual Stress Field," vol. 682, pp. 17–24, 2013.
- [3] A. K. Baliarsingh, "Prediction of fatigue crack propagation life in single edge notched beams using exponential model," National Institute of Technology Rourkela, 2013.
- [4] T. H. Topper, R. M. Wetzel, and J. Morrow, "Neuber's Rule Applied To Fatigue Of Notched Specimens," no. 11749, p. 21, 1967.
- [5] R. G. Forman, "Study of Fatigue Crack Initiation from Flaws Using Fracture Mechanics Theory," *Eng. Fract. Mech.*, vol. 4, pp. 333–345, 1972.
- [6] R. J. Mattos, "Estimation Of The Fatigue Crack Initiation Life In Welds Using Low Cycle Fatigue Concepts," The University of Illinois, 1976.
- [7] G. Glinka, "A notch stress-strain analysis approach to fatigue crack growth," *Eng. Fract. Mech.*, vol. 21, no. 2, pp. 245–261, 1985.
- [8] A. Buch, M. Vormwald, and T. Seeger, "Improvement of fatigue life prediction accuracy for various realistic loading spectra by use of correction factors," *Int. J. Fatigue*, vol. 8, no. 4, pp. 175–185, 1986.
- [9] Y. Jiang, "A continuum mechanics approach for crack initiation and crack growth predictions," *Materwiss. Werksttech.*, vol. 37, no. 9, pp. 738–746, 2006.
- [10] U. Andreaus and P. Baragatti, "Fatigue crack growth, free vibrations, and breathing crack detection of aluminium alloy and steel beams," *J. Strain Anal. Eng. Des.*, vol. 44, no. 7, pp. 595–608, 2009.
- [11] N. Ranganathan, H. Aldroe, F. Lacroix, F. Chalon, R. Leroy, and A. Tougui, "Fatigue crack initiation at a notch," *Int. J. Fatigue*, vol. 33, no. 3, pp. 492–499, 2011.
- [12] N. Benachour, A. Hadjoui, M. Benachour, and M. Benguediab, "Stress ratio and notch effect on fatigue crack initiation and propagation in 2024 Al-alloy," *World Acad. Sci. Eng. Technol.*, vol. 79, no. 7, pp. 566–569, 2011.
- [13] M. R. Ayatollahi, S. M. J. Razavi, and M. Y. Yahya, "Mixed mode fatigue crack initiation and growth in a CT specimen repaired by stop hole technique," *Eng. Fract. Mech.*, vol. 145, pp. 115–127, 2015.

- [14] S. Kadioğlu, E. Ciğeroğlu, and G. Özgen, “Çatlak içeren kırılgarlığın titreşimlerinin deneysel incelenmesi. Tübitak 1001 proje raporu, proje no 214M065,” 2017.
- [15] I. Stephens, Ralph, A. Fatemi, R. Stephens, Robert, and O. Fuchs, Henry, *Metal Fatigue in Engineering*, Second. JOHN WILEY & SONS, INC., 2001.
- [16] R. E. Peterson, “Discussion of a Century Ago Concerning the Nature of Fatigue, and Review of Some of the Subsequent Researches Concerning the Mechanism of Fatigue,” *ASTM Bull*, vol. 164, p. 50, 1950.
- [17] “Wohler’s Experiments on the Strength of Metals,” *engineering*, p. 160, 1967.
- [18] wikipedia, “August Wöhler.” [Online]. Available: [https://it.wikipedia.org/wiki/August\\_Wöhler](https://it.wikipedia.org/wiki/August_Wöhler). [Accessed: 01-Mar-2018].
- [19] J. Bauschinger, “On the change of position of the elastic limit of iron and steel under cyclic variations of stress,” 1886.
- [20] Y.-L. Lee, M. E. Barkey, and H.-T. Kang, *Metal Fatigue Analysis Handbook*. Elsevier, 2012.
- [21] G. Masing, “Eigenspannungen and Verfestigung beim Messing,” in 2nd international congress for applied mechanics, 1926, pp. 332–335.
- [22] J. Collins, H. Busby, and G. Staab, *mechanical design of machine elements and machines*, Second. Wiley, 2015.
- [23] efatigue, “Constant Amplitude Strain-Life Technical Background.” [Online]. Available: <https://www.efatigue.com/constantamplitude/background/strainlife.html>. [Accessed: 22-Mar-2018].
- [24] O. H. Basquin, “The Exponential Law of Endurance Tests,” in *ASTM*, 1910, vol. 10, p. 625.
- [25] S. S. Manson, “Behavior of materials under conditions of thermal stress,” in *Heat transfer symposium*, 1953, pp. 9–75.
- [26] L. F. Coffin, “Experimental Support for Generalized Equation Predicting Low Cycle Fatigue,” *ASME*, vol. 84, no. 4, p. 533, 1962.
- [27] K. S. Lee and J. H. Song, “Estimation methods for strain-life fatigue properties from hardness,” *Int. J. Fatigue*, vol. 28, no. 4, pp. 386–400, 2006.
- [28] M. A. Meggiolaro and J. T. P. Castro, “Statistical evaluation of strain-life fatigue crack initiation predictions,” *Int. J. Fatigue*, vol. 26, no. 5, pp. 463–476, 2004.
- [29] M. R. Mitchell, “Fundamentals of modern fatigue analysis for design,” in *ASM symposium on fatigue and microstructure*, 1979.
- [30] J. D. Morrow, “fatigue design handbook, section 3.2,” in *SAE Advanced in Engineering*, 1968, pp. 21–29.
- [31] S. S. Manson and G. R. Halford, “Practical implementation of the double

- linear damage rule and damage curve approach for treating cumulative fatigue damage,” *Int. J. Fract.*, vol. 17, no. 2, pp. 169–192, 1981.
- [32] Kn. Smith, T. H. Topper, and P. Watson, “A stress-strain function for the fatigue of metals (Stress-strain function for metal fatigue including mean stress effect),” *J. Mater.*, vol. 5, no. April, pp. 767–778, 1970.
- [33] N. E. Dowling, “Mean stress effects in strain-life fatigue,” *Fatigue Fract. Eng. Mater. Struct.*, vol. 32, no. 12, pp. 1004–1019, 2009.
- [34] N. E. Dowling, *Mechanical Behavior of Materials*, Fourth ed. Pearson Education, 2013.
- [35] C. W. MacGregor and N. Grossman, “NACA TN 2812,” Washington, DC, 1952.
- [36] W. Yao, “Stress field intensity approach for predicting fatigue life,” *J. Fatigue*, vol. 15, no. 3, pp. 243–245, 1993.
- [37] G. Qylafku, Z. Azari, N. Kadi, M. Gjonaj, and G. Pluinage, “Application of a new model proposal for fatigue life prediction on notches and key-seats,” *Int. J. Fatigue*, vol. 21, no. 8, pp. 753–760, 1999.
- [38] H. Adib and G. Pluinage, “Theoretical and numerical aspects of the volumetric approach for fatigue life prediction in notched components,” *Int. J. Fatigue*, vol. 25, no. 1, pp. 67–76, 2002.
- [39] R. E. Peterson, *Stress Concentration Factors*. New York: John Wiley and Sons, 1974.
- [40] H. Neuber, “Theory of Stress Concentration for Shear-Strained Prismatical Bodies With Arbitrary Nonlinear Stress-Strain Law,” *J. Appl. Mech.*, vol. 28, no. 4, pp. 544–550, 1961.
- [41] K. Molski and G. Glinka, “A method of elastic-plastic stress and strain calculation at a notch root,” *Mater. Sci. Eng.*, vol. 50, no. 1, pp. 93–100, 1981.
- [42] A. A. Griffith; and M. Eng, “VI. The phenomena of rupture and flow in solids,” vol. C, pp. 163–198, 1920.
- [43] G. R. Irwin, “analysis of stresses and strains near the end of a crack traversing a plate,” *Appl. Mech.*, vol. 24, p. 361, 1957.
- [44] P. C. Paris and F. A. Erdogan, “A Critical Analysis of Crack Propagation Laws,” *J. Basic Eng. (Trans. ASME)*, vol. 85, no. 4, pp. 528–534, 1963.
- [45] T.L. Anderson, *Fracture mechanics : fundamentals and applications*. 2005.
- [46] ASTM E399, “Standard Test Method for Linear-Elastic Plane-Strain Fracture Toughness K<sub>1C</sub> of Metallic Material,” E 399, pp. 1–33, 2013.
- [47] L. P. Borrego, J. M. Ferreira, J. M. Pinho da Cruz, and J. M. Costa, “Evaluation of overload effects on fatigue crack growth and closure,” *Eng. Fract. Mech.*, vol. 70, no. 11, pp. 1379–1397, 2003.
- [48] S. R. Alfredo and M. P. de J. Abílio, “Fatigue behaviour of welded joints made

- of 6061-T651 aluminium alloy,” *InTech, Alum. Alloy. Theory Appl.*, vol. 7, pp. 135–156, 2011.
- [49] “Matlab.” .
- [50] X. Chen, Y. Peng, S. Peng, S. Yao, C. Chen, and P. Xu, “Flow and fracture behavior of aluminum alloy 6082-T6 at different tensile strain rates and triaxialities,” *PLoS One*, vol. 12, no. 7, pp. 1–28, 2017.
- [51] T. Mann, “The influence of mean stress on fatigue crack propagation in aluminium alloys,” *Int. J. Fatigue*, vol. 29, no. 8, pp. 1393–1401, 2007.
- [52] D. Pósalaky and J. Lukács, “The Properties of Welded Joints Made by 6082-T6 Aluminium Alloy and their Behaviour under Cyclic Loading Conditions,” *Mater. Sci. Forum*, vol. 812, pp. 375–380, 2015.
- [53] “RUMUL.” [Online]. Available: [http://www.rumul.ch/250\\_products.php?lang\\_choose=1](http://www.rumul.ch/250_products.php?lang_choose=1). [Accessed: 10-May-2018].